From Computational Studies on the Mechanism of the Formation of Organic Heterocyclic Compounds to Spin Crossover Studies in Prussian Blue

Damiano Portinari

A thesis submitted in partial fulfillment

for the degree of Doctor of Philosophy

in the

University of Glasgow

Department of Chemistry

September 2009

i Declaration of Authorship

I declare that this thesis titled, 'From Computational Studies on the Mechanism of the Formation of Organic Heterocyclic Compounds to Spin Crossover Studies in Prussian Blue' and the work presented in it are my own. I confirm that :

- This work was done wholly while in candidature for a research degree at this University.
- Where I have consulted the published work of others, this is always clearly attributed.
- Where I have quoted from the work of others, the source is given. With the exception of such quotations, this thesis is my own work.
- I have acknowledged all main sources of help.

"I would never die for my beliefs because I might be wrong"

Bertrand Russel

ii Abstract

Understanding with the use of computational tools the mechanism of reactions in organic chemistry or the electronic transitions in solid state is a quite challenging problem. The main methods utilised for this research are Density Functional Theory (DFT) and time dependent DFT. The software utilised is GAUSSIAN03 for the reaction mechanism studies and CRYSTAL06 for the study of the spin crossover transition in a Prussian Blue analogue.

In chapter 2, we investigate the first two reaction steps of the synthesis reaction mechanism of Dihydro-Imidazo-Phenathridinium (DIP) derivatives, which are a novel class of compounds that intercalate DNA, possessing anticancer properties.

In chapter 3, we examine the last step of the DIP synthesis reaction, which is a hydride transfer, in particular it is considered the solvent effect on the excitation energies of the molecules involved in the hydride transfer.

In chapter 4, we consider the hydride transfer reaction of heteroaryl-dimethylbenzimidazoline derivatives (HDBMZ-H) with benzyl-carbamoylpyridinium (BCPY) and benzyl-nitrosoquinolinium (BNIQ) ions.

In chapter 5, we study the spin crossover transition (SCO) in the $CsFe^{II}[Cr^{III}(CN)_6]$ Prussian Blue analogue. This transition can be induced experimentally by variations of temperature or pressure and more light on this mechanism can be useful in information processing and display technologies. Those fields, in fact can benefit from the application of molecular electronic bistabilities in which the SCO phenomenon can be classified.

iii Acknowledgments

memori mente

- ★ to my supervisors Prof. Lee Cronin and Prof. Chick Wilson that followed with patience and comprehension my progresses during my research, giving support and encouragement when it was needed;
- ★ to Prof. John McGrady who provided me his experience and professionalism with great generosity: a great help for my research;
- ★ to Dr. Derek Middlemiss for collaborating and supervising me;
- ★ to Dr. Alexis Parenty for helping me to understand the "experimental side" of organic chemistry;
- ★ to Dr. Dimitrios Pantazis for very useful discussions;
- ★ to the Wilson Group and the Cronin Group;
- ★ to Dr. Marc Schmidtmann and Dr. Lynne Thomas for their kind support;
- ★ to Stuart MacKay, Dr Geoff Cooper, Duncan Sneddon, Gordon Cunningham for solving the problems I had with my DELL windows computer;
- ★ to Lorreta Lawton, Stephen Cairns, Martin Adam, Craig Martin, Andrew O'Neal, Bryan Boyle, Duncan Sneddon, Andràs Kàllay for being great friends;
- ★ to Thomas Davin for his help with LATEX software which has been utilised for writing this thesis.

A sad and joyful memory to Dr. Andy Parkin, an enthusiastic person in his work, his friends and of nature, that I have been really happy to meet.

Contents

List of Figures

List of Tables

1

Introduction

With the advent of computers in the early fifties quantum mechanics started to be applied to chemistry. This is a period that signals the birth of computational chemistry. One of the first issues tackled was solving the H*ü*ckel molecular orbital problem on some aromatic hydrocarbons, but the problems faced, such as insufficient data storage space and the slow speed of computing machines, rendered that task quite difficult to solve. The machine used in the initial applications was performing about 68 million integer instructions in 24 hours, slightly more than what an obsolete Intel 486 processor would do in 1 second! Although quantum mechanics thus did not reveal its power in solving concrete problems early after his formulation, its impact in our life could hardly be greater. The advances made in chemistry, biology, engineering and also in other fields would not have been possible without quantum mechanics tools. Here, from all contributions to quantum mechanics one is particularly relevant in our studies : the Schr*ö*dinger equation. In 1924 adopting the idea given by De Broglie on the dual nature of light, Erwin Schr*ö*dinger conceptualized a theory that described this behavior by a wave equation whose solutions are wave functions that are related to thele occurrence of physical events. The most familiar form of this equation is: $\hat{H}\Psi = E\Psi$ where $\hat{H}$ is the Hamiltonian operator that acts upon a wavefunction Ψ which returns the total energy of the system E. The molecular Hamiltonian for a time-independent

multielectron system is :

$$\hat{H} = -\frac{1}{2}\sum_{i=1}^{N}\nabla_i^2 - \frac{1}{2}\sum_{A=1}^{M}\frac{1}{M_A}\nabla_A^2 - \sum_{i=1}^{N}\sum_{A=1}^{M}\frac{Z_A}{r_{iA}} + \sum_{i=1}^{N}\sum_{j>i}^{N}\frac{1}{r_{ij}} + \sum_{A=1}^{M}\sum_{B>A}^{M}\frac{Z_A Z_B}{R_{AB}} \quad (1.1)$$

In this equation A and B define the nuclei and i and j relate to the electrons of the system. In order, the first two terms depict the kinetic energy of electrons and nuclei respectively, the third term expresses the electrostatic interaction between the nuclei and the electrons, the fourth and fifth terms represent the electron-electron and nucleus-nucleus repulsive interactions. Furthermore, simplifications of the Schrödinger equation can be achieved considering the Born-Oppenheimer approximation that has its basis in the fact that the nuclei motion is slower than that of the electrons. Thus, considering electrons moving in the field of fixed nuclei, the Schrödinger equation can be simplified as:

$$\hat{H}_{elec} = -\frac{1}{2}\sum_{i=1}^{N}\nabla_i^2 - \sum_{A=1}^{M}\frac{Z_A}{r_{iA}} + \sum_{i=1}^{N}\sum_{j>i}^{N}\frac{1}{r_{ij}} \quad (1.2)$$

The solution of the electronic Hamiltonian is an electronic wavefunction. The energy obtained therefore depends only on the electronic coordinates.

The wavefunction is a probability amplitude. This statistical interpretation was given by Born in 1926. This concept can be represented considering a high number of identical systems where in each one there is a moving particle influenced by a force. This ensemble can be defined by a single wavefunction that contains all information available in such systems. If measurements are made on the position of the particle on every system, the probability of finding the particle in the volume element $dr \equiv (dx, dy, dz)$ around the point $r \equiv (x, y, z)$ at time t is

$$P(\mathbf{r}, t)d\mathbf{r} = |\Psi(\mathbf{r}, t)|^2 d\mathbf{r} \quad (1.3)$$

Moreover, the wavefunction should be integrated over all space, normalising its value to unity since the probability of finding the particle somewhere should be equal to that.

$$\int |\Psi(\mathbf{r}, t)|^2 d\mathbf{r} = 1 \quad (1.4)$$

The variation method has very important implications in quantum mechanics because in order to find the best wavefunction, which represents the ground state of a system, it is possible to guess its value by arbitrarily defining its associated energy. The lowest energy found gives the best wavefunction. When the wavefunction is normalized to unity that principle assumes the following form :

$$\langle \Psi_{trial} | \hat{H} | \Psi_{trial} \rangle = E_{trial} \geq E_0 = \langle \Psi_0 | \hat{H} | \Psi_0 \rangle \tag{1.5}$$

This equation tells us that the expectation value of the Hamiltonian operator corresponding to a trial wavefunction is always higher than the expectation value of the Hamiltonian of the ground state wavefunction.

The solution of the electronic Hamiltonian of equation (1.2) implies the solution of a many body problem where the many body wavefunction contains the quantum probability amplitude for every possible configuration of electrons and nuclei in a three dimensional system. In order to solve such complex problem it is possible to place the wavefunction of single particles in a Slater determinant.The single particle wavefunctions described by this determinant minimize the energy utilised in the wavefunction and are termed Hartree-Fock orbitals if the Hartree-Fock method is utilised or Kohn-Sham orbitals if within the DFT method. This determinant satisfies the **Pauli Principle** which affirms that the total wavefunction must be antisymmetric under the interchange of any pair of identical electrons (fermions) and symmetrical under the interchange of any pair of identical bosons.

$$\Psi = \frac{1}{\sqrt{N!}} \begin{vmatrix} \chi_1(\overrightarrow{\chi_1}) & \chi_2(\overrightarrow{\chi_1}) & \cdots & \chi_N(\overrightarrow{\chi_1}) \\ \chi_1(\overrightarrow{\chi_2}) & \chi_2(\overrightarrow{\chi_2}) & \cdots & \chi_N(\overrightarrow{\chi_2}) \\ \vdots & \vdots & \vdots & \\ \chi_1(\overrightarrow{\chi_N}) & \chi_2(\overrightarrow{\chi_N}) & \cdots & \chi_N(\overrightarrow{\chi_N}) \end{vmatrix} \tag{1.6}$$

In eq 1.6 $\chi_i(\overrightarrow{\chi_i})$ terms are called spin orbitals, which are spatial orbitals times a spin function.

1.0.1 The Hartree-Fock approach

In the Hartree-Fock method,[1] where the wavefunction is expressed as a Slater determinant, the electron-electron repulsions are handled in an average way. Every electron moves in the field of the nuclei and in the averaged potential of the remaining electrons. The application of the variation method, illustrated above, leads to the Hartree-Fock equations. The equation for the spin orbital $\phi_a(1)$ where the electron 1 assigned to that orbital is :

$$f_1\phi_a(1) = \epsilon_a\phi_a(1) \tag{1.7}$$

in which ϵ_a is the energy of the orbital and f_1 is the Fock operator that can be written as:

$$f_1 = h_1 + \sum_u \{J_u(1) - K_u(1)\} \tag{1.8}$$

In equation 1.8 h_1 is the core Hamiltonian for electron 1 in the field of all nuclei present with charge Z_e. J_u is the Coulomb operator and K_u is the exchange operator, these are defined as :

$$J_u(1)\phi_a(1) = \left\{ \int \phi_u^*(2) \left(\frac{e^2}{\pi\epsilon_0 r_{12}} \right) \phi_u(2) dx_2 \right\} \phi_a(1) \tag{1.9}$$

$$K_u(1)\phi_a(1) = \left\{ \int \phi_u^*(2) \left(\frac{e^2}{\pi\epsilon_0 r_{12}} \right) \phi_a(2) dx_2 \right\} \phi_u(1) \tag{1.10}$$

These operators depend on the orbitals generated by the Hartree-Fock operator and the solution of the Hartree-Fock equations normally proceeds by iterative matrix diagonalisation of the Fock matrix, method termed self-consistent field (SCF). This method consists of choosing a starting set of orbitals which are used to construct an initial approximation of the Coulomb and exchange operators which constitute the Hartree-Fock operator. Iteratively are genereated new set of orbitals that are used to redefine the Hartree-Fock operator until self consistency is achieved which means that something stops changing on repeated iteration of

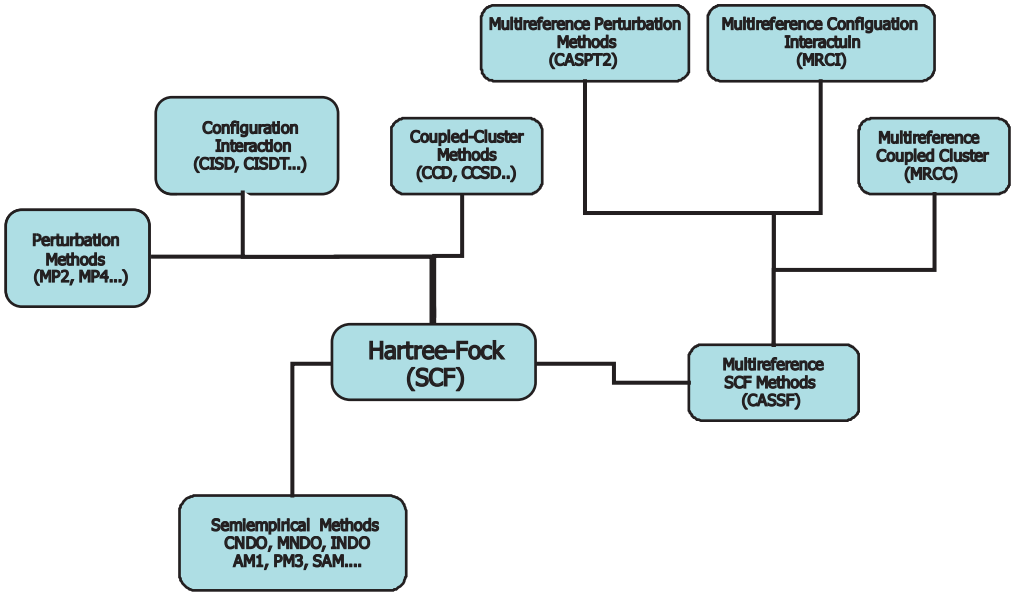

Figure 1.1: Connection between various types of ab-initio methods

the set of coupled single particle equations, be it the energy, or some collective metric of the single particle wavefunctions.

1.0.2 Semiempirical molecular orbital methods

Semiempirical methods[2] appeared from the 1930's to the 1950's, the most important of these are the Hűckel method and the Pariser-Parr-Pople method. Since the 1960s, several all valence electron methods have been developed that have found extensive use in predicting energetic and spectrospic properties of diverse systems, (fig 1.1). The most important characteristics of these methods are the explicit treatment of valence electrons, the pseudo minimal basis sets, the neglect of the three and four center integrals and the use of parametrized expressions for two center integrals. The four basic methods are : extended Hűckel theory (EHT),complete neglect of differential overlap (CNDO), intermediate neglect of differential overlap (INDO) and neglect of diatomic differential overlap (NDDO). In EHT the basis functions are used in calculating only the overlap integrals, all the other contributions to the Fock matrix are empirical. A significant improvement of NDDO has been achieved with the modified neglect of differential overlap (MNDO)

which methods use a multipole expansion for the calculation of two-center two-electron integrals. In MNDO a Pauli repulsion term has been included that is not present in CNDO and INDO.This term is added to the core-core repulsion term, which is therefore expressed as :

$$V_{nn} = \sum_{A>B} Z_A^* Z_B^* \gamma_{AB} + f_{AB} \tag{1.11}$$

where Z^* is the effective core charge and γ_{AB} is a Coulomb integral, f_{AB} is a correction term that with the Coulomb integral replaces the analytical $1/R_{AB}$ potential. Other modifications of the MNDO method, both in the parameterization and the empirical function f_{AB}, lead to the widely used AM1, PM3 and PM5 methods. AM1 and PM3 have also been extended to transition metal compounds by inclusion of d orbitals in the valence basis. While semiempirical methods cannot handle systems bigger than 10000 atoms, a solution of this problem has been achieved by developing parallelised program codes that can be used on modern parallel computers.

1.0.3 Inclusion of electron correlation

The Hartree-Fock method,[3] as stated above, treats the electron-electron repulsions in an average way, and specifically does not consider the instantaneous electrostatic interactions between the electrons and the quantum mechanical effect on electron distributions. However, the HF method does include some of the QM interactions between electrons i.e. the non-local exchange repulsion. It does not include correlations between electrons of opposite spin which means that the only repulsion between such states arises from the classical Hartree term. Moreover, the Fock operator, unlike the Hamiltonian operator, is not a single operator but a group of interdependent one-electron operators that give single electron molecular orbitals defined by a single determinantal wavefunction. In order to obtain a lower energy wavefunction, that by the variational principle should be more accurate, it is

possible to construct a wavefunction that is a linear combination of multiple determinants. Each determinant, or a linear combination of a small number of them constructed so as to have the correct electronic symmetry, is called a configuration state function (CSF). In a given basis set expansion there are Θ basis functions, while the number of different spin orbitals are 2Θ. In the SCF method the n spin orbitals lowest in energy, occupied by the n electrons are taken to construct the Hartree-Fock wavefunction, therefore there are still 2Θ - n unoccupied spin orbitals or virtual orbitals that can be used to construct an excited state by replacement of one or more occupied orbitals and representing the promotion of electrons from the occupied orbitals to the virtual orbitals. Moreover, in addition to the replacement of an occupied orbital by one virtual orbital two occupied orbitals can be replaced by two virtual orbitals and so forth...

From a defined number of spin orbitals, the number of Slater determinants can be large and the ground and excited state wavefunctions can be defined by their linear combination in the Configuration Interaction method (CI). If we start to promote for example the electrons from the occupied orbitals a, b, c, to the virtual orbitals p,q,r , the total wavefunction assumes the following form :

$$\Psi = C_0\Phi_0 + \sum_{a,p} C_a^p \Phi_a^p + \sum_{a<b,p<q} C_{ab}^{pq} \Phi_{ab}^{pq} + \sum_{a<b<c,p<q<r} C_{abc}^{pqr} \Phi_{abc}^{pqr} + \dots \qquad (1.12)$$

The C_s are the expansion coefficients, and a condition in the summation is that an excited determinant must appear only once. The correlation energy can now be formulated as the difference between the non-relativistic ground state energy defined in the equation above and the Hartree-Fock limit. A CI calculation where all CSF with a correct symmetry are used in a defined basis set is called full CI and the difference between the energy obtained within this calculation and the energy from the Hartree-Fock method is called the basis set correlation energy. In CI calculations a state s is determined by a wavefunction that is a linear combination of Slater determinants. The expansion coefficients are determined through the variation theory, with the condition that the Slater determinants form an orthonormal

set, thus the overlap integrals are equal to the identity matrix:

$$\mathbf{HC} = \mathbf{EC} \tag{1.13}$$

Diagonalisation of H generates the set of coefficients that defines the configuration interaction wavefunction.In cases where the number of determinants to be calculated is far too large and a full CI calculation is not necessary,a truncated CI scheme can be used where the number of the CSF is limited. For example,in the calculation of the electronic ground state of a system most of the configurations do not contribute to the wavefunction or the correlation energy therefore a full CI does not make sense. A first approach on the truncation method is to reduce the list of the excited determinants to the singly and doubly excited. If only singly excited determinants are included the method is called CIS, if doubly excited are also included the method is called CISD. Another method is the multiconfiguration self-consistent field where the coefficients of the CI expansion plus the basis functions coefficients in the Roothan-Hall equations are determined simultaneously. Thus, this method is computationally expensive, so, a better method has been developed and is called complete active space self consistent method (CASSCF) in which the orbitals have been divided in three types : inactive orbitals, lowest in energy and doubly occupied in all determinants, virtual orbitals, high in energy and unoccupied in all determinants and active orbitals with an intermediate character. The active electrons are the electrons not present in the inactive orbitals. In this method the CSFs are defined from all possible configurations of the electrons into the active orbitals. The CI method is variational but not size consistent. Another method useful in finding the correlation energy and not variational but size consistent is the many body perturbation theory, and its application in 1934 by C. Moller and M.S. Plesset[4] led to the Moller-Plesset perturbation theory (MPPT). In order to find the correlation energy for the ground state, the zero-order Hamiltonian is taken from the Fock operators in the Hartree-Fock SCF method and can be defined by the sum of all one electron Fock operators, while the total Hamil-

tonian H can be expressed as the sum of the zero order (ground state) and first order (excited state) Hamiltonians : In conclusion, the HF energy is given by the sum of the zero order and the first order energy correction :

$$E_{HF} = E_0^{(0)} + E_1^{(1)} \tag{1.14}$$

Perturbation theory is more efficient than CI, but is not variational. This fact means that at any particular order, the energy may be above or below the actual energy. Moreover, because the perturbation is not really small with inclusion of higher order perturbations, it is not guaranteed to converge.

1.0.4 Density Functional Theory

As seen in the previous methods, in order to obtain reasonably accurate electronic energies estimations, computationally expensive calculations have to be made. The HF approach which is a simpler method, suffers from errors correlated to the neglect of the correlation energy. An alternative to the HF approach, the DFT method, allows accurate results to be obtained with less computationally demanding calculations.[5,6]

The principal difference between DFT and the methods previously mentioned is that the main variable is not the wavefunction but is the electron density $\rho(r)$:

$$\rho(r) = N \int \cdots \int |\psi(X_1, X_2 \ldots X_N)|^2 dx_1 dx_2 \ldots dx_N \tag{1.15}$$

$\rho(r)$ at a defined point is the number of electrons per unit volume at that point. The concepts that make DFT possible are two theorems proved by Hohenberg and Kohn in 1964.[7] The first theorem shows that if the electronic density is known for a determinate system then all the properties of the ground state can be obtained. The second shows that for any ρ which may or may not be the true density for

the ground state, the relation $E_\rho \geq E_0$ is satisfied. E_0 is the energy of the ground state. The energy functional in DFT can be expressed as :

$$E[\rho] = T[\rho] + V_{en}[\rho] + V_{ee}[\rho] \tag{1.16}$$

In this equation, $T[\rho]$ accounts for the kinetic energy, and $V_{en}[\rho]$, $V_{ee}[\rho]$ represent the potential energy of the electron-nucleus and electron-electron interactions respectively. The latter can be further divided in two components as in the following equation :

$$V_{ee}[\rho] = V_{coul}[\rho] + V_{xc}[\rho] \tag{1.17}$$

where $V_{coul}[\rho]$ is the potential energy of the Coulomb interaction and $V_{xc}[\rho]$ is the exchange-correlation energy. Comparing the Hartree-Fock method with the DFT method, it is therefore possible to say that within the DFT method the correlation energy is included in the term $V_{xc}[\rho]$ together with the exchange potential, whereas in HF only the exchange part is accounted for. If $E[\rho]$ is known, finding the ground state energy can be achieved with a minimization problem thorough the iterative solution of the Kohn-Sham equations which is less computationally demanding and work in the same manner of the HF method. The Kohn-Sham equations are the following :

$$\hat{E}_{KS}\psi_i = \upsilon_i\psi_i \tag{1.18}$$

here $\hat{E}_{KS}$ is the one-electron Kohn-Sham operator. It is clear that ρ determines the ground state and any system with the same ρ as the real system will have the same ground state properties. The problem has been simplified via the KS equations introducing a set of non-interacting electrons which give the same ρ as the real system. If this approximation is made, the exchange-correlation term must contain all missing effects in terms of the wavefunctions of these non-interacting electrons. The electronic density could therefore be written as :

$$\rho(r) = \sum_{i=1}^{N_{orb}} |\psi_i(r)|^2 \tag{1.19}$$

The exchange-correlation potential V_{xc} has been explored in order to obtain more accurate results. The simplest approximation is the Local Density Approximation (LDA) that defines the exchange-correlation energy at a position r as the same as that of an uniform electron gas of density ρ, where ρ equals the local electron density at r in the actual system. The exchange-correlation potential $V_{exc}[\rho]$ can therefore be defined if the exchange-correlation energy is known as a function of the density, thus :

$$V_{exc}[\rho] = \int dr \rho(r) E_{exc}[\rho(r)] \tag{1.20}$$

When DFT is formulated for open-shell or in spin-polarization systems the electronic density is different for spin-up and spin-down electrons therefore the approximation is the Local Spin Density (LSD) instead of LDA. A more accurate treatment of the electron-density lies in the generalized gradient approximation (GGA)[8] in which the exchange-correlation energy depends also on the gradient of the electronic density in r. The most commonly used functionals are the Becke-Perdew (BP) functional, the Becke-Lee-Yang-Parr (BLYP)[9] functional and the Perdew-Burke-Ernzerhof (PBE) functional. Newer GGA functionals are the OLYP which is a combination of OPTX of Handy and Tozer and the Lee-Yang-Parr correlation functional, and the second is the Hamprecht-Cohen-Tozer-Handy functional (HCTH). In other widely used exchange-correlation functionals, a contribution from the exact exchange is present, for example the exchange energy calculated with the HF approximation. A functional of this type is the Becke3-Lee-Yang-Parr (B3LYP).

The application of LDA to molecules led to an initially poor reputation of the DFT method amongst chemists. The widespread adoption of this method occurred when GGAs were introduced, improving massively the situation. The DFT method is

developed only for obtaining ground state properties. However, DFT has been subject of several implementations in order to treat excited states, resulting in the following methods:

- restricted open shell Kohn-Sham (ROKS)
- the density functional theory/single configuration interaction (DFT/SCI)
- time-dependent density functional theory (TDDFT)

The second limitation of the DFT method is that its accuracy strongly depends on the quality of the exchange-correlation functional utilized. The DFT formalism is exact, although the exact form of the functional is currently unknown, which is different from semi-empirical methods because in such an approximation there must exist a V_{exc} potential that makes the results precise. In general, improvements of the outcomes of both DFT and HF calculations are related to the increase of the size of the basis sets and to the choice of the functional. Current improvements of the DFT method, as stated above, are for example the meta-GGA approach where some contribution is included in the xc potential that varies with the Laplacian of the density, or hybrid functionals where some orbital dependence is introduced and removes part of the self-interaction error that plagues normal DFT functionals.

1.0.5 Limitations of density functional theory

The exchange-correlation functional is the key to the success or failure of DFT. The exchange derives from antisimmetry due to the exclusion principle of Pauli and the correlation includes other many-body effects which need many determinants to be properly described. DFT normally leads to very significant errors because of the inadequacies of currently used approximate exchange-correlation functionals. The principal failures of DFT that depend also of the functional utilized are :

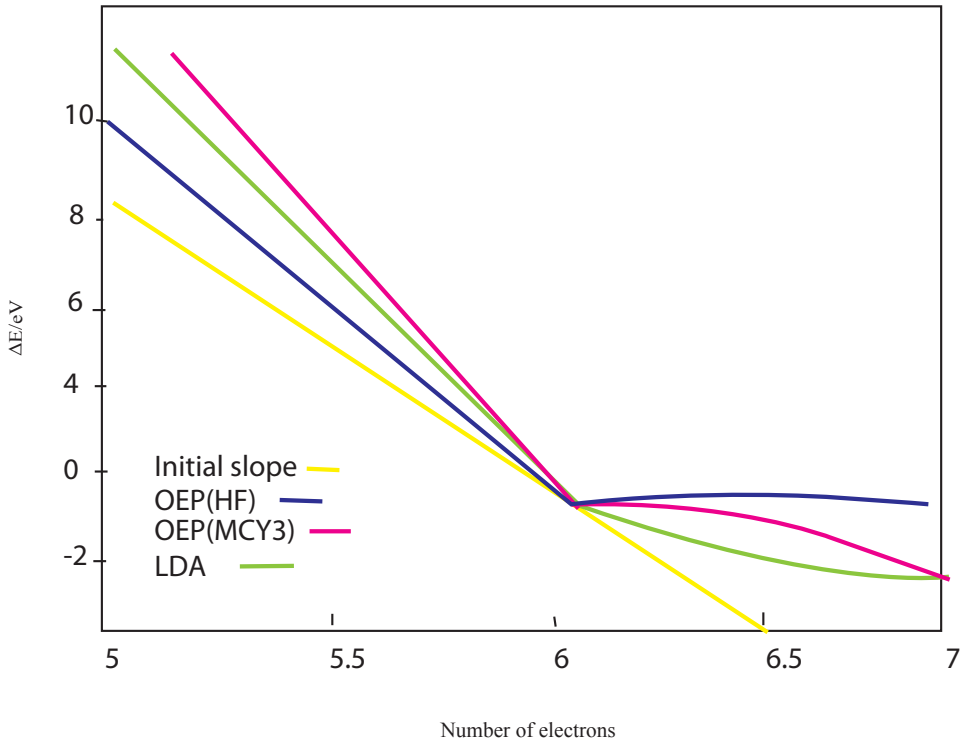

Figure 1.2: This diagram shows the energy difference of a carbon atom against the number of electrons calculated with different methods. The convex behaviour shown by pure DFT functionals such as the LDA leads to a delocalisation error; the concave behaviour shown by the Hartree-Fock approximation leads to a localisation error. The MCY3 functional lead to a better approximation with a closer behaviour to the exact.

- under- or overestimation of the barriers of chemical reactions
- band gaps of materials
- energies of dissociating molecular ions
- charge transfer excitation energies
- under- or overestimation of the binding energies of charge transfer complexes
- under- or overestimation of the response to an electric field in molecules and materials

These failures[10–12] are related to the delocalisation error in approximate functionals that spread the electron density artificially because of their dominating Coulombic term. Cohen et al.(2008)[13] explained the nature of the delocalisation error

considering the H_2^+ molecule. Chemical bonding is normally described well by functionals, but significant errors arise when the bond is stretched. At the dissociation limit the two H atoms share half electron each, with an energy that is too low. The delocalisation error of such functionals lead to an incorrect convex behaviour between the integers with a too low energy for fractional charges such as in the case described above. In general, pure DFT functionals such as the LDA approximation show a convex behaviour with therefore a significant delocalisation error that leads, for example, to the well known underestimation of the band gap. Functionals with incorrect concave behaviour such as the Hartree-Fock approximation have opposite characteristics showing a localisation error. Hybrid functionals contain concave and convex components with error cancellation in some cases (fig 1.2).

Failures in DFT functionals are present in transition metal chemistry where in situations of degeneracy or near-degeneracy a static correlation error arises. Cohen et al. show the presence of this error in the H_2 molecule dissociation limit where an H atom with half spin-up and half spin-down electron is present. The authors indicate a way to resolve this problem which is to impose the constancy condition on an approximate functional. This condition in fact requires that systems with fractional spins have energy equal to that of the normal-spin states (fig 1.3).

1.1 Basis sets

A spatial orbital $\psi_i(r)$ is a function of the position of a single electron i constructed in a way that the probability density of finding the electron in a position r is $|\psi_i|^2$.[14] Moreover, the spin of a electron can have two values which are "spin up" and "spin down" therefore every spatial orbital generates two spin orbitals. Any electron can be described by a single spin orbital. In order to solve the HF-SCF procedure it is necessary to define a spatial orbital in its mathematical form

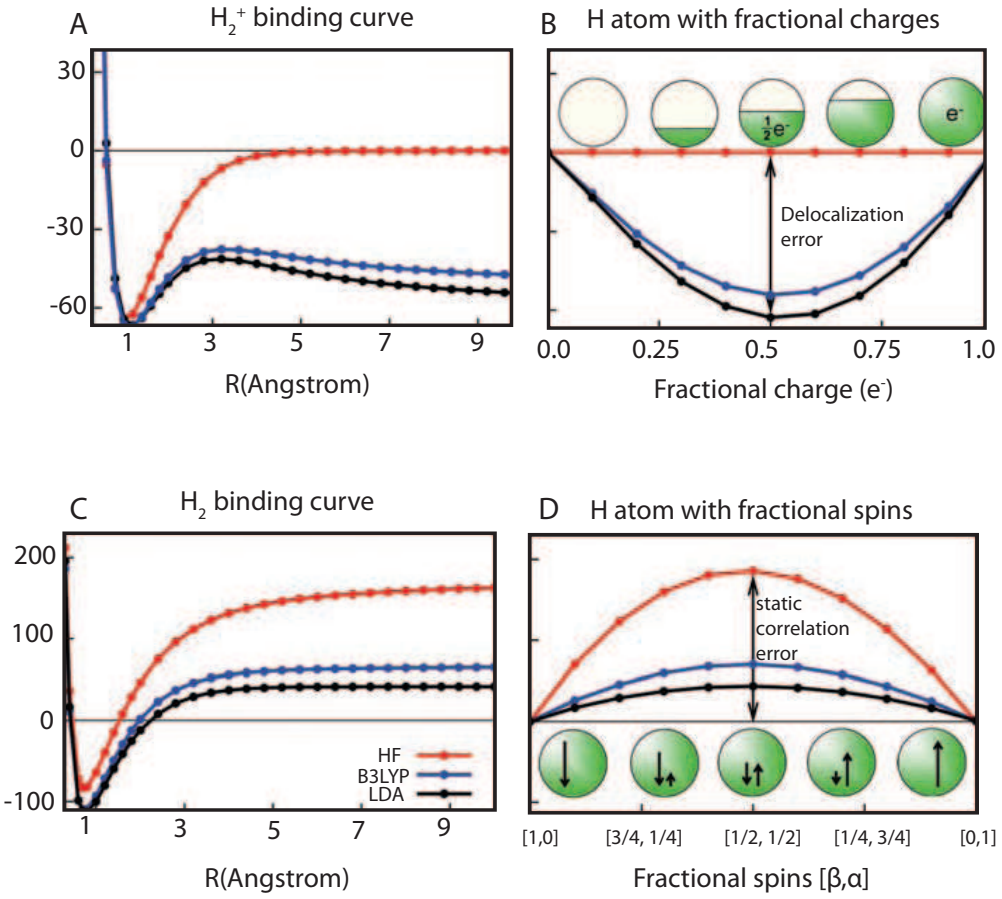

Figure 1.3: Dissociation curves of H_2^+ (A) and of H_2 (B) calculated with the HF, B3LYP, LDA approximations leading to a delocalisation error and a static correlation error respectively. Picture taken from Cohen et al. 2008.

which is achieved by introducing basis function. The basis functions are usually centered on the nuclei, when such functions are centered at different nuclei in a molecule, they are combined linearly and therefore the Linear Combination of Atomic Orbitals (LCAO) representation is defined. When a set of basis functions is chosen, the problem of finding the molecular orbitals reduces to finding the expansion coefficients. In general, increasing the size of the basis sets leads to an augmented accuracy, but the computational cost increases rapidly as the number of two-electron integrals needed for a basis set containing K functions ($O(K^4)$ or more), therefore, it is important to carefully choose the basis set. In general is possible to say that a basis function is the mathematical description of one atomic orbital, a molecular orbital therefore is given by the sum of several basis

functions. The Slater Type Orbitals (STOs) are basis functions inspired by the form of the analytical solution of the Schrödinger equation for the hydrogen atom. The normalised STO for a 1s orbital centered at R_A is expressed as :

$$\phi_{1s^{STO}} = \left(\frac{\zeta^3}{\pi}\right)^{\frac{1}{2}} e^{(-\zeta|r-R_A|)} \tag{1.21}$$

where ζ is the Slater orbital exponent. There are published values of the best Slater exponents for each atomic species which are used to avoid non-linearity problems. Within the vast majority of ab-initio methods, the integrals have to be computed in order to obtain the expectation values of the terms of the Hamiltonian. Those integrals do not have an analytical solution for STOs. The alternative is the use of Gaussian type orbitals (GTOs); the normalized GTO centered at RA is

$$\phi_{1s^{GTO}} = \left(\frac{2\alpha}{\pi}\right)^{\frac{3}{4}} e^{(-\alpha|r-R_A|^2)} \tag{1.22}$$

The major difference between GTOs and STOs is that the GTOs decay much faster when the distance increases and have value zero when $R_A = r$. In general STOs give better results than GTOs; it is very useful fitting the STOs using the GTOs therefore keeping the precision of the STOs with the lower computational cost associated with the GTOs. The basis functions obtained are called STO-NG where N is the number of Gaussians used to fit the STO. The STO-3G is given by

$$\phi_{1s}^{STO-3G} = d_1\phi_{1s}^{GTO}(\alpha_1) + d_2\phi_{1s}^{GTO}(\alpha_2) + d_3\phi_{1s}^{GTO}(\alpha_3) \tag{1.23}$$

where the d_i are the contraction coefficients. In a defined STO it is possible to find these coefficients and therefore the related Gaussian coefficients which give the best fit. Another way utilised to add more flexibility into the basis sets is to describe each atomic orbital with more than one basis function. Those orbitals are defined as multiple-zeta or split basis sets. Most of the chemistry is defined by the valence electrons, therefore, it is common to use split basis sets on them, with single STO-NG functions used for the core electrons. A basis set constructed

in this way is called a split valence basis set. Split valence basis sets are normally labeled by three numbers :

- one number which gives the GTOs employed to represent the STO for the core electrons
- two numbers which give the GTOs employed to represent the two STOs for the valence electrons

This treatment can be extended to multiple zeta basis for the valence electrons such as in the 6-311G basis which use STO-6G functions for the core electrons, one STO-3G and two GTOs for the valence electrons. The basis sets can be improved by addition of polarization and diffuse functions. Adding polarization means including the contribution from higher angular momentum orbitals and giving therefore more angular freedom with a consequent better description of bond angles. The polarization function is indicated by a star (*) symbol. In the case of the 6-31G*, called also 6-31G(d), basis set, this indicates that for the first and the second row atoms on the periodic table, the basis set is like the 6-31G but with an additional set of 3d GTOs. In the 6-31G** basis, or 6-31G(d,p), p-type GTOs for hydrogen atoms are included. Diffuse functions that are additional GTOs with smaller exponents can be included and are indicated with the symbol "+" or "++". When "+" is used this means that a set of s and p functions are added on the heavy atoms while "++" is used when an additional set of s-diffuse GTOs are included for the hydrogen atoms. Other common basis sets in use are the correlation-consistent basis sets of Dunning (cc) which are designed to recover the correlation energy of the valence electrons. Their acronyms are : cc-pVDZ, cc-pVTZ, cc-pVQZ, cc-pV5Z and cc-pV6Z (the last of these in words is correlation-consistent Polarized Valence Sextuple Zeta). These basis sets are called correlation-consistent because the functions which contribute similar amounts of correlation energy are included at the same stage independently of the function

type. The prefix aug, if used in those basis sets, indicates the presence of diffuse functions.[14]

The Effective Core Potential basis sets have been developed for systems from the third or higher row of the periodic table where there is a large number of core electrons which usually are unimportant, chemically speaking. The core electrons are treated by a suitable function and the valence electrons are modelled explicitly. The most popular pseudopotentials in use are the Los Alamos National Laboratory or LANL ECPs developed by Hay and Wadt, the ECPs developed by Stevens and the Stuttgart-Dresden pseudopotentials developed by Dolg and co-workers.

1.2 The Time Dependent Density Functional Theory method

The Time Dependent Density Functional Theory method (TDDFT) utilizes the principles of solving time dependent problems. In TDDFT a series of time-dependent Kohn and Sham (TDKS) equations are defined in which N non-interacting electrons evolve to an effective potential $v_s(rt)$ but have as result a $\rho(r,t)$ equal to the interacting system of interest. Thus, the many body Schrödinger equation is replaced by a set of time dependent single particle equations in which the orbitals own the same time-dependent density $\rho(r,t)$. The TDDFT method can be used to predict different phenomena which can be distinguished in

- non perturbative regime : systems in intense laser fields. Currently solving the full time-dependent Schrödinger equation of two interacting electrons is almost impossible and because in those fields interactions between electrons are important, this method in such cases reveal its usefulness.

- the linear response to a spatially uniform electric field, which finds great applications in chemistry. The TDDFT method leads to predictions of posi-

tions and intensities of electronic excitations.

Most of the applications of the TDDFT method are within the linear response regime, for example in inorganic chemistry, the optical response of transition metal complexes.[15,16] In organic chemistry, a review can be seen in chapter 2. Other areas of application are

- electronic excitations
- solvation
- electronic and magnetic circular dicroism

Currently, the TDDFT method is still in development when compared with the ground state method and its capabilities are still being explored. Thus, the method is likely to find new applications than those mentioned above in the near future. The TDDFT method, however, presents several sources of error that are :

- errors correlated to the ground state. If the orbital energies are wrong, further corrections with the TDDFT method cannot result in accurate predictions.
- errors correlated to local approximations,
- neglect of phenomena when the adiabatic approximation is made in properties which require nonlocality in time,
- errors on the wavefunction : the solution of the TDKS equations results in the TDKS non interacting wavefunction which can differ dramatically from the true wavefunction.

Other phenomena can be studied with the TDDFT method, even only within the linear response regime, which are : double excitations, second ionization thresholds, transport through single molecules, optical response of solids, band gaps in

solids. If the TDDFT method is combined with the fluctuation-dissipation theorem, it results in predictions on Van der Waals forces and bond breaking with symmetry problems. In the non perturbative regimes there are phenomena to be explored like : high multiphoton ionization, harmonic generation, above-threshold ionization, quantum nuclear motion, quantum control.[15,17]

1.2.1 The Kohn-Sham scheme and the solution of the Time dependent Schrödinger equation

The Time Dependent Schrödinger equation expresses one of the most fundamental postulates of quantum mechanics and an important discovery of physics of the 20th century.

$$i\frac{\partial}{\partial t}\psi(r,t) = \hat{H}(r,t)\psi(r,t) \tag{1.24}$$

The Hamiltonian can be written in the following form :

$$\hat{T}(r) + \hat{W}(r) + \hat{V}_{ext}(r,t) \tag{1.25}$$

The first term is the kinetic energy of the electrons, the second expresses the Coulombic repulsion between the electrons and the third is the time dependent potential experienced by the electrons. The Hamiltonian describes physical and chemical situations in which arbitrary time-dependent electric or magnetic fields are present. The many body Schrödinger equation has been solved only for very small systems because of its comple ity, therefore over the years, methods have been developed in which the basic equations are transformed with approximations to a manageable form, one such method is the TDDFT method.

The Hoheberg-Kohn theorem states that from the density which is a property of the quantum mechanical system, it is possible to obtain the external potential.

The wavefuction determines every observable of the system which implies that *every observable can be written as a functional of the density.* The time dependent extension of the Hoheberg-Kohn theorem is defined through the Runge-Gross theorem. Within a time dependent system, in which the Runge-Gross theorem has been developed, there are several differences when compared to the static environment. One difference is that in time dependent systems, there is not a variational principle on the basis of the total energy. The energy in static systems, therefore, is replaced by the quantum mechanical action. Moreover, a time dependent problem is an initial value problem, thus, the wavefunction, or the density, depends on the initial state, therefore the Runge-Gross theorem holds for a fixed initial state. In conclusion the differences between time dependent and time independent systems are underlined by the Schrödinger equation which is in the form of a first order partial differential equation in the time dependent environment, and of a second order in the time independent. The Runge-Gross theorem[18] states that all observables can be defined by knowledge of the one-body density. Kohn and Sham had the idea, instead of calculating the interacting Schrödinger equation, of introducing an auxiliary non interacting system subject to an external local potential in which the density of the Kohn-Sham electrons is the same as the interacting system. The Kohn-Sham electrons within the time dependent case obey the time dependent Schrödinger equation :

$$i\frac{\partial}{\partial t}\psi(r,t) = \left[-\frac{\nabla^2}{2} + \upsilon_{ks}(r,t)\right]\psi(r,t) \tag{1.26}$$

The Kohn-Sham orbitals give the density of the interacting system :

$$n(r,t) = \sum_{i}^{occ} |\psi_i(r,t)|^2 \tag{1.27}$$

The Kohn-Sham potential is divided into the following parts :

$$\upsilon_{ks}(r,t) = \upsilon_{ext}(r,t) + \upsilon_{Hartree}(r,t) + \upsilon_{xc}(r,t) \tag{1.28}$$

The first term is the external potential, the second is the Hartree potential which includes the classical electrostatic interaction between the electrons, and the last term accounts for all non-trivial many body effects. The solution of the time-dependent KS equations gives the time-dependent electron density, from which the dynamic polarizability $\alpha(\upsilon)$ is obtained. This quantity can be expanded in terms of energies of the electronic transitions n and the corresponding oscillator strengths f_n

$$\alpha(\upsilon) = \frac{4\pi^2 e^2}{m_e} \sum_n \frac{f_n}{(E_n - E_0)^2 - E^2} \tag{1.29}$$

In this equation, E_0 and E_n are the energies of the ground and the nth electronic excited state. The transition energies E_n-E_0 are the poles of the frequency dependent polarizability, they can be discontinuities of this function which occur every time the incident light energy equals the excitation energy. Description of excited states through TD-DFT can be accomplished through constructing Slater determinants from ground state KS orbitals replacing one KS spin orbital which is occupied in the ground state with a virtual one and defining a linear combination of them. This method therefore allows each electronic transition T to be represented by a linear combination of one electron excitations between pairs of ground state KS orbitals ϕ_i ϕ_j :

$$\sum_{i<j} c_{ijT}(\phi_i \rightarrow \phi_j) \tag{1.30}$$

The square of the expansion coefficient c_{ijT} specifies the contribution of the one electron excitation from the orbital ϕ_i to the virtual orbital ϕ_j , usually expressed as a fraction of 1 or as percentage. Within this method it is possible to visualize electronic transitions by comparison of the shapes of the initial and final optical orbitals, but it often happens that the electronic transitions affect many electrons in a molecule and the corresponding expansion contains many one-electron excitations with a similar weight therefore causing problems on the orbital picture. The natural transition orbitals which are constructed by an unitary transformation of

the whole set of the occupied and virtual KS orbitals allow this problem to be overcome. Moreover, it is possible to describe excited states by differences of electron densities, calculated by subtracting the excited and ground state electron densities. The electron density subtraction representation shows regions of increased and decreased electron population. In charge transfer excitations in which areas in which the electron density increases are separated from where it decreases, such plots are very useful. However, there is also the opposite situation than the charge transfer case where the excitation is highly localised in the same region of space due to constructive and destructive additions where the density difference is not very clear.

1.3 Modelling the solvent effect in chemical reactions

The microscopic description of solvation is possible with molecular dynamics (MD) or Monte Carlo (MC) simulations. In those methods the solvent molecules are represented explicitly, thus simulations are computationally demanding. Over the last 30 years lots of effort have been put in order to replace the explicit molecules with a structureless dielectric medium. With parameterizations such as the choice of the atomic radii, the implicit solvent models can describe correctly the effect of solvent molecules on structure and energetics of the solute. However, the first solvation shell creates effects difficult to be mimicked by a continuum model which are for example: the nonlinear response of the solvent when the solute is highly charged, the dispersion and hydrogen bonding interactions between solute and solvent, and the hydrophobic effect. In order to overcome such problems it is possible to utilise two different approaches: the supermolecule and the solute-solvent cluster.[19] In these treatments of the solvent effect, a number of solvent molecules are included explicitly to represent the first several solvation shells and the rest

of the solvent molecules are mimicked by a dielectric continuum. The treatment of the solvent with the approaches previously mentioned, can suffer from several limitations if the solute is highly charged or if solute properties sensitive to the enviroment such as nuclear magnetic resonance or absorption spectra are calculated. When the solute is a macromolecule such as an enzyme, hybrid quantum mechanical/molecular mechanical (QM/MM) methods can be utilised to describe solute and solvent molecules.[20]

"Solvent effect" can be defined as the changes experienced by a chemical system (the solute) upon transfer from the gas phase to a diluite solution.[21] The changes experienced by the solute affect its molecular structure, both nuclear and electronic, and the thermodynamics and kinetics of chemical processes. Analysing the first type of effect, changes in the nuclear configuration may be triggered by the tendency of polar solvents to stabilise structures with large charge separation such as the destabilization of conformations with intramolecular hydrogen bonds in polar solvents. The electronic distribution for a given nuclear configuration regulates the chemical reactivity, with effect on properties such as molecular electrostatic potential, molecular volume and spectroscopic properties. The solvent polarizing effect on neutral solutes is very large in aqueous solution with an increase of their dipole moment by 20-30%, while in apolar solvents such as chloroform, the polarizazion effect increases their dipole by 8-10%. The modulation effect of the solvent on chemical reactivity is very important in water where the free energy change for a chemical reaction in gas phase (GPH) can have its sign inverted. The solvent has three main types of modulation on the chemical reactivity which are :

- regulation of the intrinsic reactive characteristics of reactants,
- the introduction of viscosity effects,
- the differential stabilization of reactants, products and transition states mod-

ulated by the solvent.

The regulation of the intrinsic reactive characteristics of reactants is principally connected to the polarization of the solute charge distribution. The viscosity effects fine-tune the dynamics of the molecular system which is important when the solvent molecules are large and have low mobility or when the energy barrier is small, rather than when the solvent molecules are small and mobile with high intrinsic energy barriers. The last solvent reactivity factor is important in solvents where hydrogen bonds can be established with the reactive species leading to changes in their relative stabilities. The largest effect of the solvent on chemical interactions is expected when the polarities of reactants, transition state or products are very different and when the number of specific solute-solvent interactions, such as the number of hydrogen bond donors and acceptors, changes during the interaction. Polar solvents affect ion-molecule interactions, an important example is the nucleophilic attack of a hydroxyl group to a carbonyl center. This reaction is very exothermic and does not have an activation barrier in GPH, but is endothermic in aqueous solution with the activation barrier primarily related to the enhanced solvation of the reactants rather than TS (Transition State) and products.

1.4 Modeling the solvent as a dielectric continuum

Implicit solvation which treats the solvent as a dielectric continuum starts with the creation of a cavity inside the polarizable continuum, to contain the solute molecule. There is an energy pay off for building the cavity (ΔG_{cav}) caused by removal of solvent-solvent interactions after the solute is placed within the cavity, resulting in electrostatic ΔG_{elec} and non-electrostatic $\Delta G_{non-elec}$ interactions between solute and polarizable medium. In simple words, the solute induces a po-

larization of the dielectric continuum which afterwards generates a reaction field that polarizes the solute back. The energetic cost of polarizing the solvent and the solute is taken into account within the ΔG_{elec} term. Within the non electrostatic interactions, the main contribution to $\Delta G_{non-elec}$ is given by dispersion forces. The expression for the total solvation energy is given by the following equation :

$$\Delta G_{solvation} = \Delta G_{elec} + \Delta G_{non-elec} + \Delta G_{cav} \tag{1.31}$$

The electrostatic component is usually the dominant contribution to the solvation free energy.[22] The electrostatic term is obtained in different ways depending on the model utilised. The polarizable continuum model (PCM)[19] and the COSMO model[23] for obtaining the solute charge distribution and the solvent reaction field term, solve the Poisson equation corresponding to the solute charge distribution immersed in a continuum medium by using the apparent surface charge distribution on the cavity surface. The Poisson equation describes the electrostatics of a dielectric medium with embedded charged species :

$$4\pi\upsilon\sigma(r_s) = (\upsilon - 1)F(r_s) \tag{1.32}$$

In this equation $F(r_s)$ and $\rho(r_s)$ are the electric field perpendicular to the cavity and the charge density at point r on the surface of the cavity. When the Poisson-Boltzman equation is solved,[24] the electrostatic free energy G_p is combined with the GPH Hamiltonian H_0 to produce a non-linear Schrödinger equation which is :

$$(H_0 + 2G_p)\psi = E\psi \tag{1.33}$$

here, ψ is the solute wavefunction, and the term G_p is multiplied by 2 because it depends on the square of the wavefunction ($\psi * \psi$) and the variational treatment of the above equation leads to :

$$E_s \equiv \langle\psi|H_0 + 2G_p|\psi\rangle \tag{1.34}$$

Normally, the solute is treated by the HF and DFT methods in which the electrons move in the self-consistent field (SCF) of the others. The iterative solution of this

equation is called the Self Consistent Reaction Field method (SCRF).[25] However, the SCRF method takes into account only the physical effect of the insertion of the solute in a solvent, therefore all the other physical effects are neglected. Effects neglected are the electron correlation between the solute and the solvent which is manifest in the existence of dispersion interactions between solvent and solute, the cavitation effect, the hydrophobic effect (when a non polar solute is dissolved in water), and the dielectric saturation effect which is the breakdown of the linear response in the region near the solute. All these effects are very enhanced on the first solvation shell. Several options are available based on models which treat differently :

- the electrostatic interaction between the solvent and the solute which can utilize a numerical or analytical solution of the classical electrostatic problem (Poisson equation) (PCM), a model solution of the electrostatic problem like in the Generalized Born Approximation (SMx) or in the conductor like screening solvent model (COSMO), or are treated empirically without the solute reference.[19,26]

- the shape for the boundary between the solvent treated as a continuum and the solute, formed by taking in account the molecular shape, treating the solute as an ellipsoid or as a sphere.[19]

- the level to which the solute is treated, which is usually with polarizable charges obtained in different ways : by an approximate QM method with inclusion of the electron correlation or with a class IV charge model, by ab-initio HF method, by semiempirical MO theory, or by combination of the previous methods. Non polarizable charges could be used in MM calculations.[27]

- the non electrostatic interactions, which can be added by inclusion of empirical elements, treating one or more non-electrostatic interactions non-

empirically, by a single linear function of molecular surface area.[27]

One of the most widely used methods is the PCM which is implemented in Gaussian 03,[28] originally developed by Miertus Scrocco and Tomasi[19] several years ago and which has undergone several developments since. The most recent model utilises the integral equation formalism and is called IEF-PCM. Although the PCM model is very good, the extent of its use is largely related to the fact that it is implemented in Gaussian, as noted by Cramer.[29] " What is driving the train is that people use what is in the code that they bought. To the extent that PCM is a very successful solvation model, it is in part because it is in Gaussian. The SMX models sadly have never been available in Gaussian ". The PCM method[19] collects together all non-electrostatic interactions in one term called ΔG_{CDS} which is expressed in the following equation :

$$\Delta G_{CDS} = \sum_k A_k \sigma_k \tag{1.35}$$

In this equation, A_k is the exposed solvent accessible surface area of the atom k, and σ_k is the "surface tension" of the atom K. the σ_k values are empirical and are fitted to the experimental ones. This fitting procedure can have large errors especially where there are not large numbers of experimental measurements such as in non aqueous solvents.

The SMx (x= 1 to 8) range of models developed by Cramer and Truhlar employ the Generalised Born model with scaled atomic charges[30] for the treatment of the electrostatic interactions with the use of an interlocking spheres cavity. In these models the non-electrostatic interactions are introduced in order to describe more accurately the solvation in non aqueous solvents. The surface tensions are expressed the following equation :

$$\sigma_k = \sum_j \Gamma_j \eta_k^{\Gamma_k} \tag{1.36}$$

Here, the values $\eta_k^{\Gamma_k}$ are fitted to a number of solvent properties Γ_j, including hydrogen bonding acidity and basicity, refraction index, surface tension. Cramer

and Truhlar recently (2008) developed the latest model of the SMx series (SM8).[26] SM8 is an universal model which means that it can be applied to any phase that may be characterized by the previously mentioned empirical parameters which are components of the G_{CDS} term. The most recent SMx models have been applied successfully to a wide variety of problems such as the prediction of soil/water partition coefficients, which are of environmental importance, or the description of the two dimensional phase that is the air-water interface.[26] For this biphasic system the non-electrostatic parameters have been determined. The water in the SMx models[31] is taken to be a special case with its own parameters where the ΔG_{elec} and $\Delta G_{non-elec}$ terms are calculated with an algorithm specifically developed. The SM8 model extends also the aqueous parametrization from the previous SMx to temperatures other than 298K.

1.5 Theory of solvent effects on the UV-vis Absorption spectra

Interpreting the absorption spectra shifts caused by the solvent can be possible if the following issues are considered :

- The Franck-Condon principle which states that since the time utilised by a molecule to execute a vibration (about 10^{-12}s) is longer than that required for an electronic transition (about 10^{-15}s), the nuclei of the solute do not change their position during the transition. Thus when the excited state is formed, the solute in its excited state is surrounded by a solvent cage which temporarily has the same characteristics of a solvent cage that surrounds the solute in its ground state. The equilibrium is subsequently achieved by a relaxation process. The energy of the Franck-Condon excited state solute and its solvent cage is greater than when the equilibrium is achieved.

- the variations of the dipole moment of the solute caused by the solvent
- the temporary transition dipole moment present during the absorption
- differences in permanent dipole moment between the ground and the excited state of the solute

There are four situations related to the nature of the solute and the solvent: The first is when a nonpolar solute is solvated by a nonpolar solvent. Here only dispersion forces are active and cause a small bathochromic shift whose magnitude is proportional to the transition intensity, the solvent refractive index n, and the size of the molecule of solute.

The second is when a nonpolar solute is immersed in a polar solvent. If the solute does not have dipole moment, the solvent molecules are not oriented in any particular way around the solute molecules. In general, a red shift should occur in this case, which depends on the solvent refractive index.

The third is when a dipolar solute is immersed in a nonpolar solvent. The interactions that occur are dipole-induced dipole and dispersion forces. If during the electronic transition, the dipole moment increases, the Franck-Condon excited state is more solvated by dipole-solvent polarization. A red shift should occur in this case. If the dipole moment decreases during the electronic transition, the Franck-Condon excited states are less solvated and a blue shift should take place.

The fourth case is when a dipolar solute is in a polar solvent. The forces in solution which stabilise the solute ground state are of dipole-dipole type and the solvent cage is oriented around the solute resulting in its ground state stabilisation. If the solute dipole moment in the ground state increases when the electronic transition occurs, the excited state is surrounded by partly oriented solvent dipoles. If the solvent polarity increases there will be a bathochromic shift, resulting from an increased stabilisation of the excited state with respect to the ground state. If the solute dipole moment decreases during the transition, there will be a hypochromic

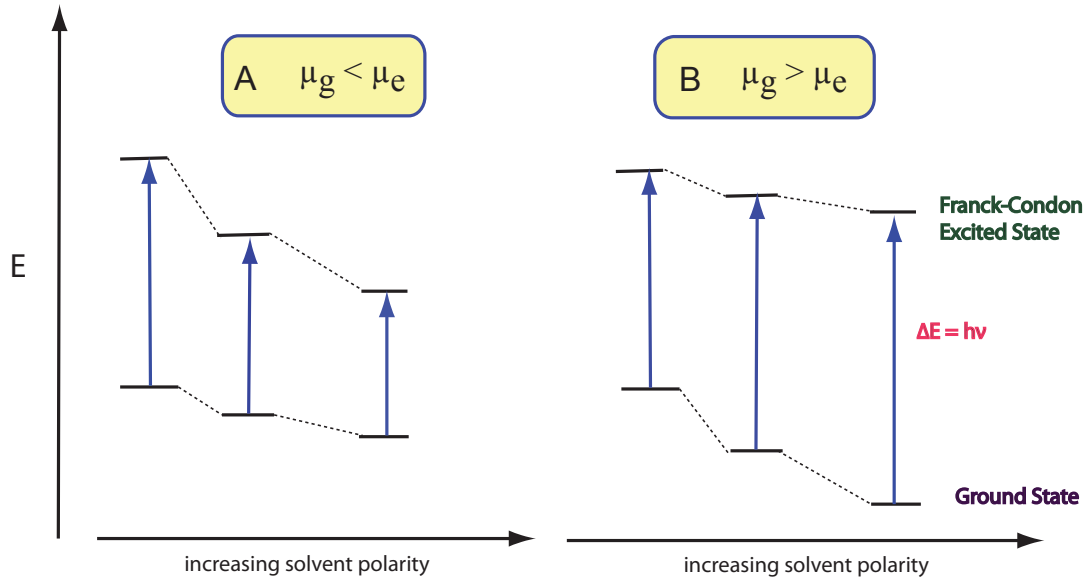

Figure 1.4: A : If the dipole moment of the ground state is lower than the excited state, then, increasing the polarity of the solvent the excited state is more stabilised than the ground state. B: If the dipole moment of the ground state is higher than the excited state, then, increasing the polarity of the solvent the ground state is more stabilised than the excited state.

shift when the solvent polarity increases because the energy of the ground state is lowered more than that of the excited state due to the fact that the solvent cage does not effectively stabilise the excited state (fig. 1.4).

1.5.1 Fluorescence and solvent effect

Fluorescence occurs when there is an emission of photons in a system that pass from an electronic excited state S_1 to the ground state S_0. The $0 \rightarrow 0$ transition normally is the same for absorption and fluorescence. Stokes' rule expresses that the fluorescence maximum is situated at lower wavenumbers than the absorption maximum due of loss of energy caused by vibrational relaxation phenomena. The gap between the maximum of the first absorption band and the fluorescence band is termed the Stokes shift. This shift is important because it gives information on the excited state. If the dipole moment of a fluorescent molecule is larger in the excited state (μ_e) than in the ground state ($\mu_e \gg \mu_g$), this means that a differ-

ential solvation leading to greater stabilisation of the excited state creates a red shift. This shift is increased in its magnitude when the solute-solvent interaction increases, thus lowering the energy of the excited state. The solvent effect on the emission bands can be investigated through the finite relaxation time τ_R for the rearrangement of the solvent around the solute in the excited state and the finite lifetime τ_e of the molecule in the excited state. In general :

- $\star$ in liquid solutions $\tau_R \ll \tau_e$ because τ_R is of order between 10^{-12} and 10^{-10} s at room temperature while τ_e is of order 10^{-8} s and the reorientation of the solvent molecules can occur after electronic excitation, resulting in a relaxed excited state where another solvation equilibrium has been defined.

- $\star$ in solid solutions $\tau_R \gg \tau_e$, since the promotion of an electron to the anti-bonding molecular orbital upon excitation takes about 10^{-15} s which is fast when compared to the molecular vibrations that are between 10^{-10} and 10^{-12} s. The emission will thus take place before any rearrangement of the solvent molecules in the solvation shell (fig.1.5).

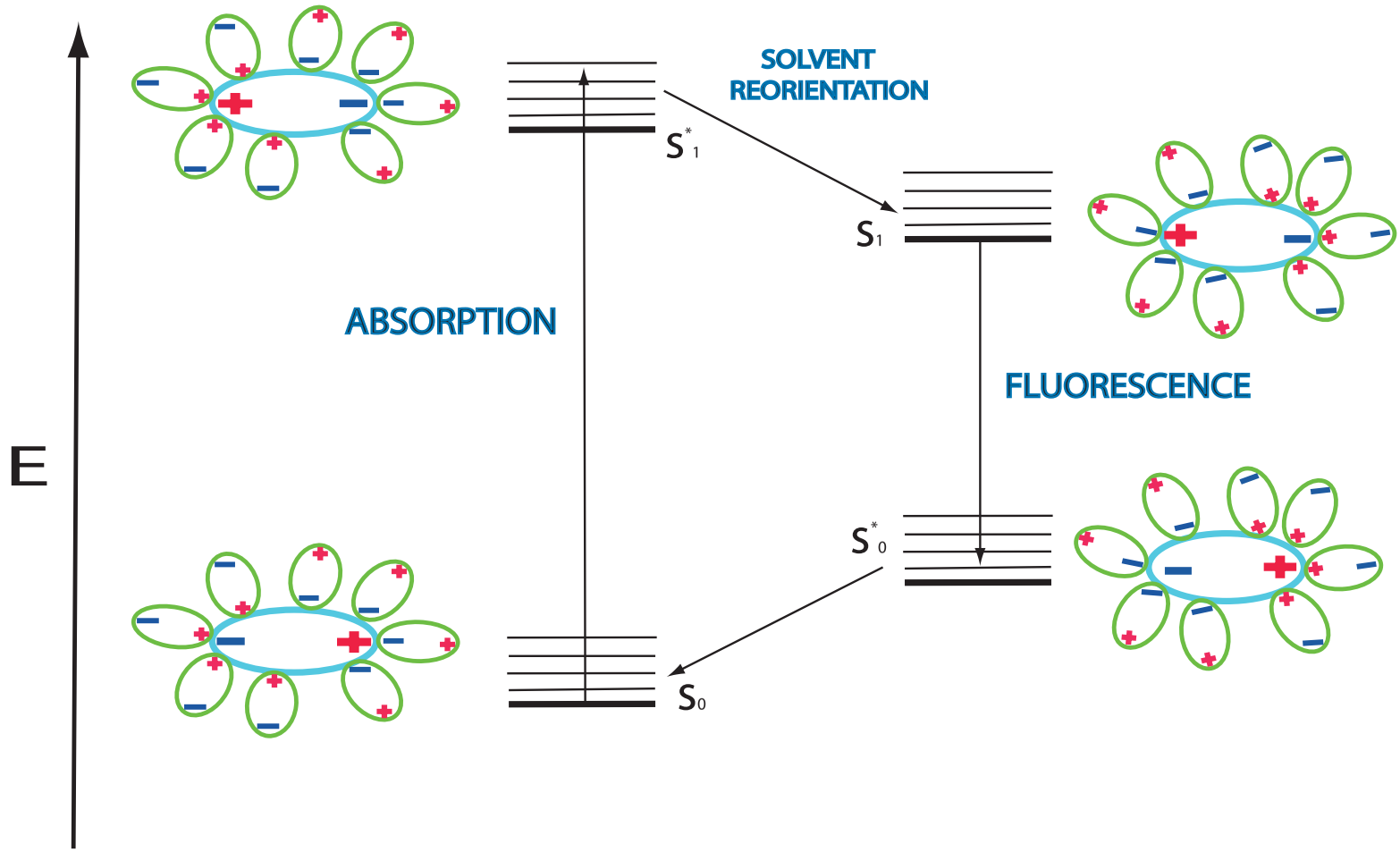

Figure 1.5: Schematic representation of the solvent effect on the fluorescence mechanism

1.6 Modelling excited states with the inclusion of continuum models

The solute-solvent interactions stabilize in a different way the ground and the excited state of a solute when it is immersed in a solvent. Thus, describing accurately the formation of the excited state and the relaxation of molecules in solution is a step toward a proper characterization of such interactions with consequent better predictions of experimental data.

It is well known that when the nature of the solvent changes, there are solvatochromic shifts on absorption or emission bands.[32] Those shifts are caused by changes within the solvation energy, and they have been used to build empirical scales for different solvents. Betaine dyes present a very strong solvatochromism demonstrated by the fact that when these compounds are in their ground state they are zwitterions, while in their excited state an electron transfer goes in the direction of canceling the charge separation. Thus, the ground state dipole moment from a high value becomes almost zero in the excited state as a result of changed solute-solvent interactions. Kamlett et al[33] proposed, in order to quantify the polarity effects, the following equation :

$$\nu = \nu^0 + s\pi^* + a\alpha + b\beta \tag{1.37}$$

here, ν and ν^0 are the wavenumbers of the band maxima in the solvent of interest and in the solvent of reference respectively. π^* is a measure of the polarity/polarizability effects of the solvent, α and β are the hydrogen bond acidity and basicity indexes of donor and acceptor respectively. This equation clearly indicates that when modeling the solvent effect on the excitation energies, the two main phenomena to consider are :

- polarity and polarizability effects
- hydrogen bonding

An example of variation of the hydrogen bonding upon excitation is on the $n \rightarrow \pi^*$ transitions in solutes with carbonyl or amide chromophores in protic solvents. After excitation the electronic density on the heteroatom decreases resulting in its decreased capability to form hydrogen bonds. A blue shift on the absorption spectrum is expected which increases upon increases of the strength of the hydrogen bond. Such phenomena can be useful in order to assign an $n \rightarrow \pi^*$ band and the spectral shift can be used to determine the strength of the hydrogen bond. The fluorescence spectrum, in contrast is less influenced by the hydrogen bonding. The solute in its excited state does not interact with the solvent significantly due to the breaking of the hydrogen bonds, with therefore an emission spectrum caused only by the solute without interactions. Hydrogen bonding can, however, be important in the $\pi \rightarrow \pi^*$ transitions. In this case, in the excited state, the electron density is more localised on the heteroatom (increase of its basicity) with an increase of its capability to form hydrogen bonds. The excited state in this case is more strongly hydrogen bonded than the ground state, thus, the emission spectrum is more sensitive to hydrogen bonding than the absorption spectrum. Hydrogen bonding therefore play a key role in defining specific characteristics of the absorption or emission spectra in several types of molecules. Hydrogen bonding must thus be carefully considered in many cases, also taking in consideration the first solvation shell. In order to take in consideration the first solvation shell it is necessary to adopt the supermolecule approach where the excitation energies are computed on clusters of solutes with several molecules of solvent. The solvent molecules considered are those that interact with hydrogen bond accepting and donating sites in the solute. However the supermolecule approach is still incomplete and a better agreement with the experimental data is found only when a continuum model is added on top of the aggregate of the solute and the solvent molecules. This improved agreement can be explained by the fact that with the inclusion of a continuum model are added the electrostatic long range interaction

that are missing in the supermolecule approach.

Polarity effects manifest with the non-equilibrium solvation.[34,35] When there is a sudden change of the solute state such as in a vertical electronic transition, it is possible to assume a Franck-Condon like response of the solvent exactly as for the solute molecule. The nuclear motions of the solvent will not be able to follow the fast changes in the solute electronic charge distribution. The polarization therefore can be divided into two components as follows[36] :

$$P = P^{fast} + P^{slow} \tag{1.38}$$

Here, fast indicates the part of the solvent response that always follows the dynamics of the process which in a vertical transition is the response of the solvent electrons, while slow refers to the remaining terms, normally related to the various nuclear degrees of freedom of the solvent. (fig.1.6).

Caricato et al.[37,38] developed a method that represents the time dependent evolution of the solvent polarization that follows the transition between two different electronic states in the solute. In this method the implementation of analytical derivatives in the TDDFT method is utilised to calculate the variation of the electron-density of the solute caused by an electronic transition and the related change in the solvent reaction field. In this method, called Time Dependent Polarizable Continuum Model (TDPCM), the complete evolution of an electronic excitation in the solute from the vertical transition in a system at the equilibrium and then going back to the ground state can be taken into account. The entire process can be divided into six steps which are :

1. electronic excitation of the solute : the solute and the solvent are in a non-equilibrium situation and the solvent is not entirely equilibrated with the electron-density of the solute in its excited state.

2. relaxation of the solvent to a new equilibrium, while the solute continues to have the ground state geometry in its excited state

3. relaxation of the solute geometry to a new equilibrium with the solvent

4. emission from the solute which returns to the ground state and the solvent is again not equilibrated with the solute

5. relaxation of the solvent to a new equilibrium with the solute in its excited state geometry

6. solute and solvent relax to the initial state of equilibrium

In this model the relaxation processes of solute and solvent are decoupled. The TDPCM method allows not only the changes in the energies of the electronic states to be studied but also the evaluation of the evolution of the solute properties. One property that can be studied is the evolution with time of the Mulliken charges for both the excited and the ground state.

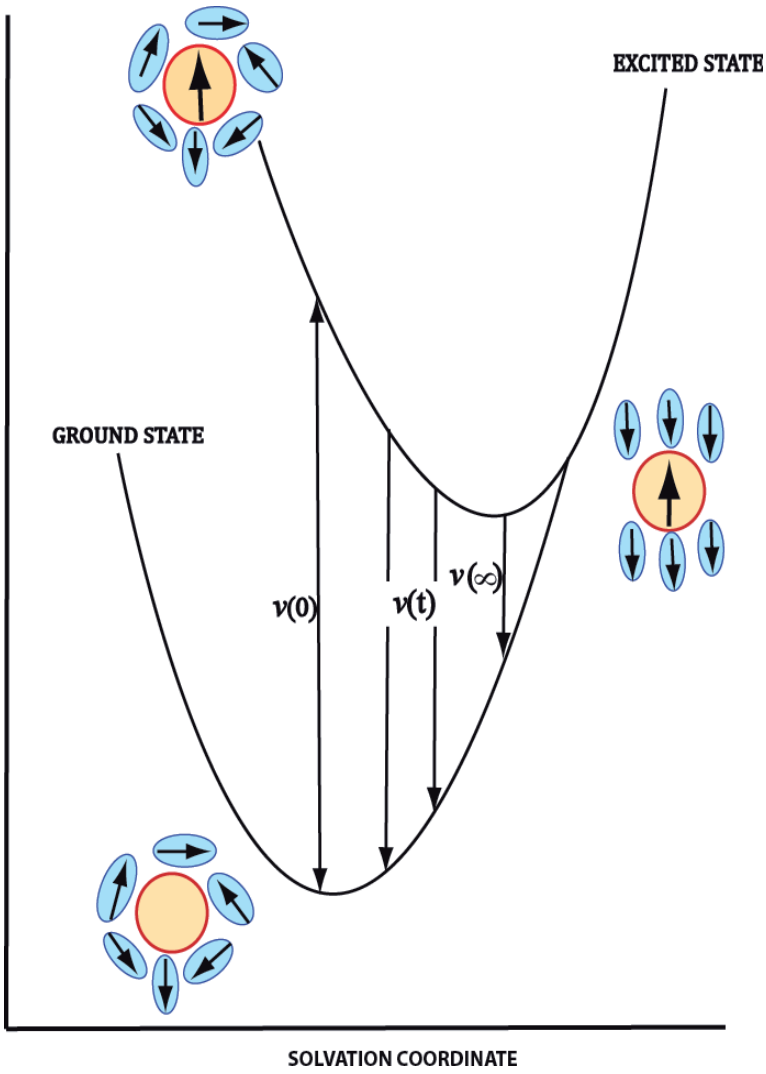

Figure 1.6: Time evolution analysis of a solvated system from the ground state to the excited state implemented in the TDPCM method.

2

Cyclizations in the Dihydro-Imidazo-Phenanthridinium synthesis reaction path

2.1 Baldwin's rules of ring closure

Jack E. Baldwin (1976)[39,40] formulated a series of rules that empirically determine if a particular cyclization reaction mode is allowed. The foundations of these rules lie in the configuration of the tetrahedral centre constituted by a carbon atom that during chemical reactions undergoes a structural transformation. (fig.2.1) Basically two main groups of reactions can be defined in which a carbon atom is a central atom :

- The nucleophilic substitution S_N2 reactions, of which an example is the Walden inversion leading to a five coordinate bipyramidal centre transition state,
- Nucleophilic or electrophilic addition/elimination reactions.

The dynamics of the S_N2 reactions are well known, where for instance an anion attacks the backside of the reacting centre displacing the leaving group. New insights about that mechanism are given by J Mikosch et al (2008).[41] This author, studying the dynamics of the substitution of a chloride anion on iodomethane found that for lower collision energies the mechanism was the well known mechanism,

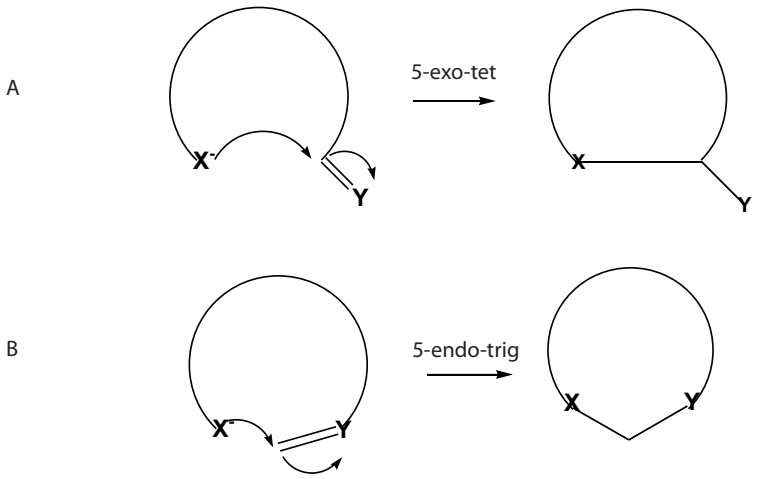

Figure 2.1: Cyclization closure modes

whereas for higher collision energies a more roundabout mechanism was found. In the principal mode of this later mechanism, the chloride anion strikes the side of the CH_3 group, causing it to rotate around the more massive I atom. Then after one CH_3 revolution, the chloride anion attacks the backside of the carbon atom displacing the iodine atom.(fig.2.2)

The second type of reaction is exemplified by the nucleophilic or electrophilic addition/elimination involving a trigonal-tetrahedral interconversion at the central carbon atom. B*ü*rgi and Dunitz (1974)[42] studied the trigonal-tetrahedral interconversion at a carbonyl centre. Using crystallographic and quantum mechanical studies they proposed an answer to the question : How do the bonds and angles in a molecule change as it moves along the reaction path? The trigonal carbonyl carbon acts as an acceptor for electron rich nucleophilic reagents that add to the carbon atom. The authors describe the generally accepted mechanism for this type of reaction which involves five steps that are: the approach of the nucleophile towards the carbonyl group, a first transition state, tetrahedral intermediate, a second transition state and formation of the products.

The authors illustrate, as example, the correlation between the distance of the nucleophile and the electrophile with the interactions that arise during the nucleophilic attack of a hydride to a molecule of formaldehyde :

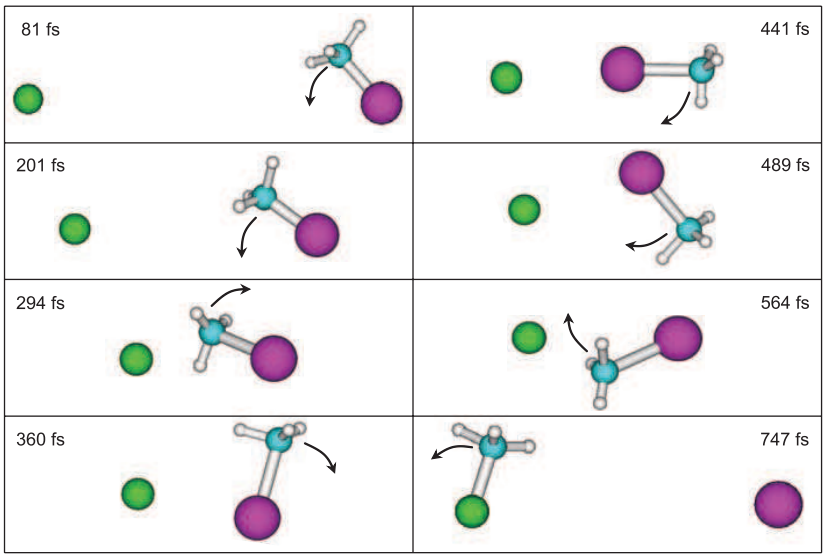

Figure 2.2: Dynamic of a nucleophilic attack of chloride anion toward iodomethane.

Picture taken from Mikosch et al 2008

- At large distances, under electrostatic control, the anion approaches the formaldehyde molecule in the molecular plane along the HCH bisector following the line of maximum electrostatic attraction to the molecular dipole.

- At shorter distances, repulsive interactions opposed to the electrostatic attraction start to come into play between the hydride and the formaldehyde hydrogens, with the angle between the carbon atom of the formaldehyde and the hydride changing from 180 to 125°.

- When the distance is below 2.5 Å, the potential energy valley starts to become steeper and narrower because the orbital interaction becomes significant.

Theoretical and experimental data agree from this study showing that when the distance between nucleophile and electrophile is smaller than 2.5 Å, the angle between these two species is about 105± 5°. In conclusion this study vitally proved, from kinetic and structural evidence, that in a nucleophilic addition to a trigonal carbon atom, into the transition state, the ideal angle between the species involved should be between 100 and 110°. Nucleophilic addition to digonal carbon atoms

instead leads to products where trajectories of 60 and 120°are followed, as will be shown in this chapter, perhaps because the triple bond has an exceptionally large "window".[43]

With knowledge of the dynamics of structural transformations of the carbon atom differently hybridized during chemical reactions, Baldwin formulated his cyclization rules (fig.2.3). The rules as stated, consider three different parameters that distinguish one type of cyclization from the other, which are:

- The number of atoms of the ring that is forming, that can vary from 3 atoms up to 7,
- The hybridization of the carbon atom that undergoes nucleophilic attack: tetrahedral, trigonal, digonal.
- The cyclization mode: exocyclic or endocyclic (fig 2.3). If the bond broken during ring closure is inside the ring that is formed : endo cyclization mode; while if it is outside : exo cyclization mode.[44]

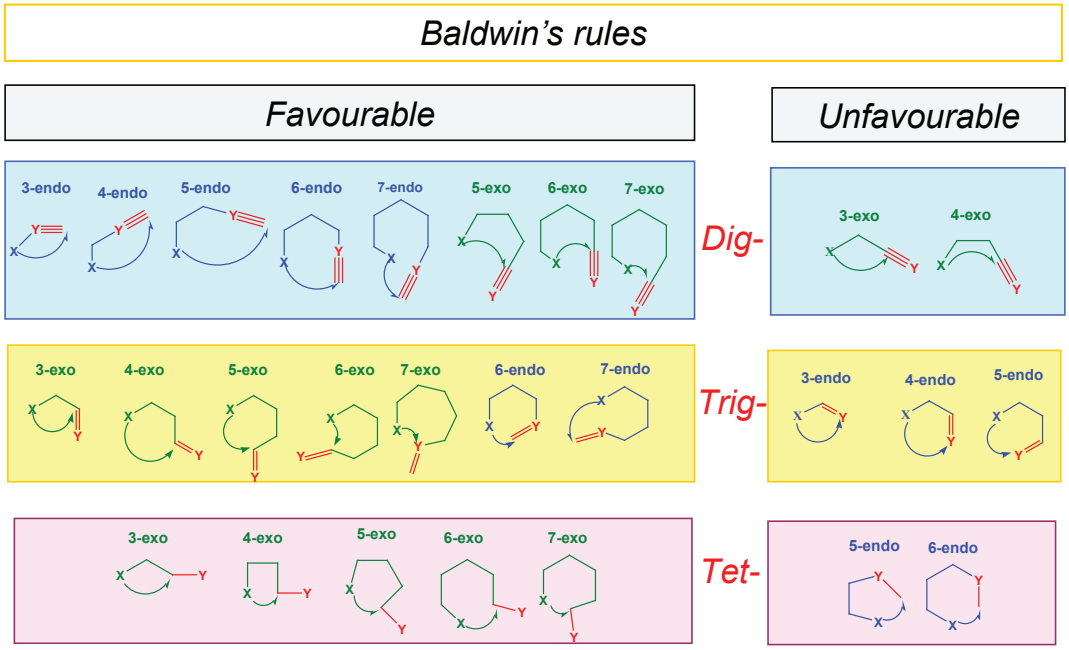

Figure 2.3: Schematic representation of Baldwin's rules

In reactions implying a nucleophilic attack at an sp^3 carbon atom, the 3-,4-,5-,6-,7-exo-tetragonal attacks are allowed, whereas the 5- and the 6- endo-tetragonal

attacks are disfavoured.

In reactions implying a nucleophilic attack at an sp^2 carbon atom, the 3- ,4-, 5- , 6- and 5-, 6-, and 7-exo-trigonal attacks are allowed processes, as well as the 6- and 7-endo endo-trigonal attacks, while the 3-,4-,5-endo-trigonal attacks are disfavoured.

In reactions which imply a nucleophilic attack at an sp carbon atom, the 5- to 7-exo-digonal attacks are favoured as well as the 3- to 7-endo-digonal attacks, while unfavoured cyclizations are the 3- and the 4-exo-digonal attacks.

Although these rules are generally respected as in the case of the hydroxyl-enone that fails to cyclise under different conditions, cases are reported where these rules are not observed. An example is the ring-chain tautomerism of 5,6-dihydro-2-hydroxy-2,3-dimethyl-2H-1,4-oxazine in which the rate constants, measured by NMR, indicated that the disallowed 5-endo-trig reaction was faster than the allowed 6-exo-trig reaction[45] (fig 2.4).

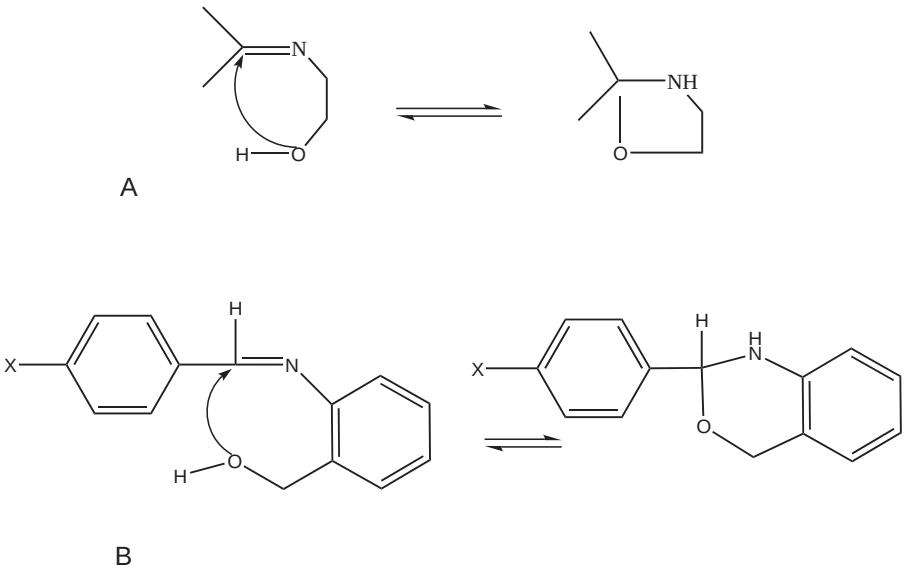

Figure 2.4: Chokotho (1985) through NMR measurements proved that the disallowed 5-endo-trig reaction (A) is faster than the allowed 6-endo-trig reaction (B)

.

2.2 Ring closures in some biological systems

Baldwin's rules are involved not only in chemical reactions at laboratory conditions but in all chemical reactions where cyclizations are involved in which the centre that undergoes a nucleophilic attack is a carbon atom. Examples can be found in the biochemical synthesis of the indole alkaloid physostigmine. Three mechanisms can be hypothesized, 1) a concerted 5-endo-trig ring cyclization with a nucleophilic attack on the S-adenosyl-L-methionine (SAM) 2) a 5-endo-trig cyclization with production of a carbanion that nucleophilically attacks SAM, 3) a stepwise mechanism which implies a methylation of a double bond with a subsequent 5-exo-tet cyclization. Piccirilli (1999)[46] predicted that the mechanism that the enzyme follows in this biosynthesis is stepwise, in which Baldwin's rules are respected (fig 2.5). Another example of an enzyme that has functionally adapted to avoid violating Baldwin's rules is the 1-aminocyclopropane-1-carboxylic acid (ACC) synthase that catalyzes the formation of ACC from SAM. Piridossal phosphate enzymes in general catalyze several amino acid transformations in which a common hypothesised mechanism for the ACC synthase with SAM is a tautomerization of an aldimine to a ketimine, followed by the elimination with breaking of the C-γ-S bond with a consequent 3-endo-trig cyclization that violates Baldwin's rules. The mechanism supported by experimental evidence suggests instead that the α- carbanion displaces the 5'-5'-deoxyadenosine through an SN_i reaction therefore avoiding the prohibited 3-endo-trig cyclization. In both cases, the enzymes that involved the biosynthesis of physostigmine and of ACC evolved their active site taking advantage of the stereoelectronic principles that allow one cyclization and avoid mechanisms that violate Baldwin's rules.

Enzymes can, however, also catalyze disfavoured reactions, probably because the constraints imposed by the stereochemistry of reactants or products, or perhaps, improving a slower reaction by means of a disfavoured reaction, is not a real ne-

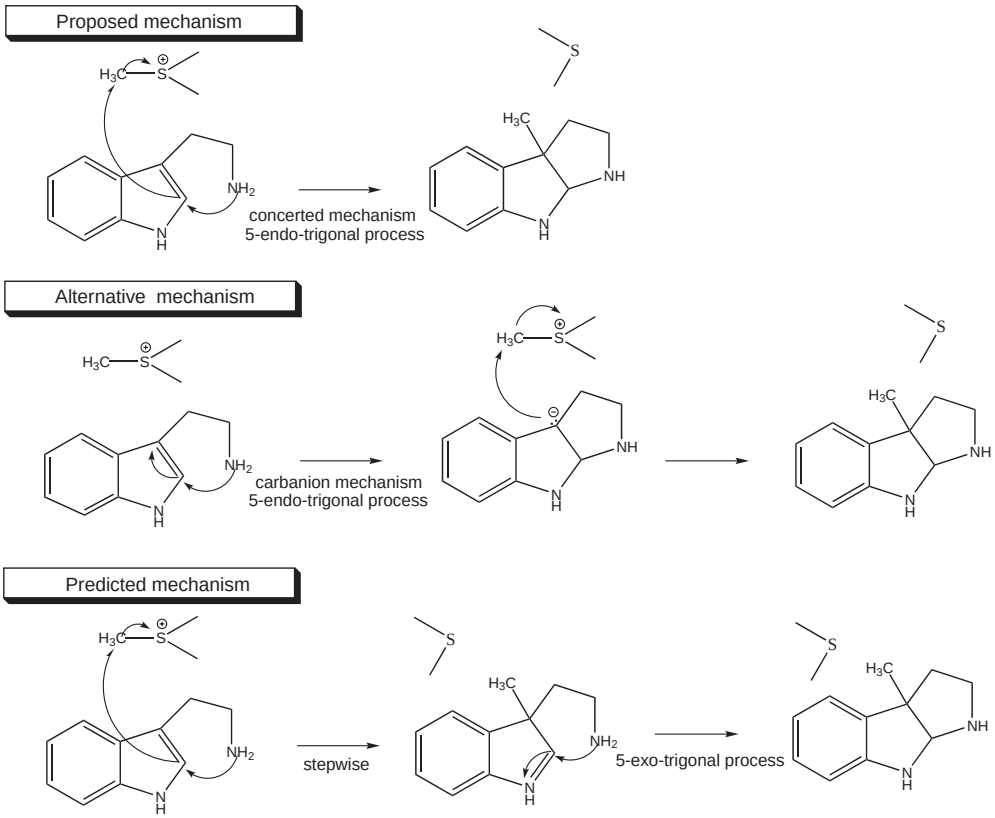

Figure 2.5: Mechanism proposed by Piccirilli for the biochemical synthesis of the indole alkaloid physostigmine

cessity for survival of the host organism. Janda et al. (1993)[47] designed antibodies that catalyze a disfavoured 6-endo-tet ring opening of an epoxide by an internal nucleophilic oxygen atom, which leads to formation of a tetrahydropyran (fig 2.6). This cyclization mode is in competition with the favoured 5-exo-tet cyclization fashion that yields an unwanted tetrahydrofuran. The author constructed a haptene surrounding the epoxide with appropriate charged amino acid residues to stabilize the C-O bond during its breaking. Gruber et al. (1999)[48] designed other haptenes to favour the 6-endo-tet cyclization. That author proposed a catalysis mechanism which implies a general acid/base catalysis with an aspartic acid residue which opens the oxirane ring and a hystidine (base) which promotes the nucleophilic attack of the alcohol group (fig 2.7).

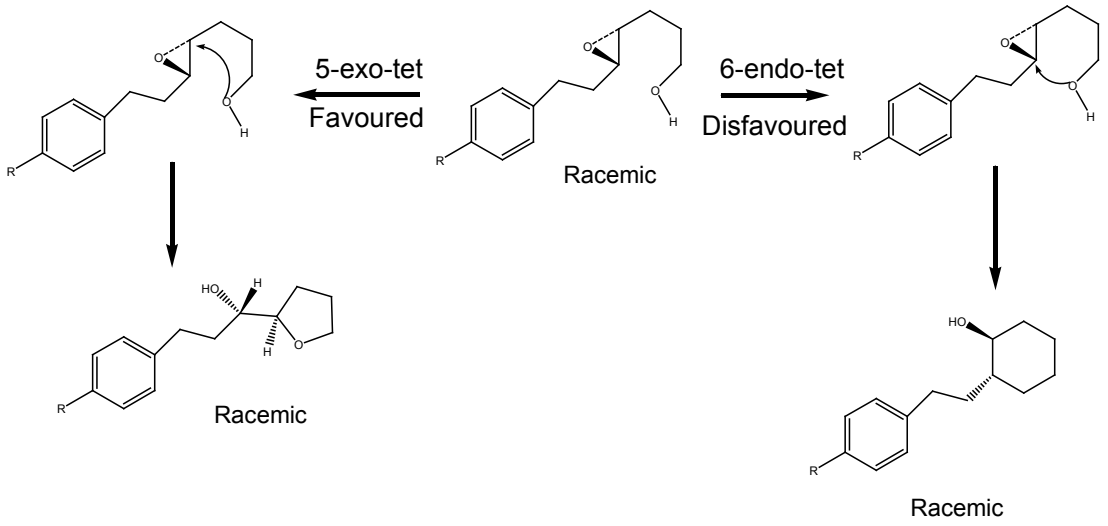

Figure 2.6: 6-endo-tet cyclization promoted by antibodies designed by Janda et al.

2.3 A survey of the cyclization reactions: a theoretical perspective

Radical cyclizations have been more widely analysed theoretically than other types of mechanism due to their large use in organic synthesis. Several applications are of interest, from synthesis of complex molecules to the discovery of bioactive natural products exhibiting both antibiotic and anticancer properties. However, anionic cyclizations, e.g. the formation of the β-lactam ring, are also pharmaceutically relevant.

2.3.1 The 4-exo ring cyclization mode.

Baldwin's cyclization rules predict that the 4-exo cyclization mode is favourable when the carbon atom that undergoes nucleophilic attack is sp^3 or sp^2 hybridized, being unfavourable only when that centre is sp hybridized. In organic synthesis, the 4-exo cyclization mode is found in general to compete with endocyclic or exocyclic modes that lead to five and/or six membered rings. Chatgilialoglu et al. (2002)[49] considered the competition between the 4-exo and the 5-endo cyclization

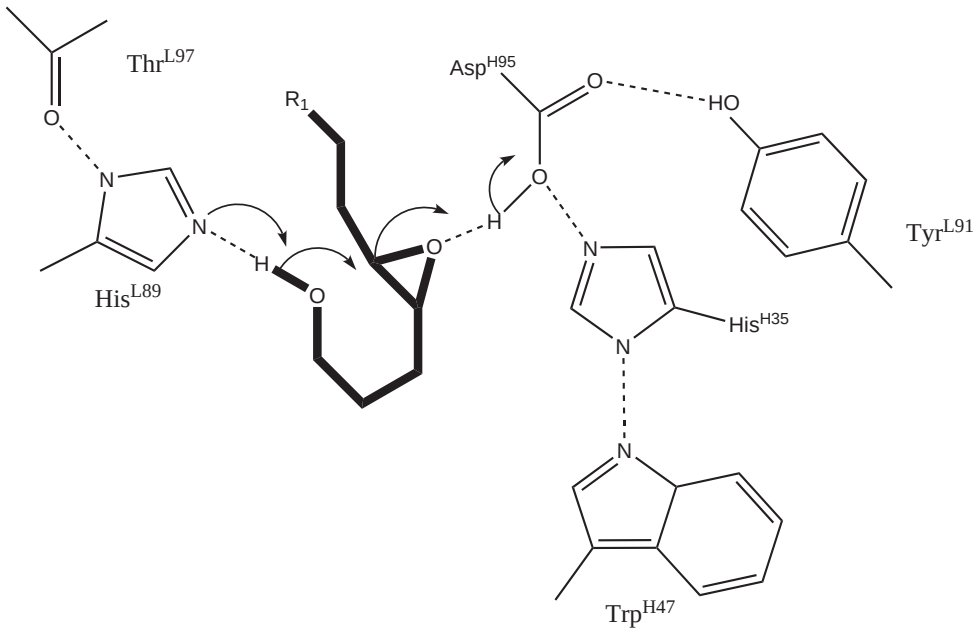

Figure 2.7: Biocatalysis in which a proposed mechanism is implied that favours the 6-endo-tet cyclization mode

modes in haloenamines, pentenyl radicals, and vinyluridines that originated from previous synthesis work of Ikeda, Ishibashi and co-workers[50,51] (fig 2.8).

This synthetic work, interestingly, was the first to show that a variety of haloenamides afford gamma-lactams in good yields under free-radical reducing conditions. The cyclizations studied can be highly diastereoselective or moderately enantioselective in which the 5-endo process is generally favoured over the 4-exo, the latter is more favourable only when there is a phenyl or other bulky substituent attached to the olefinic group where the electron can be delocalised. Also in pentenyl radicals and vinyluridines this favourability trend is respected, rationalized, in pentenyl radicals, by the ideal attack angle in the transition states of the 5-endo mode vs. 4-exo, and in vinyluridines by the fact that the uridyl group can delocalize the unpaired electron in the transition state. The kinetical and thermodynamical preference for the 4-exo mode over the 5-endo, has been confirmed by Friedrich[52] but his findings suggest that in pentenyl and related radicals there are two possible transition states for the 4-exo mode (fig 2.9).

The transition state characterized by an angle of approach of the radical toward

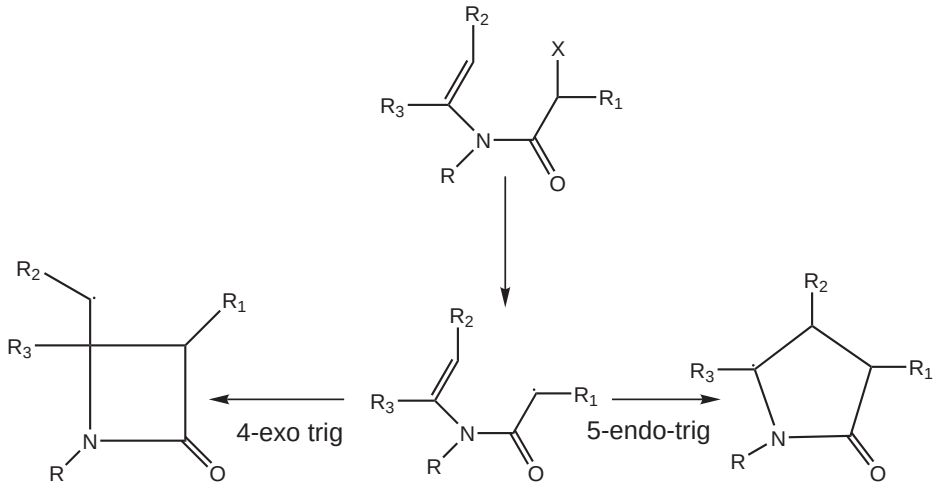

Figure 2.8: 4-exo and 5-endo cyclizations modes in haloenamines studied by Chatgilialoglu et al.

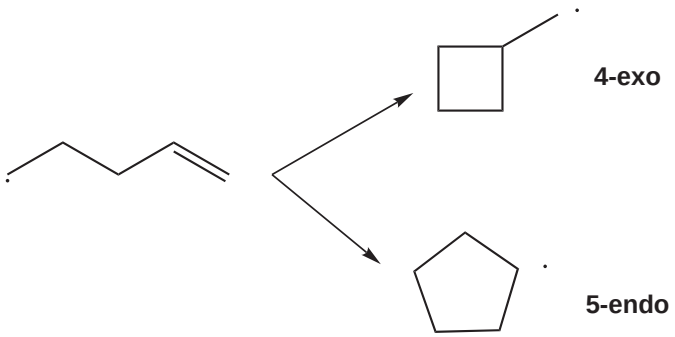

Figure 2.9: Titanocene catalyzed radical cyclization reactions studied by Friedrich et al.

the olefin of 118° is energetically more favoured than the other possible TS with an angle of 115° found by Chatgilialoglu. Moreover, the introduction of an acid group by this author in pentenyl radicals, demonstrated that 4-exo-cyclization is kinetically more favourable, while the 5-endo remains thermodynamically preferred. Analysing a series of titanocene catalyzed radical reactions Friedrich described how the gem-dimethyl effect, that is the acceleration of a cyclization due to the replacement of hydrogen atoms with alkyl groups tethering the two reaction centers, provides a means for controlling the distereoselectivity of the 4-exo cyclizations and is considered in addition to promote the reactions kinetically. The interesting preference for the formation of a four-membered ring instead of a six membered, found during the synthesis of azaheterocyclic phosphonates, has been theoretically

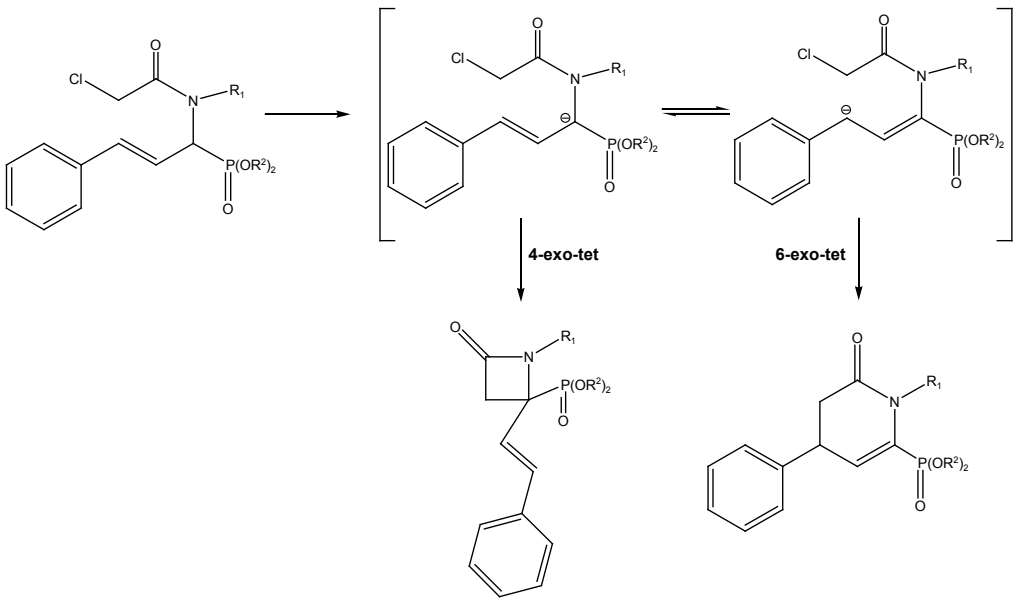

Figure 2.10: Reactions studied by Van Speybroeck et al.

disclosed by Van Speybroeck et al.(2006)[53](fig 2.10).

The transition structures for both the anionic 4-exo-tet and the 6-exo-tet cyclization modes examined resemble an intramolecular S_N2-like reaction characterized by an umbrella-like inversion at C5. The author, studying the energetics of the distortion angle involved in the nucleophilic attack to the reacting centre, shows how the origin of the 4-exo mode preferentiality should be addressed to the large distortions required in the formation of the 6-membered ring from the original geometry of the anion to adopt the S_N2-like transition structure. In contrast the 4-exo-mode has been proven unfavourable compared with other types of cyclization in the synthesis of tetrahydrofurans and tetrahydropirans via seleniranium ions, both experimentally, due to the lack of product formation and theoretically, due to the high cyclization energy barriers.

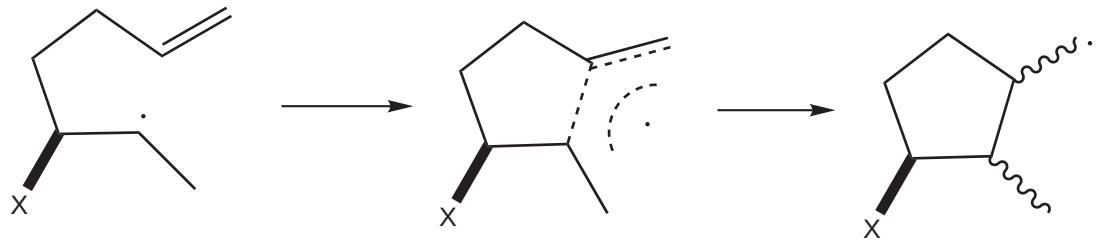

Figure 2.11: 5-exo-trig cyclizations of chiral hepta 1,6-dienes studied by D'Antuono et al.

2.4 Five and six-membered ring cyclizations

2.4.1 The 5-exo-cyclization mode.

The most basic radical cyclization is the intramolecular cyclization of alkenyl radicals, in particular the 5-hexenyl radical that cyclises in a 5-exo-trig fashion yielding five membered rings. Guan (2005)[54] studied the substituent effect on 5-exo-trig cyclizations of 6,6-diphenyl-5-hexenyl radicals. Theoretical kinetic data with the inclusion of the solvent shows that the activation free energies for all reactions analysed lowers upon inclusion of the solvent effect, indicating the role the solvent plays in such cases. In general, the substitution of these radicals with electron donor groups lowers the cyclization energy barrier, because of the stabilization effect that in the methoxy group could be of inductive fashion rather than conjugative. In contrast electron acceptor groups raise the energy barrier, with a destabilization effect that is more pronounced with the cyano group, attributed to its strong conjugation with the radical center.

D'antuono et al. (2005)[55] analysed the nature of the leading effects governing the stereochemistry of the 5-exo-trig cyclizations of chiral hepta 1,6-dienes (fig 2.11). The authors analysed two main type of substituents, bulky substituents like silated, t-Bu, and the hydroxyl group. The 5-exo-trig cyclizations with bulky substituents lead to the products through a chair-like transition state, thus are in agreement with the Houk-Beckwith model with very high level of stereocontrol due to steric

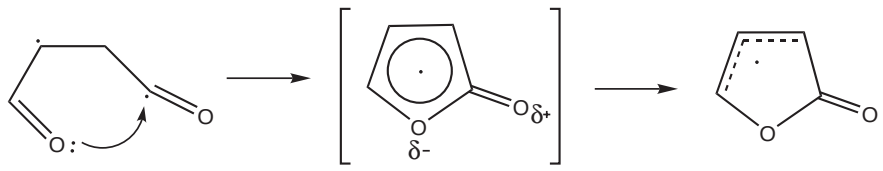

Figure 2.12: Radical 5-endo-trig cyclizations of 5-oxa-penta-2,4-dienoyl radicals studied by Yamamoto et al.

effects. Moreover, the reaction stereocontrol increases with lowering of the temperature. The cyclizations with the hydroxyl group do not have chair-like transition states and are less stereoselective with the stereochemistry of the major stereomer mainly driven by an electronic effect. It has been demonstrated also that the solvent effect for these cyclizations does not have a high impact on the stereoselectivity, somewhat in contrast to the 5-exo-trig of α-substituted 6,6-diphenyl-5-hexenyl radicals mentioned above.

2.4.2 The 5-endo cyclization mode

Yamamoto et al. (1996)[56] described an interesting case of a non-radical cyclization mechanism in radical 5-endo-trig cyclizations of 5-oxa-penta-2,4-dienoyl radicals and related systems (fig 2.12).

In this study, the author mainly compares the cyclization of the 5-oxa-penta-2,4-dienoyl radical with an analogue not substituted on position 5. Both of these radical structures have flat U shape geometry. The transition state of the oxa-substituted radical has a more planar structure than the analogue not substituted. IRC (Intrinsic Reaction Coordinate) and spin density analysis reveal the nature of the non-radical mechanism for the 5-oxa-penta-2,4- dienoyl radical. At the transition state, the radical is appreciably delocalised to give comparable spin densities on the carbon and oxygen atom. In contrast, the transition state for the analogue that can be considered as a ketene-substituted allylic radical shows that

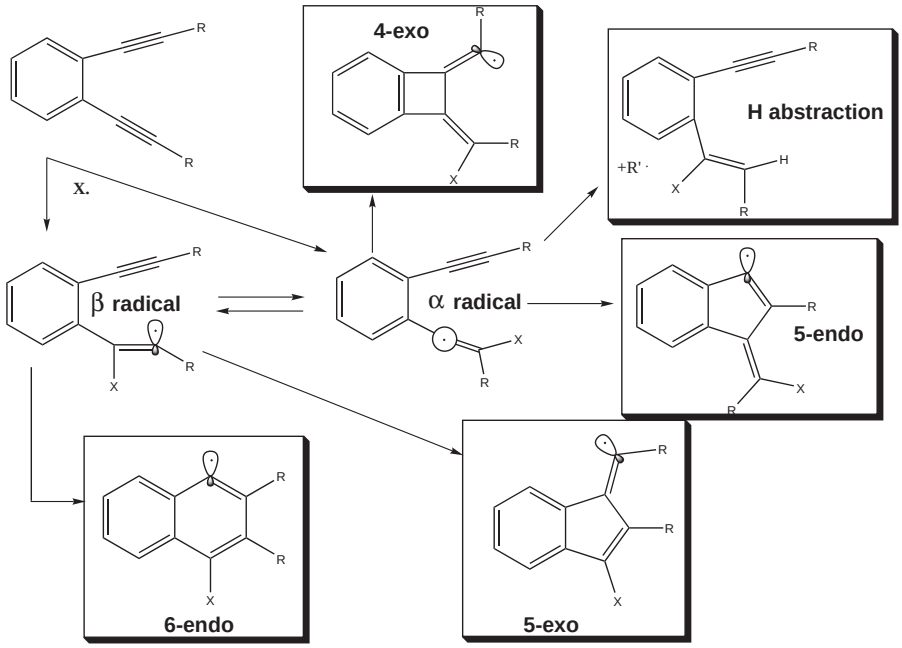

Figure 2.13: competition between 4-exo-dig, 5-endo-dig, H abstraction studied by Alabugin and Manoharan

the radical is almost completely localised on the carbon atom of the acyl group. This process could be viewed as an intramolecular addition of an acyl radical to a diene. The author, comparing the cyclization reaction of the ketene-substituted allylic radical with the cyclization of its nonconjugated version, found that the latter is more readily cyclised due to its motional flexibility. Although 5-endo-trig cyclizations are not feasible from Baldwin's rules with therefore different stereo-electronic interactions compared with the 5-endo-dig, Alaburgin and Manoharan (2005)[57] demonstrated that the 5-endo-dig radical cyclizations are similarly influenced by the conjugation effect found to be the determining factor in the reaction favourability of 5-endo-trig cyclizations studied by Yamamoto et al. (fig 2.12). Alabugin and Manoharan, studying acyclic radicals, divide the cyclization in two elementary steps:

- reorientation of the radical orbital
- new sigma-bond formation.

When a vinyl bridge is present, the reorientation of the radical causes loss of

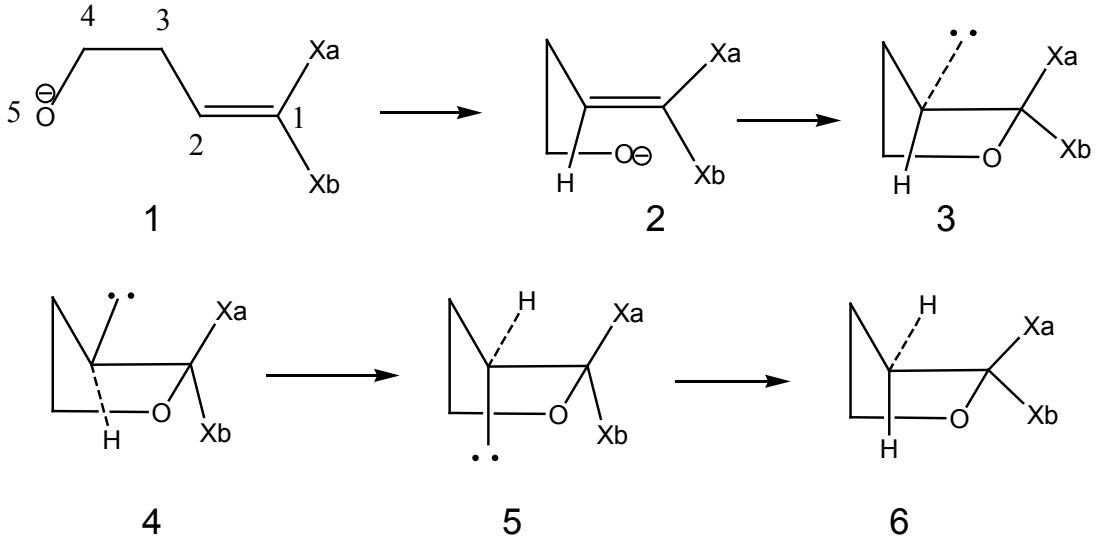

Figure 2.14: Gem-difluoroalkenes analysed by Takashi et al

conjugation, thus with unfavourable cyclization energies. Moreover, the authors show that those cyclizations are sensitive to steric effects and compete with several other mechanisms such as hydrogen abstraction, the 4-exo-dig cyclization and the isomerisation of the radical between two species. The authors show that the isomerisation of the radical in two forms α and β is slower than cyclizations, therefore the regioselectivity of the radical initiator determines if the 5-endo product will be formed. In order for the 5-endo cyclization to be favoured over the 5-exo/6-endo modes, the isomerisation energy barrier should be approximately 20 kcal mol^{-1}. When the energy difference between α and β forms is small, this cyclization has little chance to compete with the other two processes (fig 2.13).

Takashi et al. (1999)[58] studied the competition between the 5-endo-trig process with a 4-exo-trig in model systems of gem-difluoroalkenes, that cyclise with an anionic 5-endo-trig fashion in the synthesis of hydroxystirenes. The results show the 5-endo-trig cyclization process is favoured over the 4-exo-trig, thus in opposition to Baldwin's rules. The author shows also that if the fluorine atoms are not present in such system the 5-endo-trig reaction is less feasible thermodynamically and kinetically (fig 2.14). More insights on this process could be found in the work of Ando (2003),[59] which shows that the cyclization takes place in three steps, that

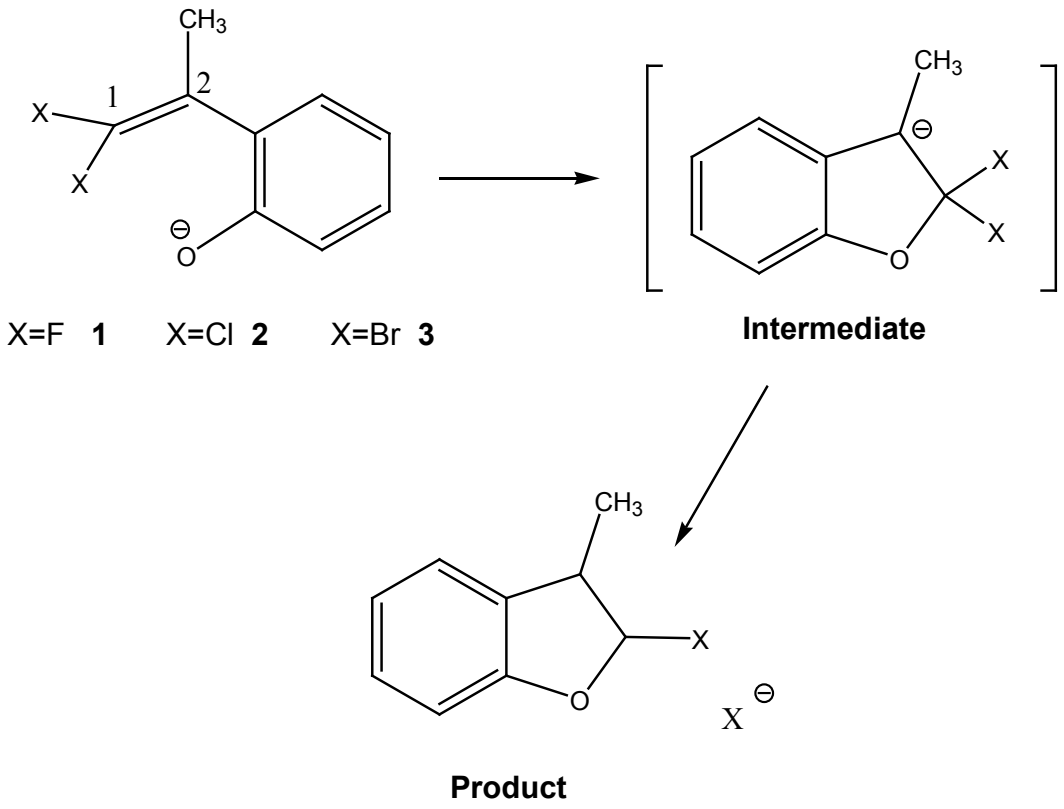

Figure 2.15: Cyclization mechanism for the cyclization of gem-difluoroalkenes proposed by Kaori Ando

is, the addition reaction to the pi-bond, the subsequent inversion of the carbanion stereochemistry, and the delocalisation of the negative charge (fig 2.15).

2.4.3 The competition of five versus six membered ring formation.

Baldwin's rules predict most of the five and six membered ring cyclizations to be favourable with the exception of 5-endo-trig and 5-exo and 6-endo-tet. Interesting insights on the competition between these two processes could be found in the thermal closure of 1,3-hexadien-5-yn-1-yl radical that is believed to be the main reaction bottleneck in polycyclic aromatic hydrocarbons in hydrocarbon combustion. Olivella and Sole' (2000)[60] showed that energetically and entropically the preferred path is the 5-exo-dig cyclization. The 5-exo cyclised product follows another cyclization to form a bicyclo-radical that leads to a ring opening of the three

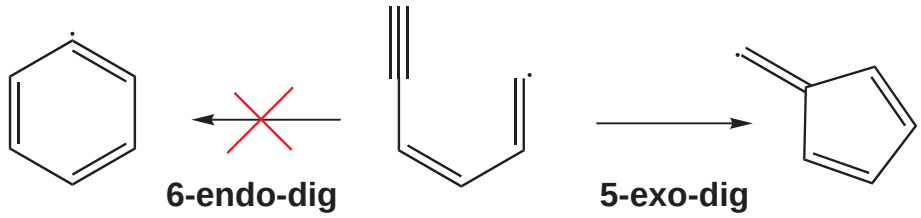

Figure 2.16: Ring closure of the 1,3-hexadien-5-yn-1-yl radical analysed by Olivella and Sole'

membered ring to finally form the 6-endo product. The 6-endo cyclization of the 1,3-hexadien-5-yn-1-yl radical in conclusion requires a higher free energy than the stepwise mechanism described. This author shows that the 5-exo-dig cyclization is a conseguence of the interplay of three main factors that are, stereoelectronics, polar and steric effects (fig 2.16).

More insights on the preference of the 1,3-hexadien-5-yn-1-yl radical for the 5-exo-dig mode and more theoretical justifications that lie behind that, can be found in the study of Alaburgin and Manoharan (2005)[61] on the influence of the thermodynamic and strain effect on vinyl and aryl radical cyclizations. These authors analyze how chemical changes on the 1,3-hexadien-5-yn-1-yl radical influence the competition between the 5-exo versus the 6-endo process and they suggest that:

- The presence of the vinyl bridge in these radicals preorganises the reacting functional groups for the bond-forming step with the effect of rendering the 6-endo process more exothermic, and lowering the energy barriers difference between the two competing cyclizations. Such preorganization provides an entropic advantage over systems in which the vinyl radical and the triple bond are connected with a flexible saturated bridge.

- When the hexen-1-ene-5-yne-1-yl radical was benzannulated in different positions, the 6-endo pathway was less exothermic because the gain in aromatic stabilisation from benzene to naphthalene is inferior to the formation of benzene.

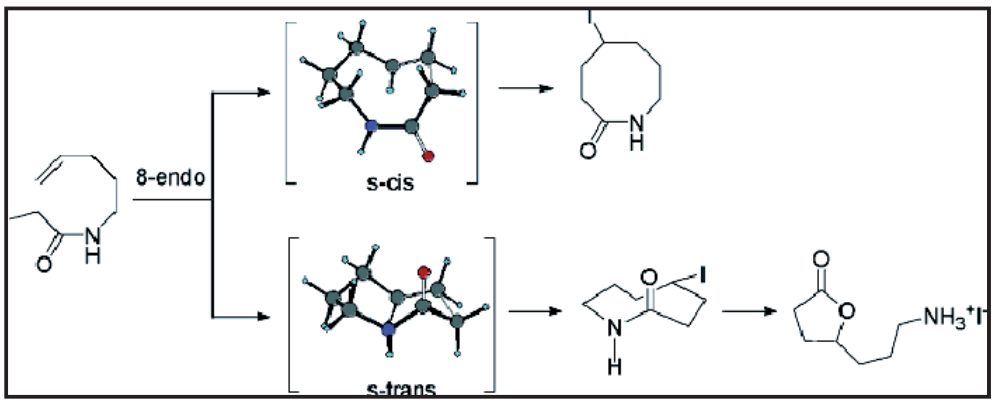

Figure 2.17: 7 and 8 ring cyclizations analysed by Liu et al.

- When aryl substituents were introduced into the benzannulated system to evaluate the steric effect, the aryl substitutions disfavour the 6-endo process, while the 5-exo mode does not suffer from steric hindrance.

- When a cyclopentene ring was annulated to the hexen-1-ene-5yne-1-yl radical and then the ring size varied, the 6-endo-dig cyclization became kinetically more favourable in presence of more strained systems.

2.4.4 Seven and Eight atom ring cyclizations.

There are not many theoretical studies that analyse seven or eight membered ring formations because the ring cyclization rules cease to exist when the number of atoms goes up to 8 and in general, rings of 7 or 8 atoms are very often readily cyclised. However, Liu et al (2005)[62] studied the competition between the 7-exo and the 8-endo cyclization modes in α-carbamoyl radicals. The authors demonstrate how the 8-endo mode cyclised products, which are stable both in a s-trans chair-chair-like conformation and in a s-cis boat-chair-like, are quite energetically lower than the 7-exo cyclised products in all conformations. Thus, in agreement with their experimental results the authors show that the 8-endo products are the only ones feasible for such systems which indicates a highly regioselective and efficient cyclization process, fig. 2.17.

In general, it has been shown that Baldwin's cyclization rules are a set of empirical

rules which enzymes in some cases have adopted in avoiding violations of these rules. With Baldwin's tools available to evaluate those processes,it is possible to note several effects in radical cyclizations, that play a key role in the preference of one mode rather than the other. Important effects are steric, from bulky substituents, conjugation and solvation. The competition between cyclization modes to achieve the stereoelectronic requirements for a given reaction is therefore intimately connected with the conformation of the reacting molecule solvated by a solvent, that sometimes is proved to be the principal factor.

2.5 The Dihidro-Imidazo-Phenanthridinium (DIP) synthesis reaction path

In this work has been computationally studied the synthesis reaction path of the DIP compound. Parenty et al. (2004)[63] described a one-pot synthesis of a series of phenanthridinium derivatives from the reaction of 2-bromoethylphenanthridinium bromide and a range of primary amines for which the reaction mechanism is shown in figure 2.18. The reaction can start with a nucleophilic attack of an amine at both a bromoalkane group (path B) and a iminium moiety (path A).

Experiments determined that path A was more favourable than path B, for example, fluoro and hydroxy analogues of **2** which were undertaking path A, were not able to cyclize with consequent isolation of the uncyclized product. The nucleophilic attack to the sp^2 carbon atom of the iminium group is more favourable than the S_N2 nucleophilic attack to the bromoalkane chain, but there is no experimental evidence that clarifies if the cyclization in path A, which within the Badwin's rules is classified as favourable, is in reality a more allowed process when compared with the 5-endo-trig cyclization in path B. Richmond et al (2008)[64] show that, controlling the pH, it is possible to convert the Tetrahidro-Imidazo-Phenanthridinium (TIP) molecule to the 5-[2-(isobutylamino)ethyl]phenanthridinium (AEP) and vicev-

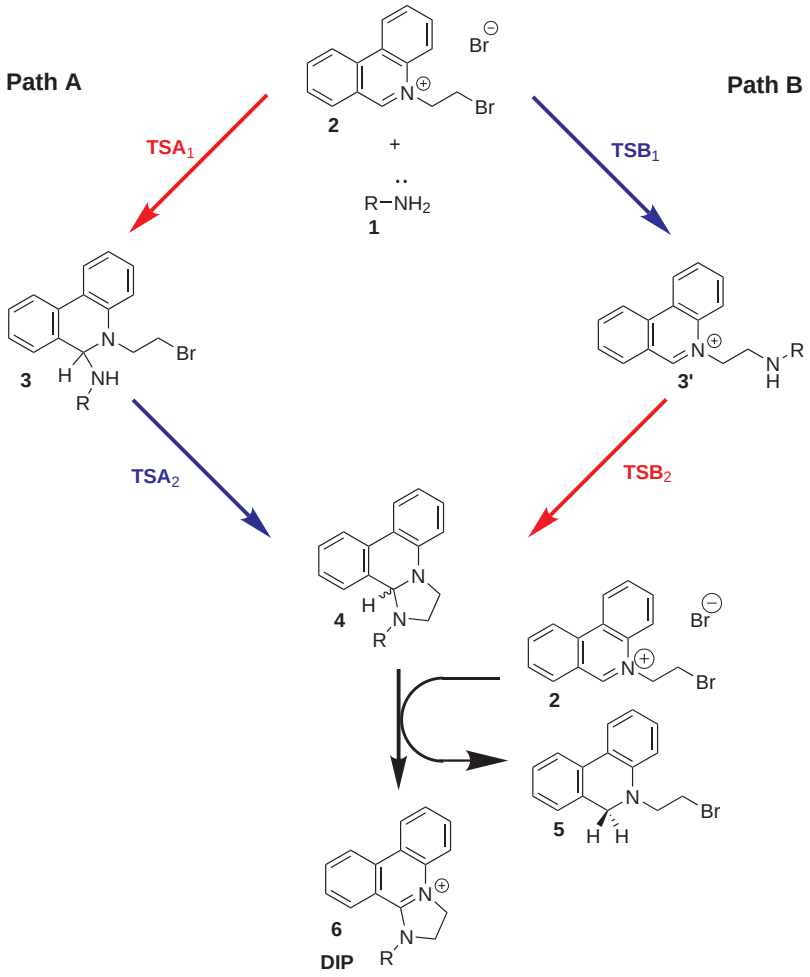

Figure 2.18: Dihidro-Imidazo-Phenanthridinium synthesis reaction path

ersa. Thus, the 5-endo-trig process in such conditions is allowed (fig.2.19).

Another experimental proof which confirms the 5-endo-trig cyclization as an allowed mechanism can be seen in the synthesis of the TIP molecule which starts with a phenanthridine that reacts with N-(2-bromoethyl)-phthalamide to form the 2-ethylamino protected molecule that in acidic conditions is hydrolised to the quaternary ammonium salt. In the biphasic conditions of an NMR tube containing D_2O and $CDCl_3$, **8** (fig 2.20) was neutralised with triethylamine and the cyclisation observed in situ. At the start of the experiment, molecule **8** is solubilised in the D_2O layer away from the bottom $CDCl_3$ layer, the only one to be read by the NMR. A control test was undertaken, showing no traces of **8** in $CDCl_3$. Upon addition of triethylamine, the quaternary ammonium moiety of **8** is deprotonated,

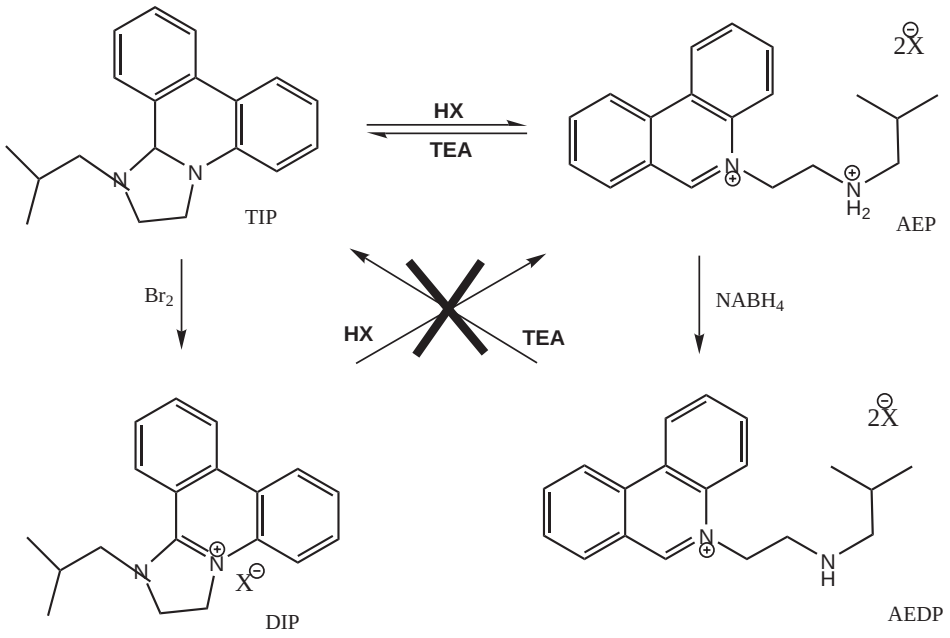

Figure 2.19: Conversion, under pH control, of the TIP molecule to the isobutylamino-ethyl-phenanthridinium

leading to the primary amine intermediate **3'** that cyclises instantaneously to form the D_2O insoluble molecule **4** that shifts to the $CDCl_3$ layer to be analysed. Attempts to examine intermediate **3'** in the D_2O layer were not successful within the 1.5 minutes necessary to run an NMR spectrum, indicating a rapid cyclisation reaction. Note that the biphasic system was also used to partition the cationic hydride acceptor **8** away from the neutral hydride donor **4**, freezing the reaction system before the redox reaction could take place. As a result, molecule **4** is highly air sensitive and can only be isolated in solution.

2.6 Computational study of the reaction mechanism

2.6.1 Computational details

It has been used the Gaussian03 suite of programs.[28] All geometry optimizations have been performed at B3LYP/6-31G* level of theory. The QST3 method has

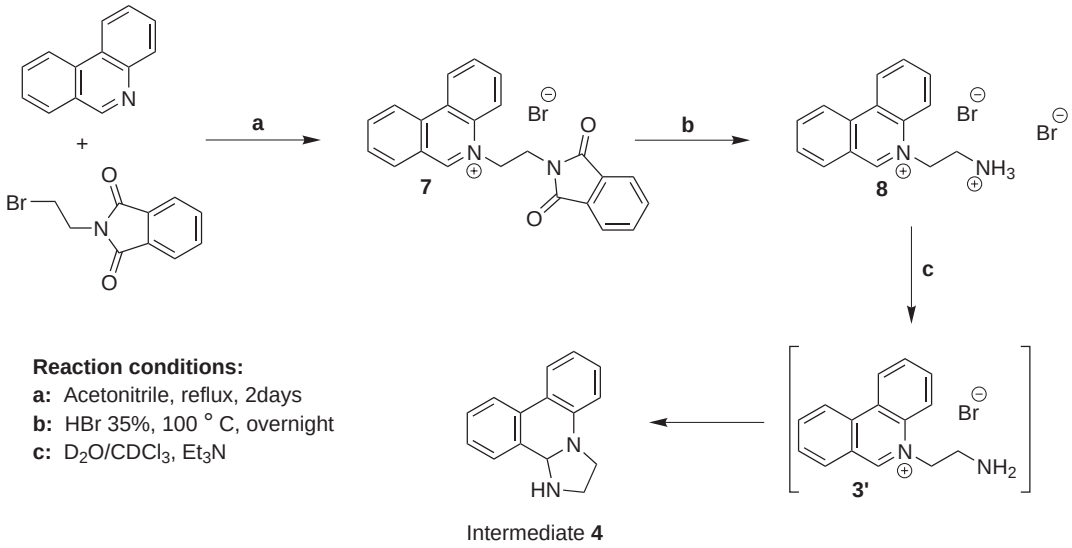

Figure 2.20: Experimental synthesis reaction path which confirm that the 5-endo-trig mode could be feasible

been employed for the transition state search calculations. The experimental data shows that both cyclizations are allowed, but the first step of the reaction path proceeds through the nucleophilic attack to the sp^2 hybridized carbon atom. Computationally, it is of interest to clarify the role of the cyclizations involved in both pathways, bearing in mind Baldwin's rules, and to prove or disprove the favourability of the nucleophilic attack to the sp^2 hybridized carbon atom (path A). The Potential Energy Surface (PES) for both pathways has been studied with several complications related to the fact that a loss of a proton or of an HBr molecule is present in some of the steps. The thermodynamics is therefore quite influenced by the solvent. The analytical treatment of HBr or H^+ is a complicated problem and goes beyond this work, but, as an approximation, one molecule of solvent (DMF) has been introduced in our computational model. Moreover, a continuum model has been included to introduce the effect of the bulk solvent on the key stationary points.

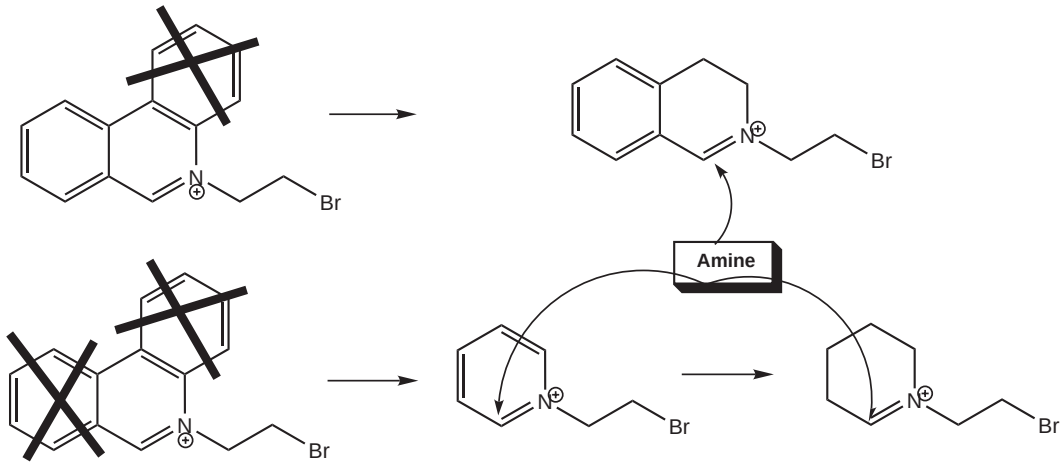

Figure 2.21: Model systems obtained from simplifications of the bromoethyl-phenanthridinium structure

2.6.2 The importance of hydrogen bonds on the DIP synthesis reaction path

All structures have been optimized with progressive increase of the level of theory from semiempirical methods to DFT. When lower levels of theory were employed such as PM3 or HF, the products of the nucleophilic attacks and of the 5-endo-trig cyclization in path B were stable. When electron correlation has been introduced within the DFT model, the C-N bond between the amine and the sp^2 hybridized carbon atom in path A or sp^3 hybridised in path B, breaks. The system thus tends to become neutral. The reasons for such effects have been explored with two model systems. The model systems considered have been obtained reducing the system size progressively with respect to the number of aromatic rings by eliminating one and then both aromatic rings from the phenanthridinium molecule which thus becomes a pyridinium. The pyridinium molecule is further simplified breaking the system aromaticity by reducing its double bonds with exception of the double bond involved in the nucleophilic attack (fig 2.21). The basis sets used are the Pople basis sets 3-21G* and the functional employed is B3LYP.

The first thing to note is that when the aromaticity is broken in all systems opti-

mized in which the starting geometry is the amine bonded to the α carbon atom, the distance between the amine and the α carbon atom increases to a maximum of 2 Å. When the phenanthridinium has been depleted by only one benzene ring, the α carbon atom and the amine nitrogen distance was found to be the longest. However, the geometry of such systems, in which the amine is orientated with an angle of about 109°that from Burgi and Dunitz can be ideal for a nucleophilic attack to a double bond, suggests that it may be possible that eventually distances between the α carbon and the amine nitrogen above 1.7 Åcould be defined as stretched bonds. If that speculation it is accepted, is possible to say that the amine can more easily give a nucleophilic attack to the double bond when its nature is not aromatic and the non stability of the amine nitrogen α carbon bond is correlated to the fact that the system aromaticity in gas phase (GPH) tends to disfavour such nucleophilic attack "pushing away" the amine. The pyridinium model and its tetrahydro derivative has been further explored in order to deeper understand the nature of such instability. Substitution of hydrogens on the alkane chain and on the aromatic moiety with halogens has been effected. The reasons for such substitutions are to explore if it was necessary to make more positive the α-carbon through electron withdrawal atoms in order to favour the nucleophilic attack. The major effect that probably such atoms like F, Cl, Br have, is when they are located on the alkane chain with formation of hydrogen bonds with an amine hydrogen, resulting in the stabilisation of the nitrogen α carbon bond to its normal length of about 1.5 Å. However, such effects should be further investigated with higher basis sets and also post-Hartree-Fock methods. In conclusion it is possible to say that in an aromatic system such as the phenanthridinium molecule, hydrogen bonds play a key role in the stabilisation of the amine nitrogen and the α-carbon bond, as seen on halogen substitution on the alkane chain. Therefore solvation may play an important role in driving that nucleophilic attack reaction. Halogens on the phenanthridinium alkane chain may facilitate that nucleophilic attack and proba-

bly the bromine atom on the alkane chain may play a substantial role on easing that reaction. Solvation may play a role on the first solvation shell that surrounds the amine nitrogen atom through hydrogen bonds that stabilise the positive charge and by long range interactions defined by the bulk solvent effect (and taken into account on the polarizable continuum model, PCM) that stabilises the nitrogen positive charge.

After having noticed the stabilisation effect through hydrogen bonds of halogens on the alkane chain with the amine hydrogen, the idea of introducing one molecule of solvent that may form some hydrogen bonds has been somewhat straightforward. One molecule of dimethylformamide (DMF) has been introduced into this model with consequent stabilisation between the amine and the phenanthridinium moiety. With only one molecule of solvent introduced in this model, it is far from representing the first solvation shell of the entire molecule. However, the portion of first solvation shell surrounding the nitrogen atom and thus influencing its reactivity, should not be too large. Consequently, one molecule of solvent on that portion of solvation shell is determinant on characterising the nucleophile reactivity and the contribution of the other solvent molecules can be more appreciated on the bulk electrostatic effect of the solvent. It is probably difficult, however, to quantify which of those contributions have more influence on defining globally the DIP synthesis reaction path : the hydrogen bond formation or the bulk dielectric effect. The amine during the S_N2 type nucleophilic attack is also stabilised by hydrogen bonds with the solvent, although it shows different characteristics (with an ideal attack angle of 180°) than the other that occurs toward a double bond.[65]

2.6.3 Formation of the TIP molecule

The potential energy surfaces are summarized in fig 2.22. In every step of each pathway, the energy of the reactants has been taken as reference point. The two steps that constitute every pathway are not placed on the same scale because of

the difficulty in computing the energies related to the dissociation of H^+ or HBr. Looking the PES, the S_N2 nucleophilic attack to the saturated haloalkane chain in both pathways will be rate-limiting compared with the nucleophilic attack to the iminium moiety. A comparison can be made between step 1 of path A which is the nucleophilic attack at the iminium group by a free amine, with step 2 of path B which is the related step where the cyclization takes place. The transition states comparison shows a relatively small incipient strain in TS2B which represents the basis of Baldwin's rules. The developing N-C bond is slightly longer in the transition state of the ring formation (1.83 Å vs 1.88 Å), with therefore signs of an earlier transition state. The N-C-N bond angle in TS1A, in which there are no constraints for the nucleophilic attack, is close to its ideal value of 109°, while this angle is reduced to 97.6° in TS2B. A partial deprotonation is present in both transition structures where the NH bond length adjacent to DMF is 1.04 Å compared to values of about 1.01 Å within the equilibrium structures. Although there are relatively small differences in the transition structures, the barriers for these two mechanisms are almost identical (7.6 kcal mol^{-1} vs 7.8 kcal mol^{-1}). It is possible to say, therefore, that the constraints related to the ring formation are quite small and counterbalanced by the greater nucleophilicity of the primary amine compared to ammonia.

The transition states related to the S_N2 type nucleophilic attack to the haloalkane chain demonstrate less evidence of strain involved in the cyclization. The N-C bond that is developing shows a similar length in both transition structures (2.03 Å in TS1B vs 2.02 Å in TS2A) and also the elongated C-Br bonds show a similar trend (2.54 kcal mol^{-1} vs 2.53 kcal mol^{-1}). The elongation of the NH bond and the contracted H-DMF bond length are also present in that case. The bond angles in both transition structures are close to their ideal values. The nucleophilicity of the primary amine compared with ammonia also in that case plays a key role in determining a higher value for the S_N2 of the latter (TS1B) which is of 27

kcal mol^{-1} versus the S_N2 of the former (TS2A) which is of 20 kcal mol^{-1}, in absence of strain formation in both steps. The absence of strain within the S_N2-type steps results in an activation energy difference of 7 kcal mol^{-1} and gives us a qualitative measure of the energetic cost of the 5-endo-trig cyclization described above considering that the strain involved in this process was counterbalanced by the higher nucleophilicity of the primary amine compared with ammonia. In support of the previous statements the activation energy barrier of step 1 of path B has been calculated where the nucleophile is methylamine instead of ammonia, showing a decrease of 4 kcal mol^{-1} (fig 2.23).

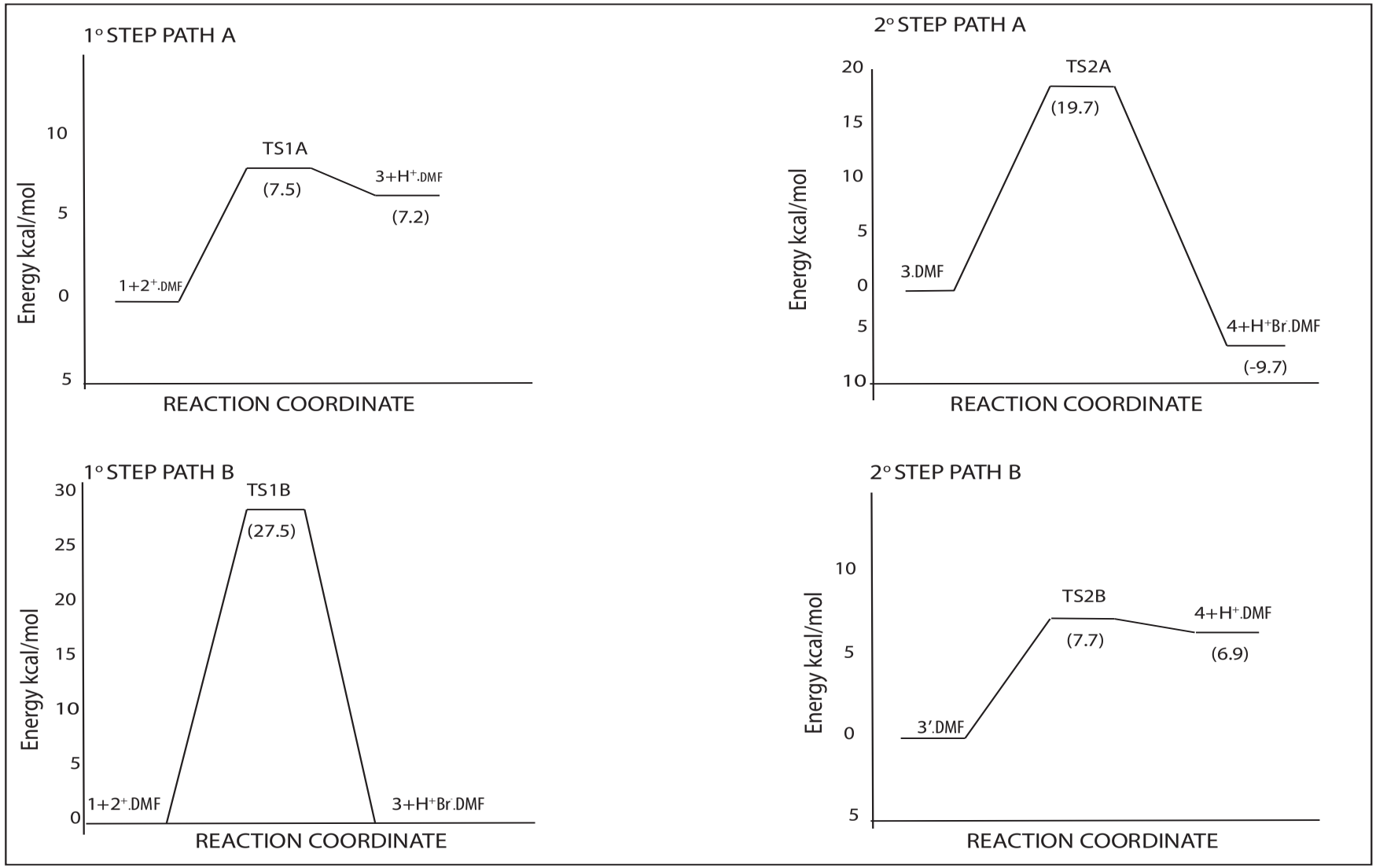

Figure 2.22: Potential Energy Surface of the four steps of the DIP synthesis reaction path

For this step there is a transition from a thermoneutral reaction, when ammonia was the nucleophile, to an exothermic reaction when methylamine was employed with an overall exothermicity of 17.5 kcal mol^{-1}. Thus, in GPH, the nucleophilicity is probably the most important factor in modulating the DIP synthesis reaction path. The alkyl group of the methylamine on one hand, shields the reaction center restricting the approach of the reactants to each other which can be seen on the TS in which the angle N-C-Br is of 162° deviating signficantly from its ideal value. On the other hand, replacing the hydrogen of ammonia and increasing the steric hindrance, theoretically, should change the bond angles at the nitrogen atom allowing its $sp^3 \rightarrow sp^2$ rehybridization and an increase in the p character of the nitrogen lone electron pair that is responsible for the increased nucleophilicity. In practice, looking at the bond angles of the methylamine nitrogen at stationary points of this step, it seems that in this case the lone electron pair is not more available than in ammonia. The major evidence of an increased exothermicity when methylamine was the nucleophile could be found in an increased stabilisation of the product. In the product, both N-H bonds of the methylamine group are stretched, one because of the interaction with the DMF molecule as in ammonia, the other because of a stabilising complexation with the bromine atom 2.07 Å distant from the hydrogen, which allows an overall stabilisation of the product.

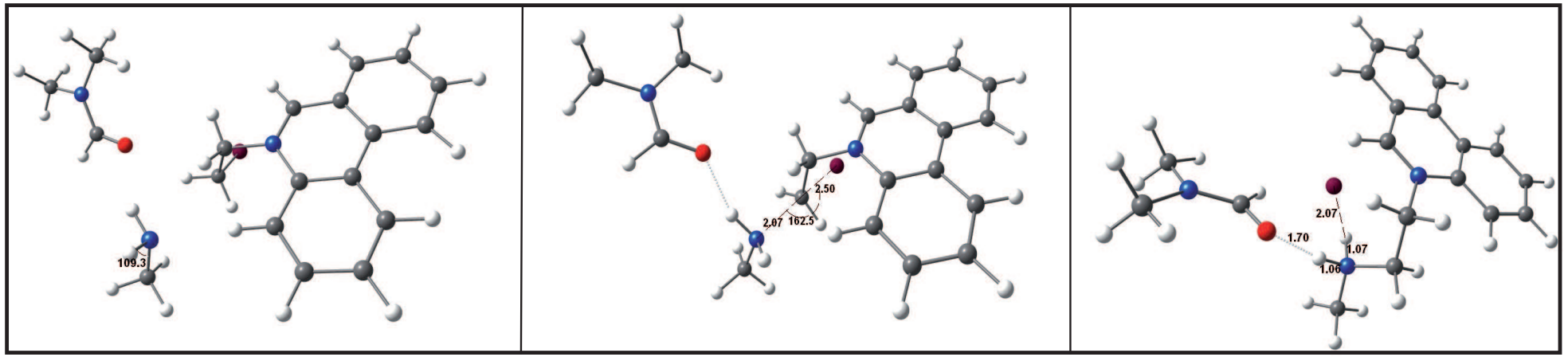

Figure 2.23: Nucleophilic attack of methylamine toward the bromoethyl-phenanthridinium molecule. Reactants (left), transition structure (middle) and products (right).

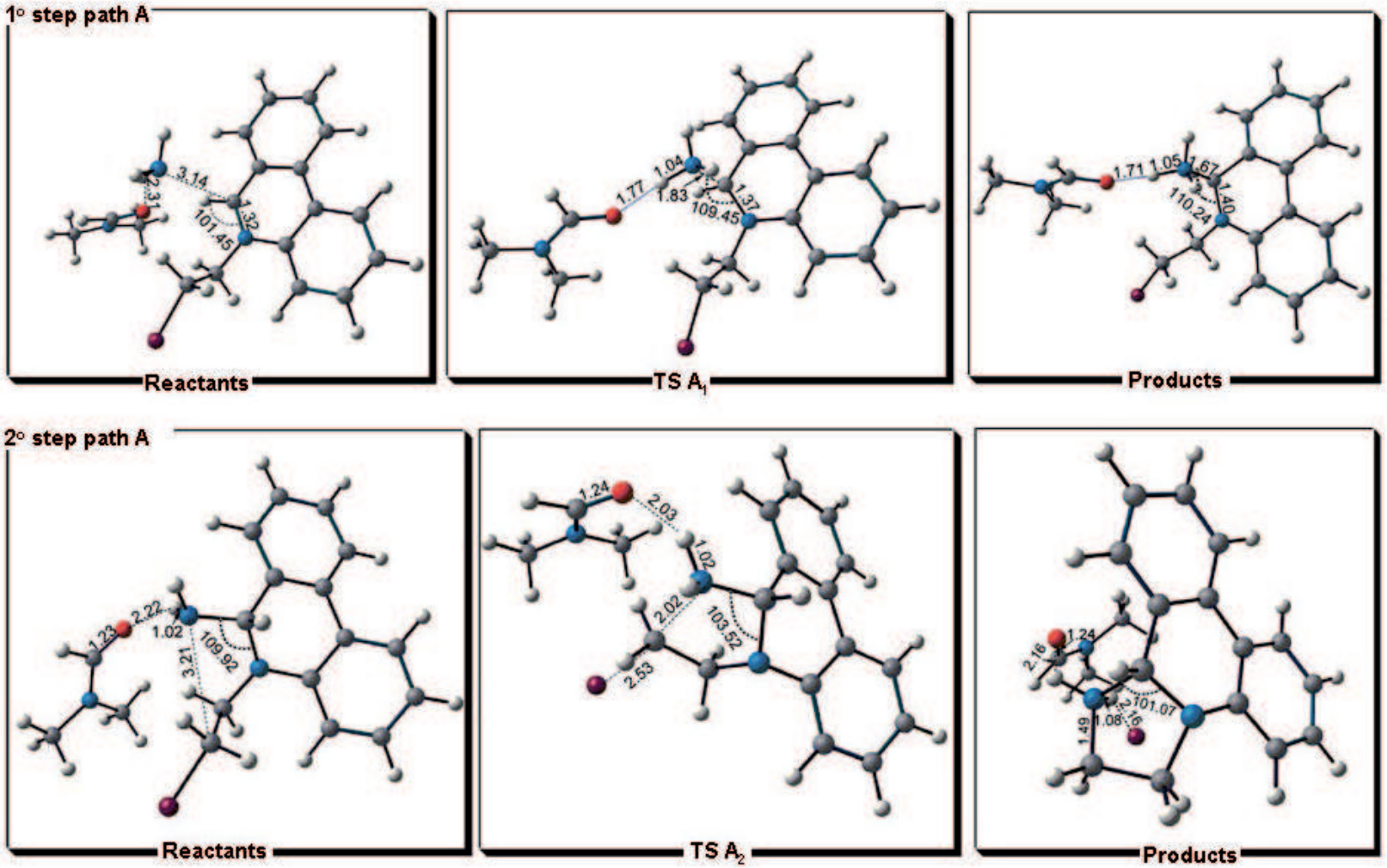

Figure 2.24: Steps of path A where one DMF molecule has been introduced into the model

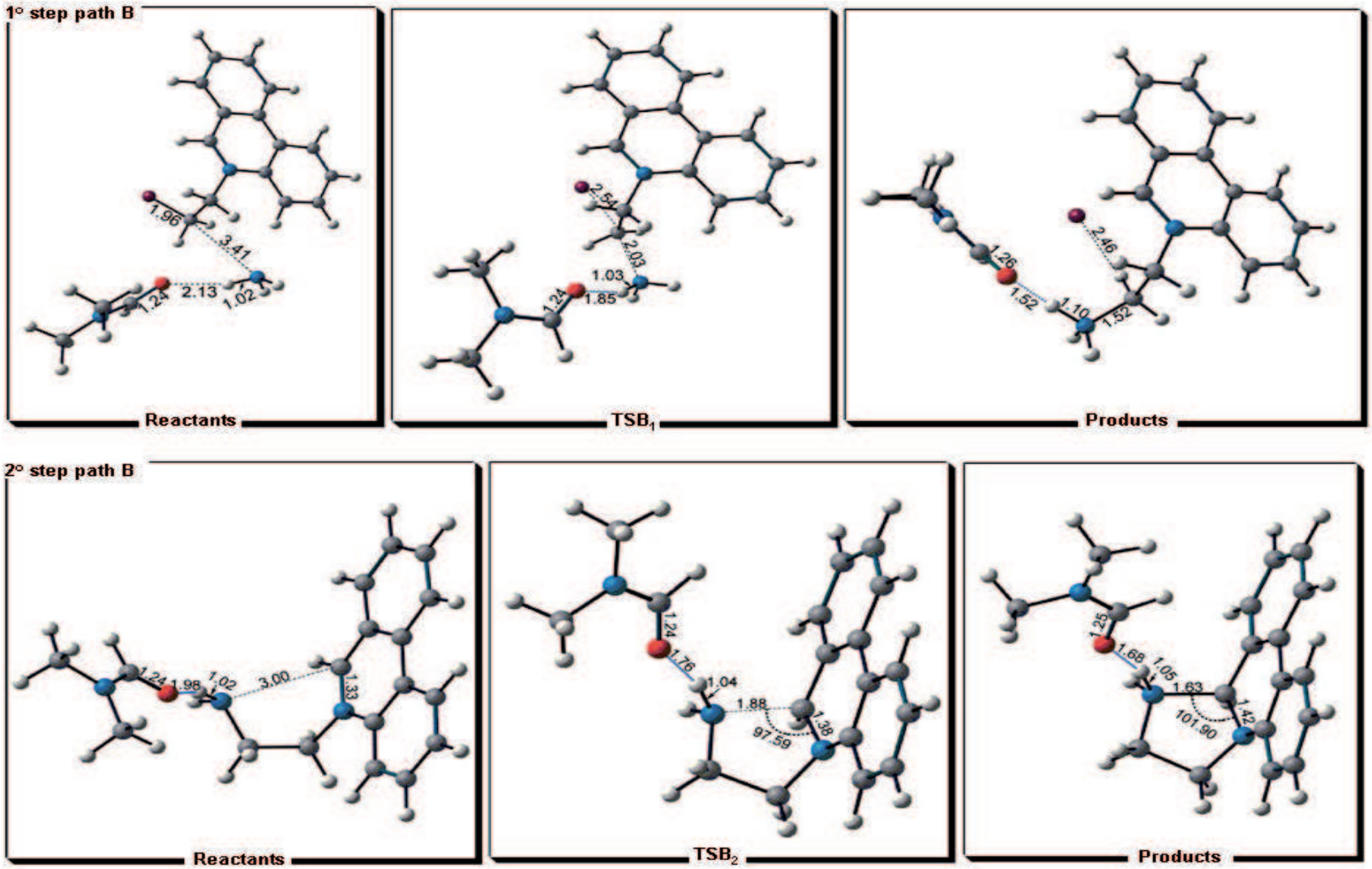

Figure 2.25: Steps of path B where one DMF molecule has been introduced into the model

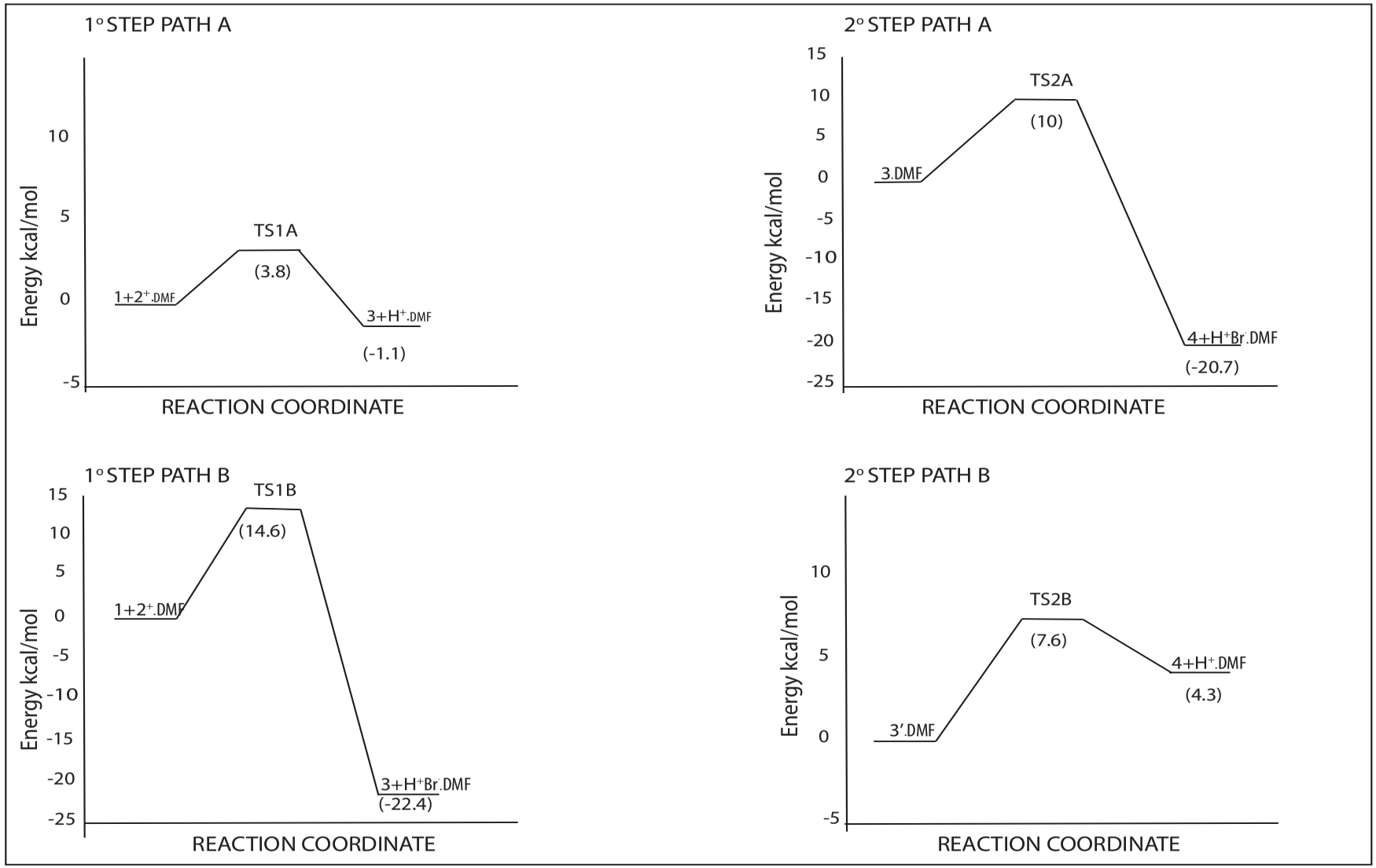

Figure 2.26: Potential Energy Surface of the four steps of the DIP synthesis reaction path in the presence of a continuum model for the solvent

The introduction of one DMF molecule in this model can be defined as a supermolecule approach, although, in this method, normally several molecules of solvent are included. It is important to remark that the model utilised in order to compute the synthesis reaction path is minimal, but sufficient for constructing the PES with the limitations described above. Ideally a statistical sampling for defining the first solvation shell of the molecule, with wide use of hybrid quantum mechanical/molecular mechanics (QM/MM) methods, should have been made. However, it should be stressed that while certainly the portion of the first solvation shell that surrounds the reactive center constituted by the developing N-C bond is made by several molecules of DMF, probably only one hydrogen bond between the ammonia or the primary ammine and a DMF molecule might be sufficient to allow the reaction to proceed. Hence the use of an initial model with a single solvent molecule.

The introduction of a continuum model has been explored with DMF as solvent at the stationary points shown in fig 2.22 in order to add the bulk electrostatic effect and therefore including the long-range electrostatic interactions. As shown in fig 2.26 the results are that, in each step, the activation energy barriers are lowered and the products are stabilised by the solvent, except in the 5-endo-trig cyclization step. The solvent stabilisation effect as a continuum model, reduces the barrier of the S_N2 reaction, which is the rate-limiting step in path B, by about 12.9 $\mathrm{kcal\,mol^{-1}}$(27.5 $\mathrm{kcal\,mol^{-1}}$ to 14.6 $\mathrm{kcal\,mol^{-1}}$) whilst the S_N2 reaction involved in the 5-exo-tet cyclization reduces its barrier by about 9.7 $\mathrm{kcal\,mol^{-1}}$(19.8 $\mathrm{kcal\,mol^{-1}}$ to 10.1 $\mathrm{kcal\,mol^{-1}}$). The resulting effect of the solvent on the S_N2-type steps could be attributed to steric considerations. Chen et al.(2009)[66] explained that the shielding effect of the extra alkyl groups of substituted nucleophiles compared with the unsubstituted one makes the former more poorly solvated than the latter. The nucleophile within the S_N2 transition state in solution has to be partially desolvated with therefore less energetic cost for this process when bulky

nucleophiles are used. Thus, the S_N2 reaction barrier in solution is lower for bulky nucleophiles, making the steric effect apparently smaller than in the gas phase. In our case, the S_N2 reaction of ammonia on the haloalkane chain, in solution the barrier is dramatically decreased and slightly more so than in the S_N2 related to the 5-exo-tet step. The solvent effect on the nucleophilic attack of a free amine to an iminium moiety (step 1 of path A) shows that the barrier decreases by half (7.5 kcal mol^{-1} to 3.8 kcal mol^{-1}), while in the 5-endo-trig cyclization step (step 2 of path B) the barrier doesn't show any variation. If the 5-exo-tet cyclization is not very influenced by the solvent when compared with step 1 of path B, the 5-endo-trig is even less influenced comparing its barrier with step 1 of path A. It might be difficult to rationalise fully a lower impact of the solvent on decreasing the energy barrier in both cyclization steps and rendering instead the nucleophilic attack of a free amine to the iminium moiety more favourable, but a few considerations can be given. A continuum model does not include the hydrogen bonding effect in solution, thus, an hypothesis which considers this effect should be ruled out. Perhaps the most convincing suggestion is that applying a continuum model on top of a molecule of solvent complexed with the reacting molecule, allows for the steric effect involved during the cyclization not to be offset any more by the nucleophilicity of the primary amine. Regan et al.(2009)[67] compared reactions of Cl^- with two alkylchloronitriles which differ by one substituent, in one case a methyl group and in the other a tert-butyl group (or neopentyl), showing it is possible to understand intrinsic structural effects without any additional effects (fig 2.27).

The authors show that for these reactions in water there is a greater increase in the desolvation free energy of the more hindered tert-butyl group relative to the methyl chloride system. Moreover, the author explains that the basis of such differences could be found in the differential solvation of the transition states which accounts for a significant part of the barrier differences in solution. These find-

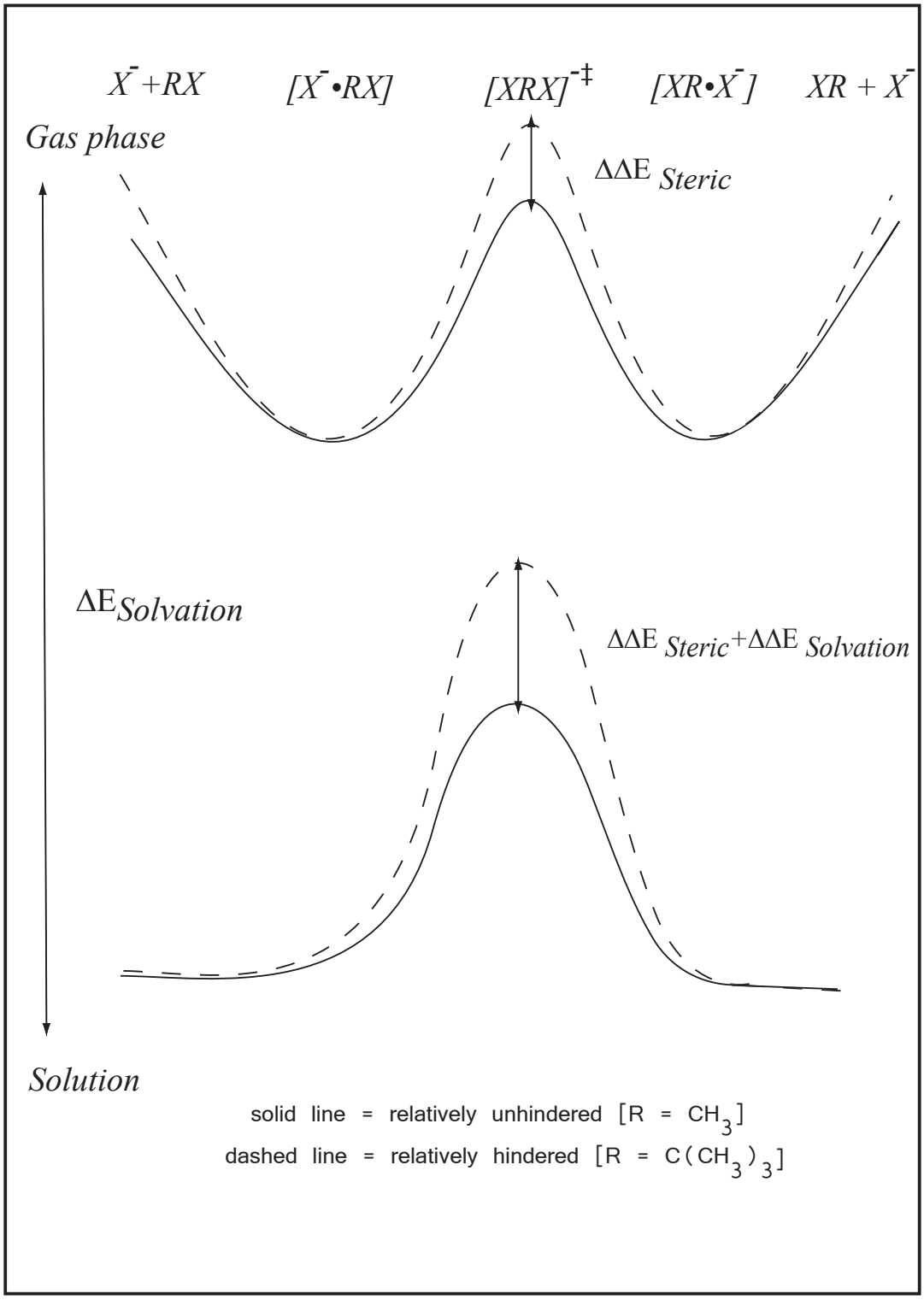

Figure 2.27: Increase of the energy barriers upon solvation in reactions of Cl^- with two alkylchloronitriles which differ by one substituent,in one R = methyl and in the other R = tert-butyl group

ings are slightly different than the findings of Chen et al. mentioned above, but this case could be used to reinforce the supposition drawn here, explaining the reasons for such diversity in the potential energy barriers in solution. In solution both cyclizations are less stabilised than the related step where a free amine is involved, where the steric hindering of the alkane chain in both cases allows the respective transition states to be differently solvated. In the 5-exo-tet cyclization transition state (step 2 of path A) the total solute-solvent electrostatic interactions are about 32 kcal mol^{-1} while in step 1 of path B these are of 72 kcal mol^{-1}. Thus in this case, the TS of the cyclization is differently solvated, explaining perhaps the lower stabilisation in solution than the free amine step. Consequently, the primary amine in solution, because less stabilised and therefore less solvated, should be more nucleophilic, but an intrinsic steric effect probably arises in this medium which partially counterbalances the increased nucleophilicity, not allowing the energy barrier to decrease more consistently. In the 5-endo-trig cyclization TS, the electrostatic interactions are of the same magnitude as in TS of step 1 of path A (54 kcal mol^{-1} vs 57 kcal mol^{-1}), thus those transition states are similarly stabilised by the solvent. It might be possible therefore that in this case in solution both the hindered primary amine and ammonia have the same nucleophilicity causing the not decreasing of the energy barrier in solution for the 5-endo-trig cyclization, imputable to a pure steric effect. The energetic cost of the 5-endo-trig cyclization in solution is therefore increased mainly by steric effects.

Hydrogen bonding plays an important role in S_N2 reactions stabilising the nucleophile and decreasing the overall thermodynamic driving force.[68] Moreover hydrogen bonding increases the intrinsic energy barrier of the reaction, slowing down the reaction. Thus, in S_N2 reactions, polar aprotic solvents increase the reactivity by several orders of magnitude compared with protic solvents. It has been estimated that the presence of only one hydrogen bond on the nucleophile can increase the barrier by 3 kcal mol^{-1} and in protic solvents this effect should

be higher because both nucleophile and leaving group are hydrogen bonded with probably multiple hydrogen bond donors available at the same time. It is widely accepted that the nucleophile is more efficiently solvated and stabilised in protic solvents. Thus water has also been used as solvent in a continuum model, added to the complex constituted by a DMF molecule and the reactants. Introducing water as continuum allows the barrier for the S_N2 reactions to decrease to the same extent as in calculations using DMF as continuum. In the nucleophilic attacks to the iminium moiety, when water as continuum was used, the energy barrier of both steps compared to the barriers where DMF as continuum was used, are higher by 1 kcal mol^{-1}.

2.7 Conclusions

Understanding the role of cyclisation reactions in organic chemistry is a very valuable opportunity because it can put light on old concepts from a different perspective. In nature enzymes adapted themselves in order to become more efficient where cyclization reactions were involved. In this chapter the relationship between nucleophilicity and steric effect has been examined, along with the role they play in cyclization reactions in which their favourability have been empirically predicted by a set of rules given by Baldwin about 30 years ago. From these findings the nucleophilicty prevails when the cyclisation are analysed in GPH, while with the inclusion of the solvent effect as a mix of explicit (one molecule of DMF) and implicit solvation (bulk electrostatic effect in PCM for DMF) the steric effect starts to prevail over the nucleophilicity. Challenging problems in computational chemistry are still waiting to be tackled such as situations where the thermodynamics of multi step reactions which differ for loss of protons or other species, at different stages, have to be compared. This will be a particular challenge, especially if in solution.

3

The Hydride transfer reaction in the DIP synthesis reaction path : a theoretical study

3.1 Hydride transfer reaction mechanism

Hydride transfer reactions are important in chemistry and biochemistry, although they are less common than proton transfer reactions.[69,70] In carbocation chemistry, intramolecular transannular and 1,2-hydride shifts are common and competitive with other processes, especially when the rearranged cation is at least as stable as the original. Industrially relevant intermolecular hydride transfer reactions include those from hydrocarbon donors to carbocations. McDonough and Dauben[71] worked on solution phase hydride transfer that involved highly stabilized carbenium ions, and Arnett[72,73] carried out calorimetric studies yielding heats of reaction for hydride transfer to these ions from cycloheptatriene and cyanoborohydride ions.

In organic synthesis useful carbon-to-carbon hydride transfers include the Clarke-Eschweiler and Leuckart reductive alkylations of amines, the Cannizaro and Tishchenko reactions, the Meerwein-Pondorf-Verley reduction, the Oppenauer oxidation and others.[74]

In biochemistry, redox reactions associated with hydride transfer processes play a leading role in many enzymatic systems.[75] Enzymes that belong to the flavoprotein reductase family, e.g. glutathione reductase, thiroedoxin reductase, or lipoamide dehydrogenase among others, present two common aspects:

1. Structural, because two coenzyme-dependent dehydrogenases are involved, NAD+/NADH and FAD/FADH2

2. Mechanistic, because of the presence of a hydride transfer step from the carbon atom of NADH to the nitrogen atom of the flavin isoalloxazine ring, FAD in the catalytic mechanism.

Computational modelling work on the hydride transfer transition state to carbonyl acceptors is abundant; the transfer of hydride from methoxide anion to formaldehyde is often used as a model system. Gronert and Keeffe[76] studied identity hydride-ion transfer from C-H donors to C acceptors, comparing those reactions with identity proton transfer reactions. These authors reported for the hydride transfer reactions that:

- Partial bonds between the transferred hydrogen and the donor and the acceptor carbons are computed to be shorter than when a proton is transferred on average by about 0.1 Å

- The angle formed by the two terminal carbons and the transferred hydrogen is often far from linear, contrasting with proton transfers where the angle lies between 175°and 180°.

- The curvature of the energy surface along the reaction coordinate in the vicinity of the transition state is sharper for proton transfers, leading to larger imaginary frequencies than for hydride transfers. The isotopic ratio of imaginary frequencies, $i\upsilon_H / i\upsilon_D$, is larger for proton transfer transition states than for hydride transfer transition states.

- The primary semi-classical KIE (KIE = kinetic isotope effect) is smaller for hydride transfer than for proton transfer.

A net hydride transfer involves the transfer of two electrons and one proton, so in principle, is a type of proton-coupled electron transfer (PCET) reaction. In the mini-review by Hammes-Shiffer,[77] a hydride transfer reaction is defined as a reaction where proton and electrons are transferred between the same donor and acceptor, as opposed to PCET,[78] a reaction involving the transfer of proton and electrons between different centers. In spite of the complexity of the hydride transfer reaction as described above, Swain, Wiles and Bader[79] gave a simple pictorial description based on molecular orbital theory, that offers some insight into the differences between the hydride transfer reaction and the proton transfer reaction. Put simply:

- In proton transfer reactions the wave function at the terminal centers in the HOMO (negatively charged) is out of phase, thus generating an antibonding interaction.

- In hydride transfer the wave function at the terminal centers in the HOMO is in phase allowing for a bonding interaction which can be improved if those sites are closer.

In the first part of this chapter we analyse the hydride transfer reaction between TIP and DIP where TIP is differently substituted with electron withdrawal and electron donor groups. The hydride transfer reactions considered are also analysed through reactivity descriptors. In the second part, we study the solvent effect on the electronic excitations of reactants and products of the hydride transfer which has been calculated using the TDDFT method. The TDDFT method although currently presenting several limitations has been employed because it still presents the best computational cost/accuracy ratio.

3.1.1 Computational methods

The TIP molecule (hydride donor), can be prepared starting from different nucleophiles that attack the phenanthridinium moiety which result in different substituents that give to the hydride donor different characteristics. Computationally, the hydride transfer has been studied when the following nucleophiles were employed:

1. ammonia
2. isopropylamine
3. methylamine
4. hydroxylamine
5. fluorophenylamine
6. difluorophenylamine
7. fluoromethylamine
8. difluoromethylamine
9. trifluoromethylamine

In fig 3.1 are shown reactants and products of the hydride transfer reaction studied. Only TIP molecules with nucleophiles 1,2,3 have been experimentally prepared. In order to search for a transition state the simplest way is trying to guess its shape by assuming that every atom is linearly moved between the position where it start and the position where it ends. This linear motion approximation is termed linear synchronous transit (LST). The method adopted in these calculations for the location of the transition structure is the extension of the LST method and is called quadratic synchronous transit method (QST).[80] The QST method considers that the atoms in the transition structure are located along a parabola between

reactants and products. In this specific case the QST3 method has been chosen where the input structures were reactants, products and a guess of the transition structure. Reactants and products have been found exploring the energy along the eigenvector corresponding to the imaginary C-H stretching frequency. It has not always been possible to terminate successfully the optimisation and achieve a minimum on the PES. The optimisation therefore for some structures, has been stopped due to slow convergence of forces after a certain number of steps (60-90 cycles) when the energy changes between cycles were of the order of 10^{-6} a. u.. The functional employed is B3LYP[81] and the basis sets used are the Stuttgard-Dresden basis set (SDD) on the bromine atom and the 6-31G* Pople basis sets on the other atoms.

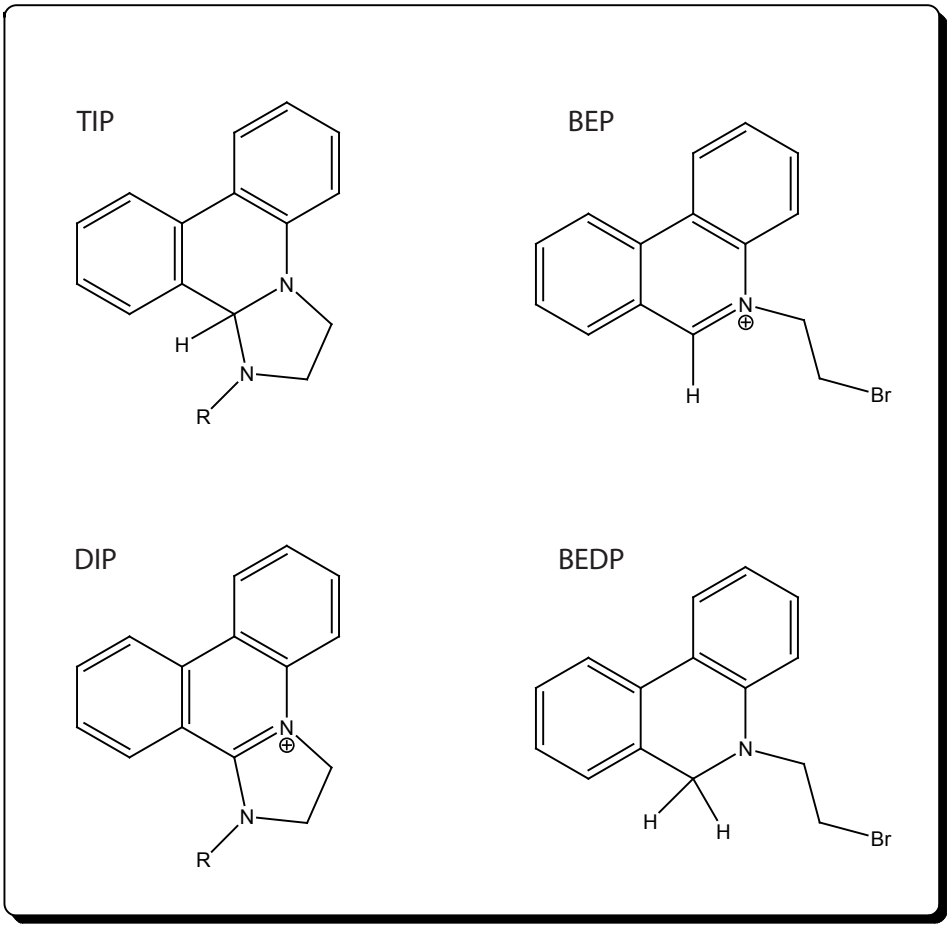

Figure 3.1: Molecules involved in the hydride transfer reaction. TIP reacts with BEP resulting in a hydride transfer that produces DIP and BEDP.

3.1.2 Characterisation of the hydride transfer reactions through the Hammond Postulate and chemical reactivity indexes

Chemical reactions can be viewed as an electron density redistribution along a reaction coordinate that can be described through Density Functional Theory. This electron redistribution can be interpreted through chemical reactivity indexes, in this section the chemical potential (μ) and the molecular hardness[82] (η) have been analysed for such reactions. The Hammond Postulate (HP) is another useful tool that helps to understand chemical reactions and correlate the position of the energy barrier along the PES with the endothermicity or exothermicity of a defined reaction. The HP states that if a TS is close in energy to a stable complex, it will have a similar structure. Thus, an exothermic reaction has a reactant-like TS, while an endothermic reaction has a product-like TS. The quantification of the Hammond Postulate can be done through a structural proximity parameter developed by Cioslowski which is defined by :

$$\beta_s = (d_{A,TS} - d_{B,TS})/d_{A,B} \tag{3.1}$$

β can have values between -1 and 1; $d_{A,TS}$ is the distance between reactants and TS, $d_{B,TS}$ is the distance between products and TS. If the reactants A are closer to the TS than the products B, the value of β_S is negative, and positive otherwise. β_s therefore is an index that helps to characterize the reactant-like or the product-like character of the TS. The electronic chemical potential (μ) expresses the tendency of electrons to escape from the equilibrium system. Electrons flow from places with higher chemical potential to places with lower chemical potential until the point where μ becomes constant through the space. The molecular hardness (η) can be seen as the resistance to charge transfer. Therefore, it is possible to discuss the thermodynamic and kinetic aspects of a given reaction through μ and (η) which

have been defined by the following expressions :

$$\mu = -\frac{1}{2}(IP + EA); \eta = \frac{1}{2}(IP - EA) \tag{3.2}$$

IP and EA are the first vertical ionization potential and electron affinity of the neutral molecule, respectively. Koopmans theorem, in which : IP $\approx -\epsilon_H$; EA $\approx -\epsilon_L$ allows μ and η to be written in terms of the energy of HOMO (ϵ_H) and LUMO ϵ_L molecular orbitals

$$\mu = -\frac{1}{2}(\epsilon_H + \epsilon_L); \eta = \frac{1}{2}(\epsilon_L - \epsilon_H) \tag{3.3}$$

The principle of maximum hardness has been expressed by Pearson[83] in the following terms: *there seems to be a rule of nature that molecules arrange themselves so as to be as hard as possible*, and later demonstrated by other authors by statistical mechanical methods. Through the demonstration of this principle it has been shown that at constant chemical potential, as the total energy increases, the hardness decreases, and as the total energy decreases, the hardness increases. A maximum in the energy corresponds with a minimum in the hardness and a minimum in the energy corresponds with a maximum in the hardness.

The change of hardness between reactants and products provides insight for the description of the thermodynamic aspects of chemical reactions :

- In endothermic reactions, $\eta_R > \eta_P$
- In exothermic reactions, $\eta_R < \eta_P$
- In isoenergetic reactions, $\eta_R = \eta_P$

Thus, η should increase in going from the TS to either reactants or products. A connection between the HP and the principle of maximum hardness can be expressed by the following rule elaborated by Datta (1992):[84] *chemical reactions tend to go in the direction that produces the hardest species.*

R_1=CH_3CHCH_3	Reactants	TS	Products
E	-1454.8127	-1454.7860	-1454.8377
ΔE	0	16.75	-32.34
ϵ HOMO	-0.2967	-0.3008	-0.3045
ϵ LUMO	-0.1993	-0.1931	-0.1840
μ	-0.248	-0.247	-0.244
η	0.049	0.054	0.029
β_s		-0.073	
R_H	1.31	0.00	1.52

Table 3.1: In this table we show the energy of HOMO (eV), LUMO (eV) orbitals, the electronic chemical potential μ (eV),the molecular hardness η (eV), the structural proximity parameter β and R_H which is the distance between reactants and TS for NH_2R and between products and TS where R= CH_3CHCH_3

The hydride transfer reaction studied is the following: TIP + BEP $\leftarrow$ DIP + BEDP, in presence of Et_3N and with DMF as solvent. Tables 3.1, 3.2, 3.6, 3.5, 3.4, 3.3, 3.7, 3.8 show the calculated reactivity indexes, the structural proximity parameter, electronic energy and the frontier orbitals for the hydride transfer reactions for the substituents in the hydride donors mentioned above (except R=H). The R_H values represent in these tables the distance of the hydride ion in the transition state structure from the reactants and the products.

All the exothermic reactions studied show a negative structural proximity parameter, with the exception of R6 in which this parameter is 0. The isoenergetic reactions R4 and R5 instead show a slightly positive value. Therefore it is possible to say that there is a good correlation between the thermodynamics of such reactions and the position of the energy barrier along the reaction coordinate. The HP postulate therefore holds for such reactions. Turning to the analysis of the hardness, immediately it is possible to see that all transition states with exception of

R_2=CH_3	Reactants	TS	Products
E	-1376.1851	-1376.1595	-1376.2118
ΔE	0	16.06	-32.82
ϵ HOMO	-0.2774	-0.3021	-0.2745
ϵ LUMO	-0.2169	-0.1949	-0.1935
μ	-0.247	-0.248	-0.234
η	0.03	0.053	0.04
β_s		-0.062	
R_H	1.32	0.00	1.49

Table 3.2: Data shown as in table 3.1, for R= CH_3

R6 CH_2F	Reactants	TS	Products
E	-1475.4272	-1475.4008	-1475.4395
ΔE	0	16.57	-7.72
ϵ HOMO	-0.3032	-0.3059	0.3017
ϵ LUMO	-0.2009	-0.1997	0.1983
η	0.051	0.053	0.052
β_s		0.00	
μ	-0.252	-0.253	-0.25
R_H	1.38	0.00	1.41

Table 3.3: Data shown as in table 3.1, for R= CH_2F

R5 CHF_2	Reactants	TS	Products
E	-1574.6729	-1574.6420	-1574.6716
ΔE	0	19.39	-0.81
ϵ HOMO	-0.3046	-0.3058	-0.3021
ϵ LUMO	-0.2014	-0.2006	-0.2027
η	0.051	0.052	0.050
β_s		0.02	
μ	-0.253	-0.253	-0.252
R_H	1.43	0.00	1.37

Table 3.4: Data shown as in table 3.1, for R= CHF_2

R4 CF_3	Reactants	TS	Products
E	-1673.9184	-1673.8870	-1673.9184
ΔE	0	19.70	0
ϵ HOMO	-0.3086	-0.2909	-0.3064
ϵ LUMO	-0.2054	-0.1923	-0.2069
η	0.051	0.049	0.050
β_s		0.02	
μ	-0.257	-0.242	-0.256
R_H	1.43	0.00	1.37

Table 3.5: Data shown as in table 3.1, for R= CF_3

R3 OH	Reactants	TS	Products
E	-1412.037	-1412.0095	-1412.0669
ΔE	0	17.26	-36.02
ϵ HOMO	-0.2806	-0.2997	-0.3068
ϵ LUMO	-0.2197	-0.1897	-0.1998
η	0.03	0.055	0.053
β_s		-0.045	
μ	-0.250	-0.245	-0.253
R_H	1.34	0.00	1.47

Table 3.6: Data shown as in table 3.1, for R= OH

R_7=C_6H_4F	Reactants	TS	Products
E	-1667.1796	-1667.1256	-1667.1483
ΔE	0	33.88	-19.64
ϵ HOMO	-0.2971	-0.300	-0.2949
ϵ LUMO	-0.1967	-0.196	-0.2036
η	0.050	0.052	0.046
β_s		-0.055	
μ	-0.247	-0.248	-0.249
R_H	1.31	0.00	1.46

Table 3.7: Data shown as in table 3.1, for R= C_6H_6F

R8 $C_6H_3F_2$(F meta)	Reactants	TS	Products
E	-1766.3799	-1766.3555	-1766.4083
ΔE	0	15.31	-17.82
ϵ HOMO	-0.2789	-0.3021	-0.2661
ϵ LUMO	-0.2197	-0.2002	-0.1913
η	0.030	0.050	0.037
β_s		-0.065	
μ	-0.249	-0.251	-0.229
R_H	1.32	0.00	1.45

Table 3.8: Data shown as in 3.1, for R= $C_6H_6F_2$

R4, have higher hardness than reactants and products, thus violating the principle of maximum hardness, perhaps because of the basis sets employed. However in general for all the exothermic reactions with exception of R1 and R6, the hardness of the reactants is lower than the products which underlines the rule elaborated by Datta. In the isoenergetic reactions in R4 and R5 (R5 is almost isoenergetic) the hardness of reactants and products is similar, as would be expected. The hardness found for the TSs is unusual because in general the hardness of a TS in a exothermic reaction should be close to the hardness of the reactants and viceversa. The chemical potential, with the exception of R3 and R7, is lower for the reactants than the products which seems counterintuitive, but several computational approximations have been made in these calculations in which substantial errors can be very common.

The correlation between the structural parameter β_s of the transition states and the reaction thermodynamics can be seen in Fig 3.3 in which the correlation between the position of the hydride atom and the thermodynamics of the reaction is evident. Correlation between the electronic chemical potential μ and energy of the calculated TSs is shown in fig 3.2 A, while correlation between hardness η and

TSs energy is shown in fig 3.2 B.

From such results it is possible to conclude that in general hydride transfer reactions in which an electron donor group such as a CH_3 or a OH is present on the hydride donor (TIP), the reaction is kinetically more favorable with an "early TS" than those when electron attractor groups like CF_3 are present.

3.2 Quantum mechanical aspects of the interaction between radiation and molecules

The time dependent DFT method can simulate accurately the interaction between electromagnetic radiation and a molecule which experiences a transition under such perturbation. The strongest transition that this molecule experiencs is caused by the interaction of the electric vector of the radiation with the electric dipole moment of the molecule. The magnitude of the electric dipole moment depends on the spatial properties of the molecule's wavefunction involved in this transition. If there is a significant charge separation between the ground and the excited state, there will be a strong interaction between molecule and radiation. The entity of this interaction is defined by the scalar product of the electric field and dipole moment vectors. The molecular Hamiltonian correlated with the interaction, can be expressed as perturbation of the ground state Hamiltonian. Thus the total Hamiltonian can be written as: $\hat{H}_{total} + \hat{H}'$. During the application of the field the molecular wavefunction passes from a state m to a state n. One way to analyse such a transition is to imagine that the molecule is in both states at the the same time and the probability for each state varies during the transition, thus the wavefunction can be assumed to be a superposition of states: $\psi = a_m\psi_m + a_n\psi_n$. The coefficients a_m and a_n are time dependent. Before the transition a_m=1 and a_n=0, after the transition a_m=0 and a_n=1. The progress of the transition can

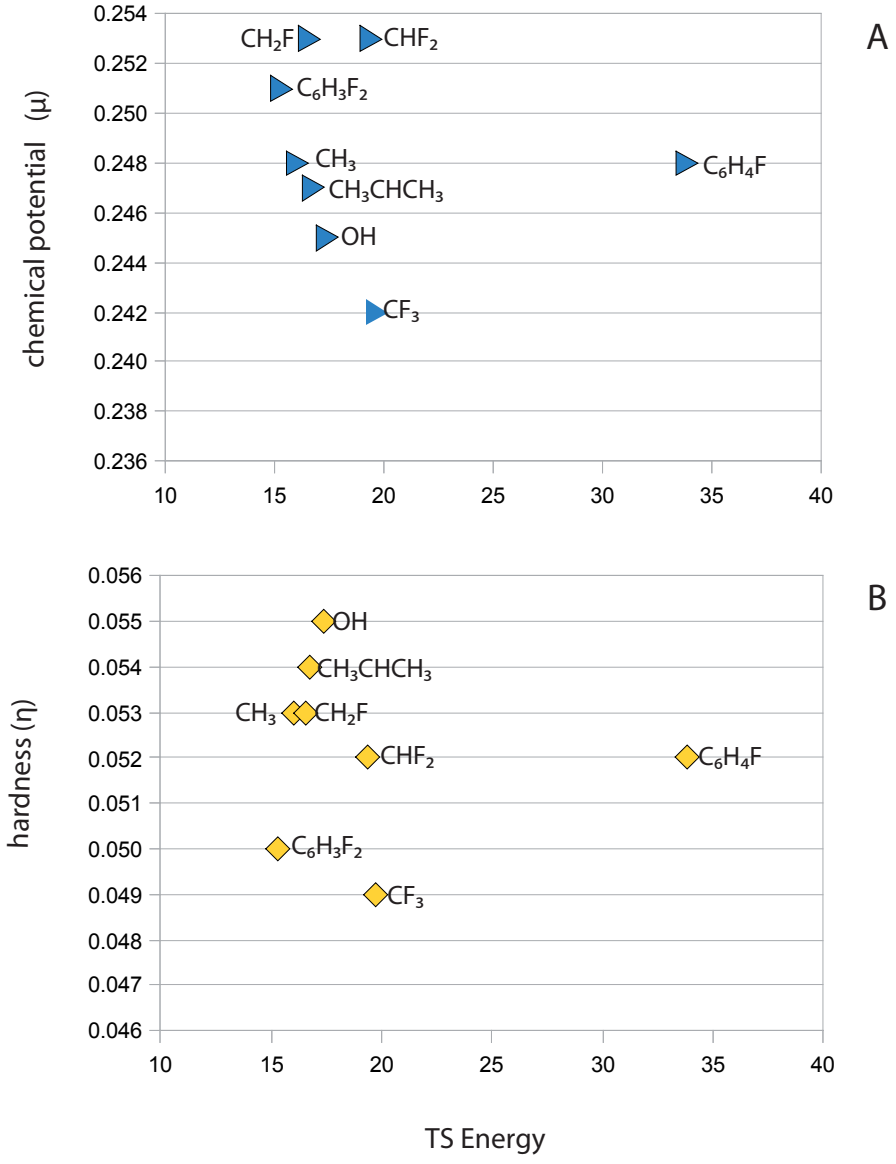

Figure 3.2: In A is shown the correlation between electronic chemical potential μ and the TSs energies. In B is shown the correlation between hardness η and the TSs energies. Values of μ and η are in eV, while TSs energies are in kcal mol^{-1}.

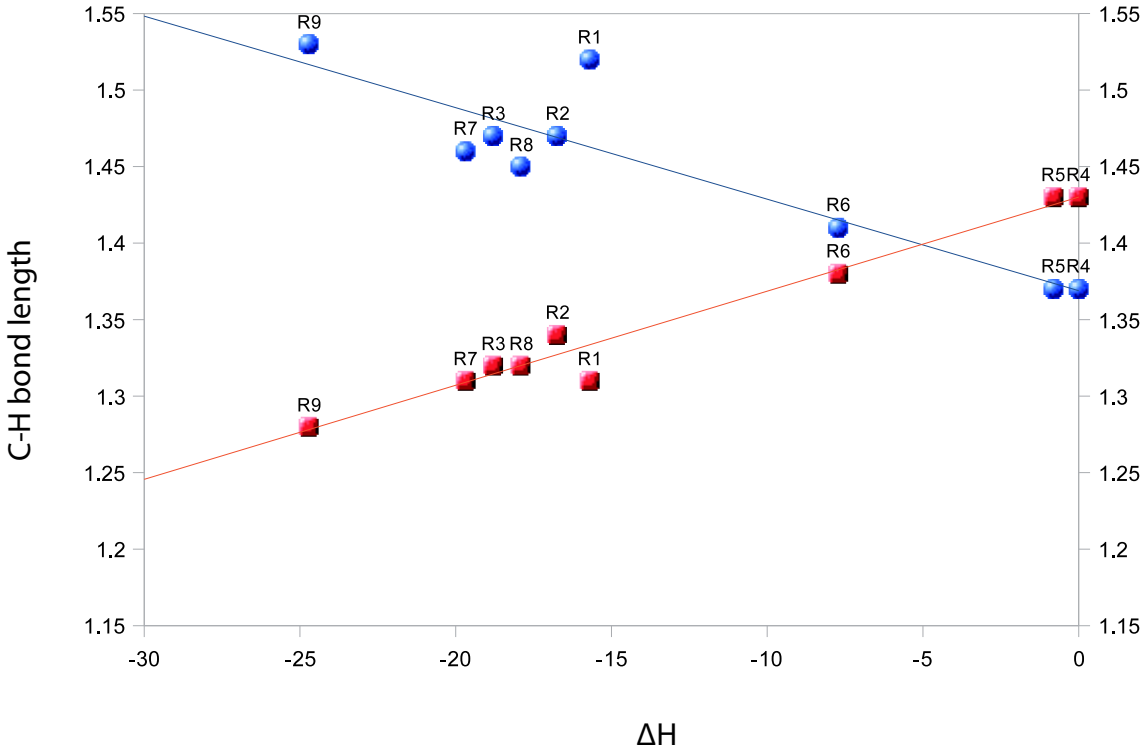

Figure 3.3: Correlation between R_H and the thermodynamic of the reaction. Red squares show the distance in the transition state (R_H) between the hydride and the hydride donor, the blue circles show the same for the hydride acceptor

be quantified by the probability (P_n) that the molecule is in the state ψ_n. This probability could be defined also as $P_n = a_n * a_n = |a_n|^2$. The transition probability is also expressed as in equation 3.4

$$P_n = \frac{4E_0^2|\mu_{nm}|^2}{\hbar^2}\frac{sin^2\frac{1}{2}\Delta\omega t}{\Delta\omega^2} \tag{3.4}$$

In equation 3.4 μ_{nm} and E_0 are the dipole moment vector and the electric field along the three coordinates. $\Delta\omega$ is the frequency difference between the transition frequency and the radiation frequency. Such expression gives the factors that determine the transition probability. When the radiation frequency is close to the transition frequency, it becomes resonant with the transition frequency allowing a rapid increase during time of the transition probability. Equation 3.4 indicates that the transition probability is directly proportional to the square of the transition dipole moment and its magnitude depends on the nature of the electronic charge

redistribution associated with the transition. The transition dipole moment μ_{nm}, therefore creates a connection between the nature of the electronic structure and the transition intensity. The factorization of μ_{nm} with consideration of the Born-Oppenheimer approximation is : $\psi = NS$ in which ψ is the electronic spatial wavefunction, N is the nuclear wavefunction and S the electronic spin wavefunction. It is therefore possible to take out of the transition dipole moment integral the electronic spin and the nuclear wavefunctions, thus :

$$\langle \psi_n | \mu | \psi_m \rangle = \langle \psi_n | \mu | \psi_m \rangle \langle S_n | S_m \rangle \langle N_n | N_m \rangle \tag{3.5}$$

The transition dipole moment obviously is zero if one of these quantities is equal to zero. The nuclear or vibrational overlap integral when squared is often called the Franck-Condon factor that tells which of the possible excited vibrational levels of the electronically excited state will be populated in the transition. The spin overlap integral tells which of the possible spin orientations will allow a transition. In general in organic molecules the spin selection favours singlet-singlet transitions and forbids singlet-triplet transitions which have a zero spin overlap integral.

3.3 Spectroscopy Basics

Spectroscopy in the gas phase allows individual rotovibronic transitions to be observed at high resolution while in the liquid phase the electronically excited molecules have many collisions and interactions with the solvent molecules with a resulting spectrum broadening correlated with a rapid redistribution of population with disappearance of the individual rotovibrational states. The experimental measurement of the absorption spectrum follows the Beer-Lambert law:

$$I = I_0 e^{-kcl} \tag{3.6}$$

which defines the intensity of the radiation that is transmitted through the sample. I_0, is the incident radiation intensity, k is the wavelength-dependent molar absorp-

tion coefficient, c is the molar concentration and l is the length of solution the light passes through. The above expression can be rearranged as: $-ln(I/I_0) = kcl$. In general reference is given to the decadic molar absorption coefficient ϵ in the expression $-ln(I/I_0) = \epsilon cl$. ϵ is a function of the radiation frequency. In general the value of ϵ is reported at the wavelength or wavenumber of maximum absorption ϵ_{max} for a given spectral feature. ϵ_{max} is correlated to the intensity of the transition but a better measure of the transition intensity is obtained by integration of ϵ over the whole absorption feature. The integrated absorption coefficient A is given by

$$A = \int_{band} \epsilon \tilde{d}\upsilon \tag{3.7}$$

giving a connection between the experimental spectrum and the theoretical quantity that is the oscillator strength f_{nm} for the transition. The oscillator strength determines the strength of the electric dipole transition compared to that of a free electron oscillating in three dimensions. The oscillator strength assumes a value equal to unity when the electric dipole transition is close to that of the oscillating free electron. The formula that highlights the relation between A and f_{nm} is shown in equation 3.8 :

$$f_{nm} = \left[\frac{4\epsilon_0 m_e c^2 ln(10)}{N_A e^2}\right] A \tag{3.8}$$

The connection between the oscillator strength and the transition dipole moment is given by equation 3.9 :

$$f_{nm} = \left[\frac{8\pi_2 m_e c}{3e^2 h}\right] \tilde{\upsilon}_{nm} |\mu_{nm}|^2 \tag{3.9}$$

$\tilde{\upsilon}_{nm}$ is the wavenumber of the transition that is equivalent to $\tilde{\upsilon}_{max}$. The physical constants in the formula above can be collected into the value $4.70210^{-7} D^{-2}$, therefore, equation 3.9 can be simplified as :

$$f_{nm} = 4.70210^{-7} D^{-2} \tilde{\upsilon}_{nm} |\mu_{nm}|^2 \tag{3.10}$$

3.4 The TD-DFT method and its limitations

Time dependent density functional theory (TDDFT) has become an important method for the calculation of excited state energies in chemistry with the capacity of predicting a very large variety of phenomena; electronic excitations are just an example of the power of this method. There are phenomena which can be analysed such as double excitations, second ionization thresholds, optical response of solids, band gaps in solids, transport through single molecules. This method however contain different sources of error that are correlated to the underlying DFT ground-state calculation, because if the Kohn-Sham orbital energies are in significant error, the TDDFT procedure cannot produce accurate results. In properties that require nonlocality on the exchange-correlation potential, the TDKS non-interacting wavefunction can be very different from the KS wavefunction with therefore inaccurate observables calculated.

TDDFT has been demonstrated to be inaccurate with production of inaccurate KS eigenvalues that are insufficiently negative, in the case where standard density functionals like LDA,GGA, and hybrids are used. The reasons for this are connected with poor asymptotic behaviour with an exponential decay of the KS potentials.[85] TDDFT has been proved quite accurate for non charge transfer valence excited states, but, for instance, in problems of particular interest in biochemistry such as intermolecular charge transfers significant errors are present due to the locality of the exchange and Correlation (XC) potential.The underlying reasons for errors in calculation of CT valence excited states are correlated with the orbital energies that from a DFT calculation suffer from the self-interaction term (SI). This error is related to the Coulomb interaction term in which all occupied orbitals are

contained in the orbital energy with inclusion of the orbital under consideration itself[86].[87]

In Hartree-Fock theory this is not a problem, because the exact exchange guarantees an exact cancellation of the artificially introduced error. In DFT, on the other hand, the HF exchange is replaced by an approximate XC-potential which does not cancel the self-interaction error in the Coulomb part correctly. In the excitation energies of non-CT states which do not require a change in electron numbers on independent subsystems, the SI error is of the same order of magnitude for the occupied and virtual orbitals. In a CT state the excitation energy is given by the difference of electron-donating and electron-accepting orbitals. When a functional such as BLYP where the exchange term =0 is utilised, the potential energy curves of CT states do not exhibit the correct 1/R shape as a function of the reaction coordinate. The correct asymptotic behavior can be obtained when nonlocal HF exchange is used as in hybrid functionals. In order to gain a more accurate excitation energy of the energetically lowest CT state,Dreuw et all (2003)[88] employed a hybrid approach to study a (1,4)-phenylene-linked zincbacteriochlorin-bacteriochlorin complex (ZnBC-BC) and a bacteriochlorophyll-spheroidene complex (BChl-Spher), that consisted of TDA/BLYP calculations for the valence excited states and CIS calculations for the energetically lowest CT states, shifting the curve by a ΔDFT value. In this method the correct asymptotic behaviour of the potential energy curve of the lowest CT states is given. TDDFT alone for both complexes was found to underestimate drastically the lowest CT states by few electron volts, therefore the authors pointed out that for large systems such as those analysed in this work, method requires experience and knowledge of the investigated system in order to gain accurate results. Peach et al. (2008)[8990] investigated further this problem employing a series of molecules in which CT excited states could occur in order to :

- assess the quality of TD-DFT excitation energies from selected GGA, hybrid and Coulomb attenuated functionals
- correlate the excitation energy errors for local, intramolecular CT,and Rydberg states with spatial overlap between the occupied and the virtual orbitals involved in the excitations for all three categories of functionals.

The functionals considered are PBE,[91] B3LYP[81] and CAM-B3LYP, the latter containing just 19% of exact exchange at short range but 65% at long range. The performance of these functionals shows that for local excitations B3LYP is a clear improvement over PBE, the CAM-B3LYP provides a mean absolute error (MAE) similar to B3LYP, but the maximum energies are slightly higher, while for both Rydberg and CT excitations, the improvement from PBE to B3LYP to CAM-B3LYP is very clear. The quantification of the correlation between the excitation energy errors and the spatial overlap between the (unperturbed) occupied and virtual orbitals involved in the excitation is given by calculating the factor Λ. In order to define Λ it is necessary to determine the spatial overlap O_{ia} and K_{ia} which delineate the contribution of each pair of orbitals to a given TDDFT excitation. The spatial overlap for a given occupied orbital ϕ_i and virtual orbital ϕ_a can be measured as the inner product of the moduli of the two orbitals,

$$O_{ia} = \langle|\phi_i||\phi_a|\rangle = \int |\phi_i(r)||\phi_a(r)|dr \tag{3.11}$$

K_{ia} is given by the sum of X_{ia} and Y_{ia} which are elements of the solution vectors of the non-Hermitian eigenvalue problem in the TDDFT scheme for Kohn-Sham orbitals. Λ therefore can be calculated with equation 3.12

$$\Lambda = \frac{\sum_{ia} K_{ia}^2 O_{ia}}{\sum_{ia} K_{ia}^2} \tag{3.12}$$

In equation 3.12, $0 \leq \Lambda \leq 1$. A low value of Λ means a long range excitation and a large value means a short range excitation. $\Lambda = 0$ in intermolecular CT excitations, which explains further the findings of Dreuw et al in TDDFT calculations

with DFT functionals in which the nonlocal HF exchange was not incorporated. In conclusion, the performance of a TD-DFT functional for defined excitation energies can be checked through the spatial overlap between orbitals. The failure of TDDFT for the determination of the intermolecular CT excited states can be explained as a lack of overlap in the orbitals involved in these excitations.

3.4.1 TDDFT studies of organic dyes and stacked compounds

TDDFT has been widely used in order to assess the accuracy of different DFT functionals and get more insights into the systems analyzed. Jacquemin et al. (2008)[92] assessed the efficiency of several functionals in the reproduction of UV-vis spectras for the $\pi \rightarrow \pi*$ transitions in more than one hundred organic dyes. The principal classes of dyes analyzed were azobenzenes, anthraquinones, indigos and diarylethenes.[93] The functionals examined were PBE, PBE0, CAM-B3LYP, LC-PBE, LC-ωPBE. The author shows that the PBE0 functional gives the smallest error followed by CAM-B3LYP that suffers from larger deviations but appears efficient in calculating the properties of dyes with a very delocalized excited state. Jacquemin et al. (2006)[94] in a previous work found the PBE0 functional quite accurate in determining the UV-vis spectra of 21 nitrodiphenylamine dyes in various solvents. The C-PCM model was included in those UV-vis predictions. In this work the authors found a very good correlation between experimental and calculated Λ_{max} . It was also noted that for these phenylamines the main transition was correlated with a $HOMO \rightarrow LUMO$ transition and in particular when one or more nitro-groups were introduced into these compounds, this excitation was corresponding to a CT excitation with the electron density moving from the phenyl rings to the electroactive side group during the absorption process. The PBE0 functional has been confirmed to be quite accurate also by Wathelet et al

(2006)[95] with predictions of the Λ_{max} of more than 100 compounds with a conjugate carbonyl chromophore. Anthraquinone dyes have been studied in another work of Jacquemin et al. (2006)[96] where the B3LYP and PBE0 functionals have been compared. The absorption spectra in this work were computed with the PCM model for ethanol and methanol. The authors found that both functionals gave similar results but with opposite errors, the PBE0 overestimating, while the B3LYP underestimates the Λ_{max}. The error determined can be decreased by statistical treatment of the theoretical data. Fluoroanthraquinones have been studied with B3LYP and PBE0 functionals by Preat et al.(2007)[97],[98] but in this case a multilinear regression scheme has been used to combine the B3LYP and the PBE0 results giving a better agreement with respect to the experimental results than any of the two functionals taken separately. This study reveals that the solvents lead to a bathochromic shift of the UV-vis spectrum. The structural sensitivity to the solvent decreases in the large systems analyzed with a possible explanation that the accessibility of the dye chromophoric and auxochromic units by the solvent molecules is lower for sterically jammed compounds or when bulky ligands are alongaside the chromophoric unit. The derivatives including sulfur atoms in their heterocyclic ring display a non-planar structure, but because of the high polarizability of the sulfur atom, these dyes show the largest bathochromic shift. Intramolecular hydrogen bonds strongly influence the geometries, charges, and therefore the excitation energies of these compounds. The PBE0 functional has been proven accurate also in the determination of the UV-vis spectra of poly(l-glutamic)acid modified with a chromophoric azobenzene side chain,[99] proving to be able to predict geometries and absorption wavelengths in good agreement with the experimental results. The author analyzed the system above studying the isolated chromophoric unit and then when this was bound to the poly(l-glutamic)acid chain. The azobenzene studied isomerizes from the trans to the cis isomer after irradiation at 350 nm with a $\pi \rightarrow \pi*$ transition, whereas the reverse reaction is

promoted by a 450 nm irradiation with a $n \rightarrow \pi*$ transition. The UV-vis spectrum has been well reproduced in gas phase and in ethanol, which consist for the cis conformer of a low lying $n \rightarrow \pi*$, allowed only in the cis derivative due to its non-planar geometry, and a $\pi \rightarrow \pi*$ transition. The bathochromic effect of the solvent on the $\pi \rightarrow \pi*$ excitation has been well reproduced. The effect of the different polypeptide stable conformations such as α helix and β sheet on the UV-vis spectra of the azobenzene derivatives show that the $\pi \rightarrow \pi*$ absorption energies are all red-shifted. This effect can be attributed to the auxochromic shift of the amide group used to link the azobenzene moiety to the carboxylic group. A blue shift has also been observed on the $n \rightarrow \pi*$ excitation that corresponds to a stabilization of the ground state compared to the excited state and derives from the interaction of the carboxylic acid hydrogen atom of the glutamic acid chain and the lone pair of the N=N unit of the trans-azobenzene moiety. Jacquemin et al. studied the $n \rightarrow \pi*$ excitation for a series of azoalkanes (2008)[100] and of thiocarbonyl dyes (2006). This transition normally corresponds to the first singlet excitation with the implication that the HOMO and LUMO frontier orbitals are localized on the two nitrogens. The PBE0 functional with the PCM model has been proved accurate when the results have been compared with experimental data, except in the case of azomethane. In order to understand more in detail the reasons for this failure, two explicit water molecules have been introduced in that model with a reduction of the difference between theory-experiments by a factor of three. The author showed that the PBE0 functional is accurate enough in predicting the $n \rightarrow \pi*$ transition that normally is hidden by a strongly dipole-allowed $\pi \rightarrow \pi*$ band with the introduction of the solvent as PCM model, except in the case of the azomethane due to the lack of explicit solute-solvent hydrogen bonds. The author compared the performance of B3LYP and PBE0 functionals in predicting the $n \rightarrow \pi*$ transitions of thiocarbonyl dyes. The B3LYP functional gave a Λ_{max} that better agreed with the experimental results, while when a linear regression

procedure has been applied there was a negligible difference between these two functionals. Thioindigo dyes have been investigated by Jacquemin et al.(2005).[101] In this investigation, for 170 thioindigo dyes, the agreement between theoretical and experimental Λ_{max} is exceptional. The solvent plays an important role in determining the Λ_{max} value that for thioindigo is consistently larger in $CHCl_3$ and CCl_4 than in ethanol or DMF while in indigo dyes the phenomenon is reversed. The different solvatochromism for these two classes of dyes can be explained by the strong hydrogen bonds between the ethanol and the carbonyl group in indigo dyes with weakening of the C=O double bond strength that allows an easier excitation and an unusual solvation process with "polar" chlorine or the formation of hydrogen bonds between the sulfur atoms and ethanol that compensates for the dielectric effect. In this study the excitation related to Λ_{max} corresponds to the $\pi \rightarrow \pi*$ transition where the HOMO lies on the sulfur atoms and the central C=C double bond, whereas the LUMO is centered on the single C-C bonds and oxygen atoms. Woodford (2005)[102] used the TDDFT method to give more insights on the Lewis structures for the ground state of anthocyanidin molecules. The TDDFT method applied to the equilibrium geometry of these molecules showed that the first excited state is determined by the HOMO to LUMO transition and a HOMO-1/HOMO-2 to LUMO transition. The author justified the different Lewis structures proposed by the electronic resemblance of the anthocyanidin molecules to the biphenyl molecule rather than the naphthalene. The biphenyl molecule is twisted in its ground state and does not show delocalization of its π electrons. The resonance structures indicated by the author show the positive charge localized alternately on C_2 and C_4. That suggestion is consistent with the structural data obtained, in fact the non-zero inter-ring torsion angles demonstrates that this system cannot delocalize the π electrons over all three rings.

3.4.2 The TD-DFT method and π-stacking interactions.

The TD-DFT method has been used to study stacked DNA bases. Varsano et al.(2006)[103] investigated the absorption spectra of five isolated nucleobases and their assemblies that resemble simple Watson-Crick pairs, π-stacks of two bases and π-stacks of GC base pairs. The calculated spectra of the single bases are in agreement with previous theoretical studies and with experiment, reproducing the ordering of the π $\pi*$ transitions with the HOMO orbitals that are of π-type for the purines and of σ-type for the pyrimidines, while the LUMO is always of π-type. With regard to the base assemblies, the presence of π stacking and hydrogen bonding interactions does not alter the absorption spectrum significantly. However, hypochromicity into the higher energy part of the spectrum can be observed which is greater when induced by the π stacking interactions, than by hydrogen bonding. The HOMO and LUMO states are delocalised on both purines and pyrimidines in the stacked case, while when hydrogen bonding is present, the HOMO is in the purine and the LUMO on the pyrimidine which denotes a charge transfer excitation. Santoro, Barone and Improta (2008)[104] gave more insights into the previous work on the excited state behaviour of the stacked cytosine dimer. The authors show in this work that the TD-DFT method is reliable for the treatment of excited states in π-stacked nucleobases with results that are very close to more computationally expensive methods such as CASPT2. The inter-ring distance in this dimer is of about 3.5Å and the molecular orbitals are quite mixed with a non vanishing orbital overlap. Thus, the TD-DFT method employed does not fail due to errors correlated with long CT excitations. In this study the TD-PBE0 has been suggested to provide the closest results to CASPT2, but the LC-ωPBE and MO52X functionals, which are designed to better describe the long range effects, can treat the dimer van der Waals interactions more accurately. Improta (2008)[105] analysed the accuracy of different functionals and solvation methods on the de-

scription of the absorption spectra of π stacked 9-methyladenine oligomers with the adoption of the B-DNA conformation. The author suggests the LR-PCM/TD-PBE0 as the best method for describing such a system. The author, moreover, compares the LR-PCM method which is the PCM method implemented with the linear response theory (LR) where the excitation energies are computed with the SS-PCM method in which the solvent effect has been treated by solving a different Schrödinger equation for each state with therefore a more accurate treatment of the solvent effect on different excited states. The TD-PBE0 method when compared with CAM-B3LYP and MO52X overestimates the stability of the CT state by about 0.5 eV. This error is compensated when this method is employed with LR-PCM which underestimates the CT state stability by the same extent. Therefore the LR-PCM/TD-PBE0 method is accurate regardless of the energy of the CT excitation due to error compensation.

3.5 Computational methods

All calculations were performed with the Gaussian03[106],[28] suite of programs. Geometries were initially optimized with the PM3 method. Final geometries were obtained with a full optimization with the B3LYP level of theory which is a combination of Becke's three parameter exchange functional with the modified Lee-Yang-Parr correlation functional. The exchange energy in B3LYP follows the structure of the hybrid functionals proposed by Becke which is:

$$E_x^{B3LYP} = 0.8E_x^{LDA} + 0.2E_X^{HF} + 0.72\Delta E_X^{B88} \tag{3.13}$$

here E_X^{LDA} and ΔE_X^{B88} are the LDA exchange and the gradient corrections from the Becke88 exchange respectively. The correlation energy is given by the following expression:

$$E_c^{B3LYP} = 0.19E_c^{VWN3} + 0.81E_c^{LYP} \tag{3.14}$$

here E_c^{VWN3}, E_c^{LYP} are the correlation energies from the Vosko-Wilk-Nusair III and the Lee-Yang-Parr correlation functionals respectively. The coefficients in the above equations are semiempirical and are determined by a linear least squares fit to atomization energies, ionization potentials and proton affinities of atoms and molecules of the G1 database. B3LYP is therefore a semiempirical functional. All stationary points have been tested with calculation of harmonic vibrational frequencies. Pople basis sets 6-31G* were used.[69] Electronic absorption spectra have been calculated with the TD-DFT method. The hydride transfer reaction considered is when the isopropylamine molecule was employed in the TIP hydride donor. The TD-DFT electronic absorption spectra have been calculated for the four species involved in the hydride transfer reaction which are DIP, TIP, BEP and BEDP. The density functionals utilized for TD-DFT computations are : B3LYP, BLYP, B3P86, BP86 and PBE0. The basis sets for TD-DFT computations are Pople 6-311G*. The TD-DFT computations are performed both in gas phase and in solution. Self consistent reaction field (SCRF) methods are employed to compute solvent effects on the energies. The integral equation formalism polarizable continuum model (IEFPCM) was employed in these calculations. Acetonitrile (ACN)(ϵ = 36.6) and Chloroform ($CHCl_3$) ($\epsilon = 4.9$) were selected as solvents. The number of tesserae on the surface of each sphere was set to 140 and the Merz-Kollman set of atomic radii has been used.

3.6 Results and Discussion

Table 3.9 shows the electronic energies calculated with the functionals tested in gas phase and with the inclusion of solvation of the four species involved in the hydride transfer reactions.

The results in table 3.9 show that for all funtionals tested, all four molecules are stabilized by increasing the polarity of the solvent. It is indicated also that in both

MOLECULE	GAS	ACN	$CHCl_3$	GAS	ACN	$CHCl_3$
		PBE0			**BP86**	
TIP	7.693	0	2.473	6.806	0	2.171
BEP	55.280	0	11.577	54.627	0	11.390
DIP	48.365	0	9.960	48.138	0	9.888
BEDP	8.647	0	2.558	7.765	0	2.271
		B3P86			**B3LYP**	
TIP	7.520	0	2.414	6.560	0	2.096
BEP	55.107	0	11.530	55.431	0	11.634
DIP	48.234	0	9.925	48.472	0	10.002
BEDP	8.470	0	2.500	7.674	0	2.245
		BLYP				
TIP	5.799	0	1.839			
BEP	55.002	0	11.516			
DIP	48.422	0	9.984			
BEDP	6.926	0	2.006			

Table 3.9: Energies (kcal/mol) of the four molecules involved into the hydride transfer in gas phase, chloroform, acetonitrile

solvents, BEP and DIP, which are more polar due to the charge present on the nitrogen atom, are more stable than the other two non charged species. Moreover, the reason for such stabilisation can be qualitatively appreciated by the electrostatic interaction energies of DIP and BEP with the solvents which are five times higher than in TIP and BEDP. The IEFPCM calculations show also that the electrostatic interactions are higher in ACN than in $CHCl_3$. Table 3.9 displays for all functionals tested the consistent energy lowering of the charged species compared with the respective non charged species when the medium polarity increases.

The heterocycles possess an uneven distribution of charge which leads to a permanent dipole moment that typically assume values in the range between 0 and 12 Debye.

The role of the heteroatom in heterocycles in determining the molecule's electronic distribution can be easily demonstrated when heteroaromatic systems are compared with their perhydro counterparts. The dipole moments of heteroaromatic systems are less directed toward the heteroatom than in the corresponding saturated counterpart. The pyrrole ring instead has its dipole moment with a reversed direction pointing to the unsaturated part and whose value is higher than that of pyrrolidine because of the acidic nature of the pyrrole ring. Pyridine has a dipole moment that points in the same direction toward the heteroatom, as for its saturated analogue, but with higher intensity. Thus, in general, in heterocycles, the dipole moments point toward the heteroatom from the ring with the exception of pyrrole. The unsaturation leads to an increase of the dipole moment with exception of pyridine. The dipole moment of BEP and BEDP points towards the ring while for both DIP and TIP it points towards the heteroatom. The dipole moment of BEP, as shown in Tables 3.10 3.11 3.12, is consistently higher than that of BEDP, therefore the charge present on the heteroatom is not effectively delocalised along the aromatic ring. The dipole moment of DIP and TIP is lower than that of BEP and BEDP which can be explained by considering that the electron density can be

well delocalised between the two heteroatoms and between the heteroatoms and the aromatic ring. In DIP the charge can be efficiently delocalised with a result that the difference between the dipole moments of DIP and TIP is lower than that between BEP and BEDP. Furthermore it is possible to say that the presence of a second nitrogen atom within the non aromatic DIP molecule allows for a better charge delocalisation than that in the BEP aromatic ring. As shown in tables 3.10 3.11 3.12, the dipole moments for all functionals tested increase with increasing the medium polarity. Therefore, the solvent increases the charge separation of the heterocycles. The DIP dipole moment is the most sensitive to the solvent polarity with an increase of almost 2D compared to the gas phase. The BEP dipole moment, in contrast, is the least sensitive to the solvent polarity. Thus in solution $\mu BEP > \mu DIP > \mu TIP > \mu BEDP$ and in relation to the dipole moment sensitivity to the solvent polarity $\mu DIP > \mu TIP > \mu BEDP > \mu BEP$.

Tables 3.10, 3.11 3.12 and fig 3.4 illustrate how the HOMO-LUMO gap varies upon increasing the medium polarity. In all the types of functionals used it is possible to observe the same general trends. The HOMO-LUMO gap obtained when the Becke three parameter hybrid functionals and PBE0 were used is about 1.3 eV higher compared with BLYP or BP86 for all four molecules in all solvents. The HOMO and LUMO of BEDP and TIP have similar energies and very close values of gap. The HOMO and LUMO of DIP have a shift to higher energies by about 1eV in gas phase and 0.6eV in solution compared to the HOMO's and LUMO's of BEP. The BEP HOMO-LUMO gap is the most sensitive to the inclusion of a polar medium with a variation of about 0.2eV when solvated by ACN. Notably, upon increase of the medium polarity the BEP and DIP HOMO-LUMO gap gradually assumes values closer to the HOMO-LUMO gap of BEDP and TIP. It is possible to say that the polarizability (which is a property that measures the softness of the molecule electron density and is directly proportional to the molecular size and inversely to the HOMO-LUMO gap and ionization potential) of BEP and DIP

increases with increasing the solvent polarity. The solvent polarity, in conclusion, affects to a greater extent the electron distribution of BEP and DIP through the stabilisation effect than the corresponding non charged species.

	GAS PHASE				CHLOROFORM				ACETONITRILE			
					PBE0							
	μ [D]	HOMO [eV]	LUMO [eV]	ΔE [eV]	μ [D]	HOMO [eV]	LUMO [eV]	ΔE [eV]	μ [D]	HOMO [eV]	LUMO [eV]	ΔE [eV]
TIP	2.14	-5.57	-0.98	4.60	2.65	-5.50	-0.90	4.61	2.89	-5.57	-0.98	4.60
BEP	6.39	-10.70	-6.43	4.27	6.82	-7.69	-3.30	4.39	6.85	-6.99	-2.53	4.46
DIP	2.77	-9.74	-5.32	4.42	3.85	-7.01	-2.54	4.47	4.44	-6.38	-1.89	4.49
BEDP	2.12	-5.64	-1.00	4.64	2.57	-5.63	-0.98	4.65	2.72	-5.64	-1.00	4.64
					B3LYP							
	μ [D]	HOMO [eV]	LUMO [eV]	ΔE [eV]	μ [D]	HOMO [eV]	LUMO [eV]	ΔE [eV]	μ [D]	HOMO [eV]	LUMO [eV]	ΔE [eV]
TIP	2.07	-5.28	-0.97	4.31	2.58	-5.26	-0.99	4.27	2.81	-5.31	-1.05	4.26
BEP	6.40	-10.47	-6.54	3.93	6.85	-7.42	-3.39	4.04	6.88	-6.71	-2.60	4.10
DIP	2.69	-9.53	-5.45	4.08	3.77	-6.77	-2.64	4.13	4.35	-6.12	-1.96	4.15
BEDP	2.13	-5.55	-1.23	4.32	2.58	-5.39	-1.07	4.31	2.73	-5.38	-1.07	4.31

Table 3.10: Dipole moments (μ) (Debye), HOMO (eV), LUMO (eV), HOMO-LUMO gap (ΔE in eV) of the four molecules involved into the hydride transfer for the PBE0 and the B3LYP functionals calculated in Gas-Phase and with the IEFPCM model for $CHCl_3$ and Acetonitrile.

	GAS PHASE				CHLOROFORM				ACETONITRILE			
					B3P86							
	μ [D]	HOMO [eV]	LUMO [eV]	ΔE [eV]	μ [D]	HOMO [eV]	LUMO [eV]	ΔE [eV]	μ [D]	HOMO [eV]	LUMO [eV]	ΔE [eV]
TIP	2.16	-5.90	-1.60	4.30	2.68	-5.92	-1.65	4.26	2.92	-5.98	-1.73	4.25
BEP	6.39	-11.13	-7.18	3.95	6.84	-8.11	-4.05	4.06	6.86	-7.41	-3.28	4.13
DIP	2.77	-10.17	-6.08	4.09	3.86	-7.43	-3.30	4.14	4.46	-6.79	-2.64	4.15
BEDP	2.13	-6.18	-1.86	4.32	2.58	-6.04	-1.74	4.30	2.74	-6.06	-1.76	4.30
					BP86							
	μ [D]	HOMO [eV]	LUMO [eV]	ΔE [eV]	μ [D]	HOMO [eV]	LUMO [eV]	ΔE [eV]	μ [D]	HOMO [eV]	LUMO [eV]	ΔE [eV]
TIP	2.19	-4.63	-1.72	2.91	2.78	-4.61	-1.75	2.86	3.04	-4.67	-1.82	2.84
BEP	6.30	-9.85	-7.23	2.62	6.76	-6.89	-4.11	2.79	6.77	-6.18	-3.34	2.85
DIP	2.83	-8.92	-6.14	2.79	3.98	-6.16	-3.35	2.81	4.61	-5.50	-2.69	2.81
BEDP	2.09	-4.91	-1.99	2.93	2.56	-4.76	-1.85	2.91	2.73	-4.75	-1.85	2.90

Table 3.11: Dipole moments (μ) (Debye), HOMO (eV), LUMO (eV), HOMO-LUMO gap (ΔE in eV) of the four molecules involved into the hydride transfer for the B3P86 and the BP86 functionals calculated in Gas-Phase and with the IEFPCM model for $CHCl_3$ and Acetonitrile.

	GAS PHASE				CHLOROFORM				ACETONITRILE			
					BLYP							
	μ	HOMO	LUMO	ΔE	μ	HOMO	LUMO	ΔE	μ	HOMO	LUMO	ΔE
	[D]	[eV]	[eV]	[eV]	[D]	[eV]	[eV]	[eV]	[D]	[eV]	[eV]	[eV]
TIP	2.10	-4.35	-1.43	2.92	2.66	-4.30	-1.42	2.88	2.91	-4.33	-1.47	2.87
BEP	6.31	-9.55	-6.93	2.62	6.77	-6.54	-3.78	2.76	6.79	-5.82	-3.00	2.82
DIP	2.72	-8.64	-5.86	2.78	3.85	-5.84	-3.03	2.81	4.47	-5.17	-2.35	2.82
BEDP	2.07	-4.62	-1.69	2.94	2.55	-4.44	-1.51	2.92	2.71	-4.42	-1.50	2.92

Table 3.12: Dipole moments (μ) (Debye), HOMO (eV), LUMO (eV), HOMO-LUMO gap (ΔE in eV) of the four molecules involved into the hydride transfer for the BLYP functional calculated in Gas-Phase and with the IEFPCM model for $CHCl_3$ and Acetonitrile.

The excitation energies (EXCEs) and the oscillator strength (OS) of the four molecules in gas phase in $CHCl_3$ and ACN have also been evaluated with all functionals considered.

The hybrid functionals B3LYP, B3P86 and PBE0 show similar trends in both excitation energies and oscillator strength intensities, while similarly the BLYP and BP86 results lead to closely associated values. The excitation energies in GPH, in ACN and $CHCl_3$ have also been compared. This comparison is focused on transitions with the more intense oscillator strengths. Another criterion utilised in order to analyse the transitions within different media is that only excitations in which the orbitals involved in the transition were similar have been compared.

Because of the similar performance of B3LYP, B3P86 and PBE0 and between the pure DFT functionals, here only the performance of the PBE0 and the BLYP functionals has been compared analytically within the criteria shown above.

Tables 3.13 and 3.14 show the results computed for the DIP molecule within the PBE0 and BLYP functional respectively. The differences in the excitation energies between GPH and solution are enhanced when the BLYP functional was utilized. The lowest excitation energies for both PBE0 (which occurs at higher energy) and BLYP correspond to the HOMO-LUMO transition. In general the solution excitation energies are red shifted by 0.05-0.1 eV. For most of the excitations in solution a hyperchromic effect is present that often increases when increasing the polarity of the solvent. Notably, within the PBE0, on the fourth excitation considered the OS increases significantly when the percentage of the H$\rightarrow$L+2 within the orbital composition involved during the transition is almost doubled. A similar behaviour can be observed within the BLYP on the third excitation. The difficulty in comparing the excitation energies is underlined by the fact that in GPH, often there are transitions in which the orbitals involved are quite different than the orbitals involved in transitions in solution. In fig 3.5 and 3.6 we show that for the DIP

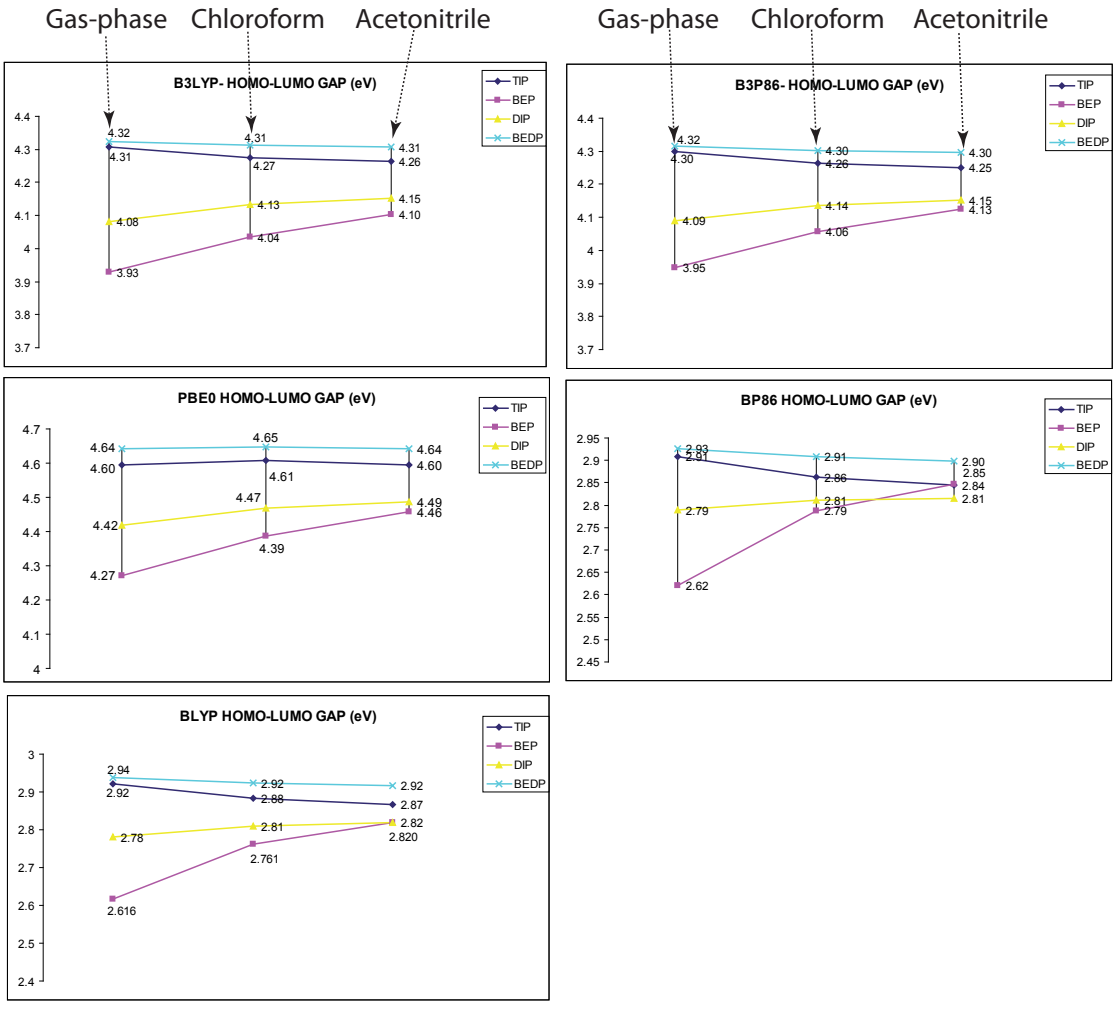

Figure 3.4: Variation of the HOMO-LUMO gap upon increasing the medium polarity

molecule the relation between gas phase and solution excitation energies is linear in both functionals, thus the solvent effect is not very pronounced with no significant EXCE differences between the two solvents. The solvent effect therefore is mainly correlated to variations of the OS, and thus to variations of the transition dipole moments.

Turning to the BEP molecule, tables 3.15 and 3.16, the PBE0 functional shows a higher number of transitions with a more intense OS, and with more differences between GPH and solution results than BLYP. The HOMO-LUMO transitions in both functionals, show an OS less than 0.05 units, thus has not been considered. Within the PBE0 results, six transitions have been considered. The shift of the EXCE between GPH and solution oscillates between 0.05 eV to 0.15 eV with the exception of the second transition analyzed, which shows a progressive blue shift that goes up to 0.2 eV in ACN. The solvent effect on the OS varies depending on the excitation. In all EXCE apart from excitations 4 and 5 a hyperchromic effect is present which increases gradually, increasing the polarity in EXCE 3 and 6 and which is higher in $CHCl_3$ in EXCE 1 and 2. In EXCE 5 a hypochromic effect is present when gradually the solvent polarity increases and possibly caused by the lowering of the percentage by which the H→L+1 is involved during the transition. In excitation 4 the OS in GPH and $CHCl_3$ is similar and the hypochromic effect is present in ACN, perhaps caused by the increase of the H-4→L percentage during the transition.

It is possible to compare to some extent the first EXCE calculated with PBE0 and BLYP because they have a similar MO composition, mainly correlated to an higher percentage of the H-1→L. In BLYP this EXCE undergoes a progressive blue shift from GPH to ACN coupled with a progressive hyperchromic effect, different than in EXCE 1 of the PBE0 in which the hyperchromic effect is similar in both solvents and there is no significant shift between the EXCEs. It is possible to compare EXCE 2 of BLYP with EXCE 4 of PBE0, perhaps because there is a

similar composition and a correlation between the H-1→L+1 percentage and the OS. In EXCE 2 of BLYP there is a blue shift of 0.2 eV in going from GPH to solution which in EXCE 4 of PBE0 is less than 0.1 eV.

The EXCE 3 of BLYP could be compared with EXCE 5 of PBE0. In both cases there is not a very significant energy shift between GPH and solution. In EXCE 3 a strong hyperchromic effect is present when passing from GPH to $CHCl_3$ and ACN while in EXCE 5 of PBE0 a hypsochromic effect is shown. The correlation between GPH and solution EXCE with the PBE0 and BLYP functionals for the BEP molecule is shown in figures 3.7 and 3.8. Notably most of the EXCEs for the PBE0 functional in ACN are blue shifted from the EXCE in $CHCl_3$. Within the BLYP functional there are no equivalent shifts. Therefore it is possible to say that in the BEP molecule, the solvent effect is more pronounced with PBE0 than when the BLYP method was used.

The TIP molecule EXCEs do not have significant energy shifts when passing from the gas phase to solvation in both functionals analysed (fig 3.9, 3.10 and tables 3.17 and 3.18). The PBE0 OS shows a hyperchromic effect on all excitations analysed with the exception of excitations 3 and 4. EXCE 3 shows a hypochromic effect with the increase of solvent polarity, while EXCE 4 shows a hypochromic effect on $CHCl_3$ and a hyperchromic effect on ACN. Such different effect in solution cannot be explained by the MO composition, these being similar in both solvents. The BLYP OS also shows a hyperchromic effect in all excitations. Given the MO compositions of the individual excitations, few EXCEs within the two functionals can be compared. The EXCE 2 in BLYP is blue shifted with respect to EXCE 2 in PBE0 with in common a higher percentage of the H-3→L orbital, while the EXCE 4 in BLYP can be compared with EXCE 5 in PBE0, with in common the higher percentage of the orbitals H-2→L+1 and H-3→L, and is red shifted by about 0.9 eV from the PBE0 EXCE.

In conclusion the DIP and BEP molecules are the most stabilized by the solvent which can be seen by the increasing of the HOMO-LUMO gap and the decreasing of the electronic energy upon increase of the solvent polarity. The solvent effect on the UV-vis of the BEP molecule is seen as a blue shift of the EXCEs with a coupled hyperchromic effect on most of the EXC. Although the DIP molecule is quite sensitive to the solvent effect, its EXCEs do not vary significantly upon solvation. The solvent effect on the DIP molecule is seen as a hyperchromic effect that increases upon increasing the solvent polarity. The effect of the solvent on the BEDP and the TIP molecules which are the uncharged species is rather different. These molecules are not dramatically stabilised by the solvent (probably because of their neutral state) which is shown by their energy in solution and by their HOMO-LUMO energy gap which does not change significantly. The calculated EXCEs of the solvated TIP molecule show an energy blue shift of the ACN results over the $CHCl_3$ results, and a hyperchromic effect when passing from the GPH to solution. The solvation effect on the BEDP molecule can be seen only on the progressive hyperchromicity when the solvent polarity increases with very small changes on the EXCEs.

DIP (PBE0/6-311G*//B3LYP/6-31G*)				
N °	PHASE	EXC E	OS	MO Composition
	Gas Phase	3.70	0.20	H→L (84)
1	CHCl3	3.68	0.31	H→L (87)
	ACN	3.71	0.29	H→L (87)
	Gas Phase	4.77	0.13	H-1→L+1 (44) H-2→L (35) H→L+2 (14)
2	CHCl3	4.74	0.17	H-1→L+1 (46) H-2→L (37) H→L+2 (10)
	ACN	4.75	0.14	H-1→L+1 (45) H-2→L (37) H→L+2 (12)
	Gas Phase	5.09	0.34	H-2→L (35) H-1→L+1 (22) H-3→L (14) H→L+1 (8)
3	CHCl3	5.00	0.64	H-2→L (45) H-1→L+1 (31)
	ACN	5.05	0.59	H-2→L (45) H-1→L+1 (30)
	Gas Phase	5.34	0.29	H→L+2 (33) H-1→L+1(15) H-2→L+1 (19) H-3→L (10)
4	CHCl3	5.24	0.42	H-L+2 (62) H-1→L+1 (8) H-2→L+1 (7) H-3→L (5)
	ACN	5.24	0.47	H→L+2 (64) H-1→L+1 (12)
	Gas Phase	5.79	0.11	H-3→L (38) H-2→L+1 (32) H→L+3 (10)
5	CHCl3	5.76	0.15	H-3→L (32) H-2→L+1 (21) H-4→L (15) H→L+3 (13)
	ACN	5.78	0.15	H-3→L (32) H-2→L+1 (12) H→L+3 (23) H-4→L (9) H-1→L+2 (8)
	Gas Phase	6.18	0.13	H→L+3 (31) H-1→L+2 (17) H-4→L+1 (10) H-3→L+1 (28)
6	CHCl3	6.10	0.18	H→L+3(43) H-1→L+2(20) H-4→L+1(19) H-3→L+1(5)
	ACN	6.10	0.17	H→L+3 (39) H-1→L+2 (24) H-4→L+1 (21)

Table 3.13: Solvent effect on the excitation energies and the oscillator strengths in the DIP molecule with the PBE0 functional. In brackets is shown the percent contribution of the excited state wavefunction

DIP (BLYP/6-311G*//B3LYP/6-31G*)				
N °	PHASE	EXC E	OS	MO Composition
	Gas Phase	3.26	0.14	H→L(78)
1	CHCl3	3.24	0.22	H→L(82)
	ACN	3.25	0.20	H→L(81)
	Gas Phase	4.48	0.13	H-1→L+1 (27) H-2→L (19) H-3→L (26)
2	CHCl3	4.44	0.32	H-1→L+1 (33) H-2→L (29) H-3→L (8) H-4→L (6)
	ACN	4.46	0.27	H-1→L+1 (30) H-2→L (30) H-3→L (10) H-4→L (6)
	Gas Phase	4.71	0.14	H→L+2 (36) H-2→L+1 (5) H-4→L (32)
3	CHCl3	4.63	0.32	H→L+2 (55) H-1→L+1 (7) H-3→L (9)
	ACN	4.61	0.35	H→L+2 (54) H-1→L+1 (12) H-3→L (6)
	Gas Phase	5.07	0.17	H-3→L (32) H-2→L+1 (17)
4				H→L+3(14) H-2→L+3 (5)
	CHCl3	5.02	0.24	H-3→L (5) H-2→L+1 (13) H-4→L (44) H-1→L+2 (9)
	ACN	5.07	0.13	H-4→L (36) H-2→L+1 (5) H→L+3 (32) H-4→L+1 (6)
	Gas Phase	5.14	0.23	H-L+3 (34) H-1→L+2 (28) H→L+2 (12)
5	CHCl3	5.07	0.21	H→L+3 (51) H-1→L+2 (23)
	ACN	5.05	0.27	H→L+3 (31) H-1→L+2 (26) H-4→L(15) H→L+2(6)

Table 3.14: Solvent effect on the excitation energies and the oscillator strengths in the DIP molecule with the BLYP functional

BEP (PBE0/6-311G*//B3LYP/6-31G*)				
N°	PHASE	EXC E	OS	MO Composition
	Gas Phase	3.79	0.12	H-1→L (80) H→L+1 (7)
1	CHCl3	3.86	0.21	H-1→L (86) H→L+1 (6)
	ACN	3.93	0.19	H-1→L (85) H-L+1 (7)
	Gas Phase	4.72	0	H-4→L (46) H-1→L+1 (21) H→L+1 (18)
2	CHCl3	4.90	0.32	H-4→L (11) H-1→L+1 (24) H→L+1 (21) H-3→L (22) H-5→L (11)
	ACN	5.11	0.17	H-4→L (13) H-1→L+1 (19) H-3→L (47) H-4→L (13) H-2→L (6)
	Gas Phase	4.91	0.12	H-5→L (51) H→L+1 (25)
3	CHCl3	4.86	0.26	H-3→L (57) H→L+1 (25)
	ACN	4.93	0.53	H-5→L (13) H→L+1 (37) H-1→L+1(26)
	Gas Phase	5.13	0.23	H-1→L+1 (42) H-4→L (18) H-5→L (11) H→L+2 (8)
4	CHCl3	5.10	0.25	H-1→L+1 (34) H-4→L (27) H-5→L (23)
	ACN	5.17	0.09	H-1→L+1 (8) H-4→L (64) H-5→L (20)
	Gas Phase	5.33	0.55	H→L+1 (29) H-5→L (19) H→L+2 (13)
5				H-4→L (10) H-2→L+1 (7)
	CHCl3	5.21	0.47	H→L+1 (14) H-5→L (43) H→L+2 (12) H-4→L (13)
	ACN	5.27	0.31	H→L+1 (10) H-5→L (35) H→L+2 (18) H-4→L (14) H-2→L+1 (6)
	Gas Phase	5.41	0.1	H-L+2 (20) H-4-L+1 (6) H-5-L (5)
6				H-1→L+1 (12)H-3→L+1 (46) H→L+2 (20)
	CHCl3	5.44	0.16	H→L+2 (54) H-4→L+1 (13) H-5→L (11) H-1→L+1 (7)
	ACN	5.47	0.21	H-5→L (20) H-2→L+1 (11) H-1→L+1 (6)

Table 3.15: Solvent effect on the excitation energies and the oscillator strengths in the BEP molecule with the PBE0 functional

BEP (BLYP/6-311G*//B3LYP/6-31G*)				
N °	PHASE	EXC E	OS	MO Composition
	Gas Phase	2.97	0.02	H-1→L (73) H-3→L (9)
1	CHCl3	3.35	0.14	H-1→L (65) H-2→L (13) H→L (6)
	ACN	3.43	0.15	H-1→L (73) H→L (7)
	Gas Phase	4.22	0.01	H-1→L+1 (27) H-5→L (52) H-3→L+1 (5)
2	CHCl3	4.44	0.19	H-1→L+1 (48) H-2→L+1 (10) H→L+2 (9) H-4→L (8) H→L+1 (6)
	ACN	4.46	0.17	H-1→L+1 (46) H→L+2 (23) H-4→L (7) H→L+1 (5)
	Gas Phase	4.84	0.06	H-1→L+2 (49) H-4→L+1 (24) H-3→L+1 (5)
3	CHCl3	4.71	0.58	H-5→L (31) H→L+1 (28) H→L+2 (7) H-4→L (6) H→L+3 (6)
	ACN	4.77	0.55	H-5→L (25) H→L+1 (23) H-4→L (8) H-3→L+1 (6) H-1→L+3 (5)

Table 3.16: Solvent effect on the excitation energies and the oscillator strengths in the BEP molecule with the BLYP functional

TIP (PBE0/6-311G*//B3LYP/6-31G*)				
N °	PHASE	EXC E	OS	MO Composition
	Gas Phase	3.76	0.12	H→L (89)
1	CHCl3	3.67	0.18	H→L (92)
	ACN	3.67	0.16	H→L (91)
	Gas Phase	5.13	0.03	H-3→L (49) H-2→L+1 (34) H→L+2 (7)
2				H→L+1 (6)
	CHCl3	5.10	0.42	H→L+2 (44) H-2→L+1 (9) H-2→L (20) H-1→L+1(10)
	ACN	5.13	0.37	H-3→L (30) H→L+2 (24) H-2→L (23)
	Gas Phase	5.23	0.32	H→L+2 (34) H-2→L (29) H→L+3 (8)
3				H-3→L (7)
	CHCl3	5.11	0.14	H-3→L (54) H-2→L+1 (16) H-2→L (8) H→L+1 (6)
	ACN	5.11	0.17	H-3→L (31) H-2→L+1 (25) H→L+2 (24) H-2→L (7)
	Gas Phase	5.59	0.16	H→L+3 (67) H-2→L+2 (11) H→L+2 (6)
4	CHCl3	5.53	0.12	H-L+3 (59) H-2→L+2 (13) H-1→L+2 (18)
	ACN	5.57	0.24	H→L+3 (58) H-2→L+2 (9) H-1→L+2 (20)
	Gas Phase	5.83	0.12	H-2→L+1 (49) H-3→L (18) H→L+4 (12)
5	CHCl3	5.78	0.20	H-2→L+1 (58) H-3→L (18)
	ACN	5.80	0.19	H-2→L+1 (56) H-3→L (17) H-2→L+2 (5)

Table 3.17: Solvent effect on the excitation energies and the oscillator strengths in the TIP molecule with the PBE0 functional

TIP (BLYP/6-311G*//B3LYP/6-31G*)				
N °	PHASE	EXC E	OS	MO Composition
	Gas Phase	4.28	0.09	H-2→L (47) H→L+2 (32)
1	CHCl3	4.24	0.14	H-2→L (58) H→L+2 (21) H-1→L+2 (5)
	ACN	4.25	0.13	H-2→L (56) H→L+2 (25)
	Gas Phase	4.48	0.02	H-3→L (43)
2				H-2→L+1 (39) H→L+2 (8)
	CHCl3	4.53	0.13	H-3→L (35) H-2→L+1 (7) H→L+2 (15) H→L+3 (18) H-2→L (10)
	ACN	4.54	0.11	H-3→L (34) H-2→L+1 (8) H→L+2 (12) H→L+3 (22)
				H-2→L (9) H-2→L+1 (8)
	Gas Phase	4.59	0.10	H→L+3 (25) H→L+4(9)
3				H-L+2 (17) H-3-L(14) H-2→L (14) H-2→L+2 (5)
	CHCl3	4.85	0.20	H→L+3 (45) H→L+4 (14) H-1→L+3 (10) H-2→L (6)
	ACN	4.87	0.22	H-L+3 (44) H→L+4 (7) H-2→L (7) H-2→L+1 (7) H-3→L (7) H→L+2
	Gas Phase	4.95	0.01	H-2→L+1 (26) H→L+4 (6)
4				H-3→L (16) H-1→L+3 (20) H→L+3 (6) H→L+4 (6)
	CHCl3	4.97	0.11	H-2→L+1 (37) H→L+4 (29) H-3→L (15)
	ACN	5.01	0.20	H-2→L+1 (37) H→L+4 (21) H-3→L (13) H-4→L+1 (6)

Table 3.18: Solvent effect on the excitation energies and the oscillator strengths in the TIP molecule with the BLYP functional

BEDP (PBE0/6-311G*//B3LYP/6-31G*)				
N°	PHASE	EXC E	OS	MO Composition
	Gas Phase	3.79	0.13	H→L (89)
1	CHCl3	3.72	0.20	H→L (91)
	ACN	3.72	0.18	H→L (91)
	Gas Phase	5.16	0.05	H-2→L (51) H-1→L+2 (31) H→L+2 (6)
2	CHCl3	5.11	0.19	H-2→L (50) H-1→L+2 (13) H→L+2 (6) H-1→L (13) H→L+3 (8)
	ACN	5.13	0.17	H-2→L (52) H-1→L+2 (14) H-1→L (12) H→L+2 (6)
	Gas Phase	5.27	0.17	H→L+3 (37) H-1→L (25) H→L+4 (10) H-1→L+1 (+9)
3	CHCl3	5.20	0.20	H→L+3 (44) H-1→L+2 (16) H-1→L (13) H-2→L (8)
	ACN	5.21	0.21	H→L+3 (45) H-1→L (15) H-1→L+2 (14) H-2→L (6) H→L+4 (5)
	Gas Phase	5.82	0.16	H-1→L+2 (42) H-2→L (17) H-1→L+3 (6)
4				H-3→L+1 (6) H→L+3 (6)
	CHCl3	5.77	0.23	H-1→L+2 (57) H-2→L (17)
	ACN	5.79	0.21	H-1→L+2 (56) H-2→L (15) H-1→L+3 (5)

Table 3.19: Solvent effect on the excitation energies and the oscillator strengths in the BEDP molecule with the PBE0 functional

3.7 Conclusions

In this chapter the solvent effect has been analysed through the simulation of the interaction of molecules involved in the DIP synthesis reaction path with light, in contrast to chapter 2 where its role on the DIP synthesis reaction mechanism was studied. The Time Dependent DFT method has been proven to offer a very good compromise between computational cost and accuracy, although still presenting errors that the scientific community is currently working to eliminate or decrease. In this chapter is possible to see how charged species such as the BEP or the DIP molecule are more susceptible to the effect of the solvent which it manifest when its polarity increases. When the polarity increases, it is possible normally to observe in all functionals analysed a blue shift and/or a hyperchromic effect. In contrast, looking the excitation energies, uncharged species are not very

BEDP (BLYP/6-311G*//B3LYP/6-31G*)				
N °	PHASE	EXC E	OS	MO Composition
	Gas Phase	3.23	0.07	H→L (84)
1	CHCl3	3.17	0.11	H→L (88)
	ACN	3.17	0.10	H→L (87)
	Gas Phase	3.41	0.11	H→L+1 (95)
2	CHCl3	3.31	0.14	H→L+1 (96)
	ACN	3.32	0.13	H→L+1 (96)
	Gas Phase	4.33	0.09	H-1→L (39) H→L+3 (32) H-1→L+1 (10)
3	CHCl3	4.28	0.15	H-1→L (48) H→L+3 (26) H-1→L+1 (10)
	ACN	4.30	0.13	H-1→L (44) H→L+3 (29) H-1→L+1 (11)
	Gas Phase	4.63	0.12	H→L+4 (27) H→L+3 (19) H-1→L (16)
4				H-2→L (13)
	CHCl3	4.55	0.22	H→L+4 (14) H→L+3 (25) H-1→L (16) H-2→L (23) H→L+4 (14)
	ACN	4.56	0.19	H→L+4 (17) H→L+3 (22) H-1→L (18) H-2→L (20)
	Gas Phase	4.90	0.03	H→L+4 (24) H-1→L+2 (19)
5				H-2→L (18)
	CHCl3	5.02	0.23	H→L+4 (16) H-1→L+2 (14) H-4→L (22) H→L+3 (8) H-2→L (6)
	ACN	5.05	0.19	H→L+4 (13) H-1→L+2 (13) H-4→L (26) H→L+3 (7) H-3→L (7)

Table 3.20: Solvent effect on the excitation energies and the oscillator strengths in the BEP molecule with the BLYP functional

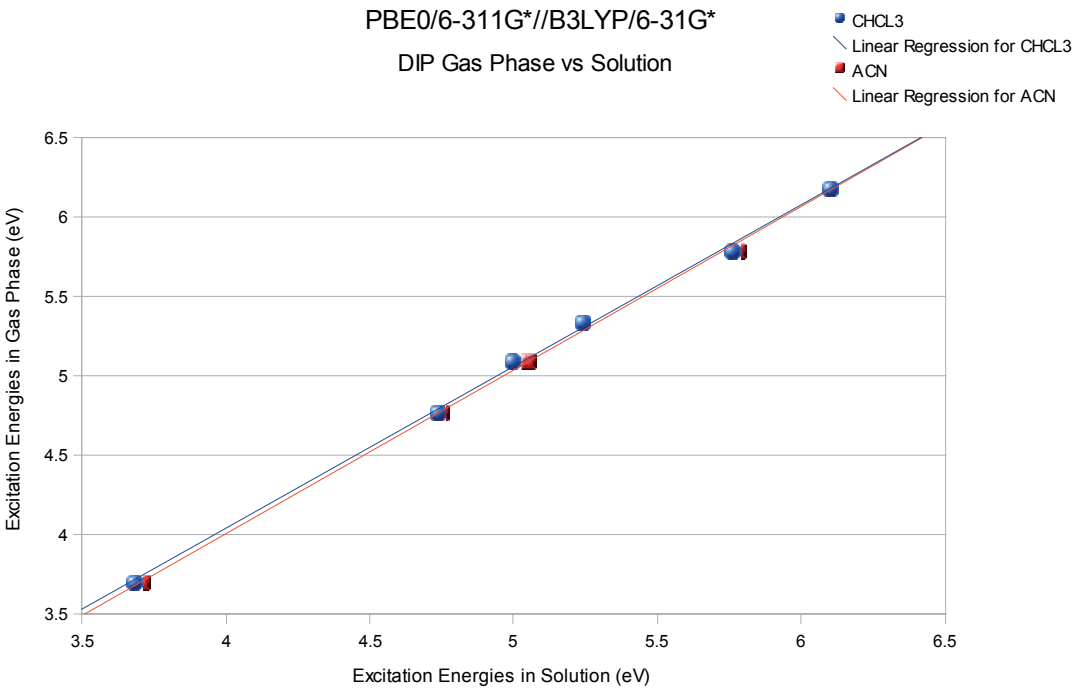

Figure 3.5: PBE0/6-311G*//B3LYP/6-31G*, correlation between gas phase and solution excitation energies for DIP

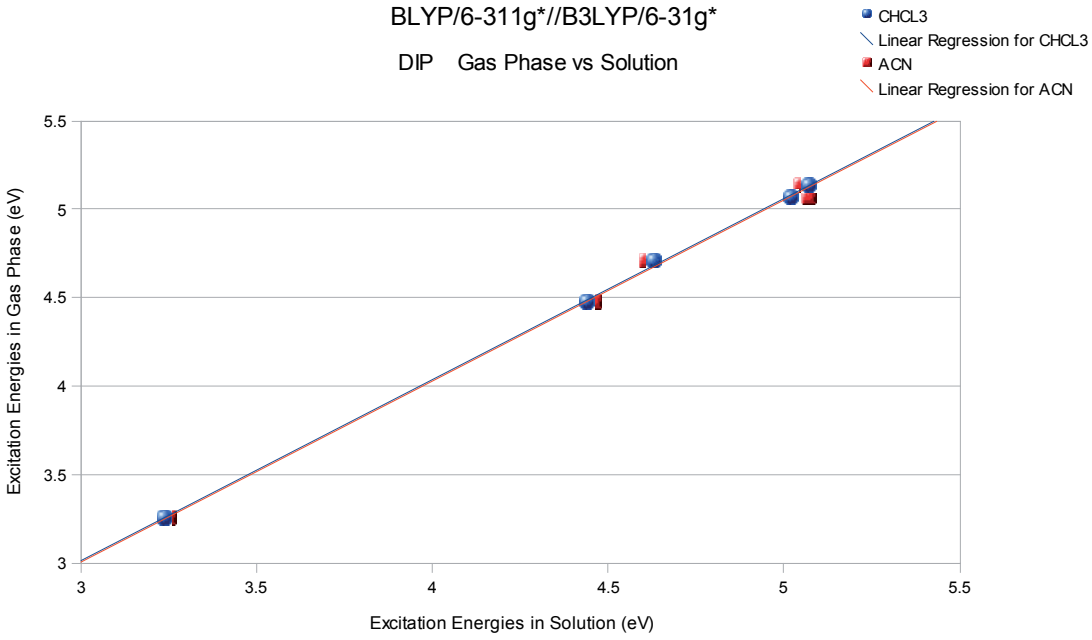

Figure 3.6: BLYP/6-311G*//B3LYP/6-31G*, correlation between gas phase and solution excitation energies for DIP

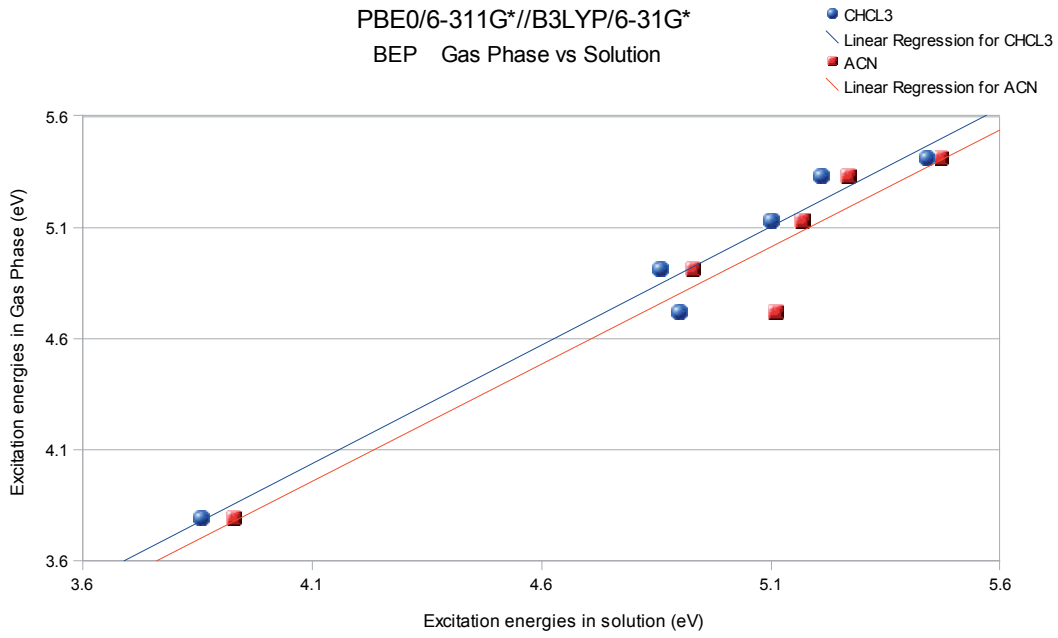

Figure 3.7: PBE0/6-311G*//B3LYP/6-31G*, correlation between gas phase and solution excitation energies for BEP

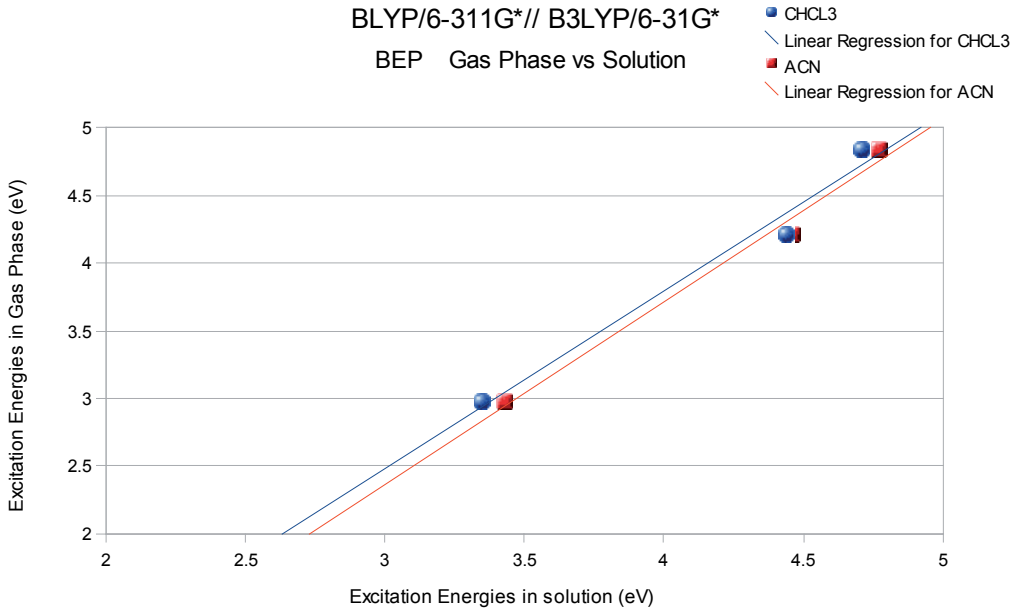

Figure 3.8: BLYP/6-311G*//B3LYP/6-31G*, correlation between gas phase and solution excitation energies for BEP

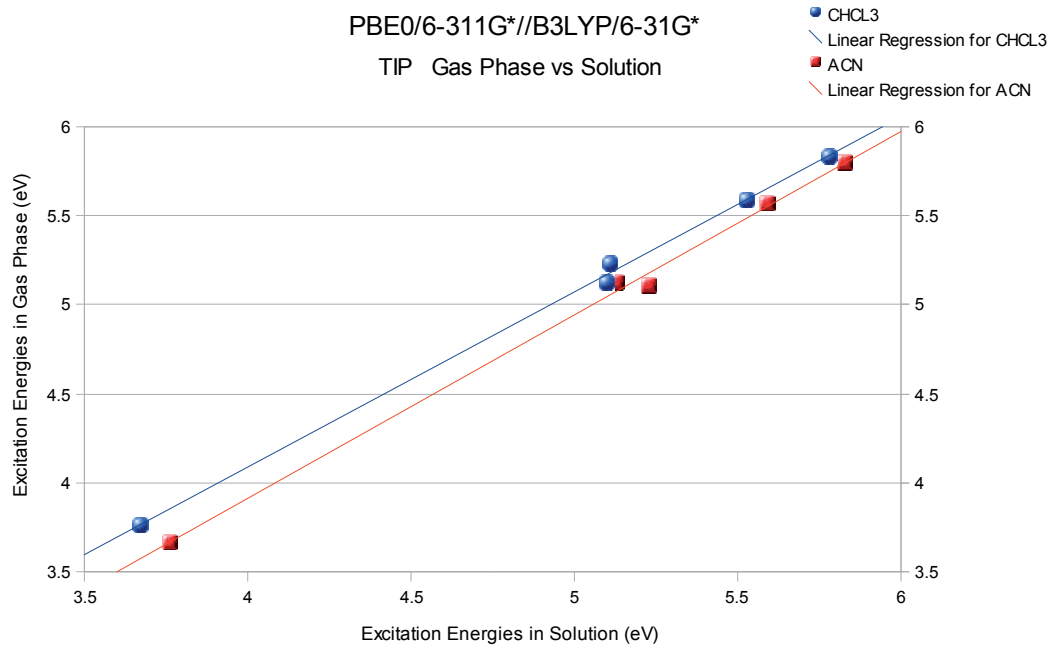

Figure 3.9: PBE0/6-311G*//B3LYP/6-31G*, correlation between gas phase and solution excitation energies for TIP

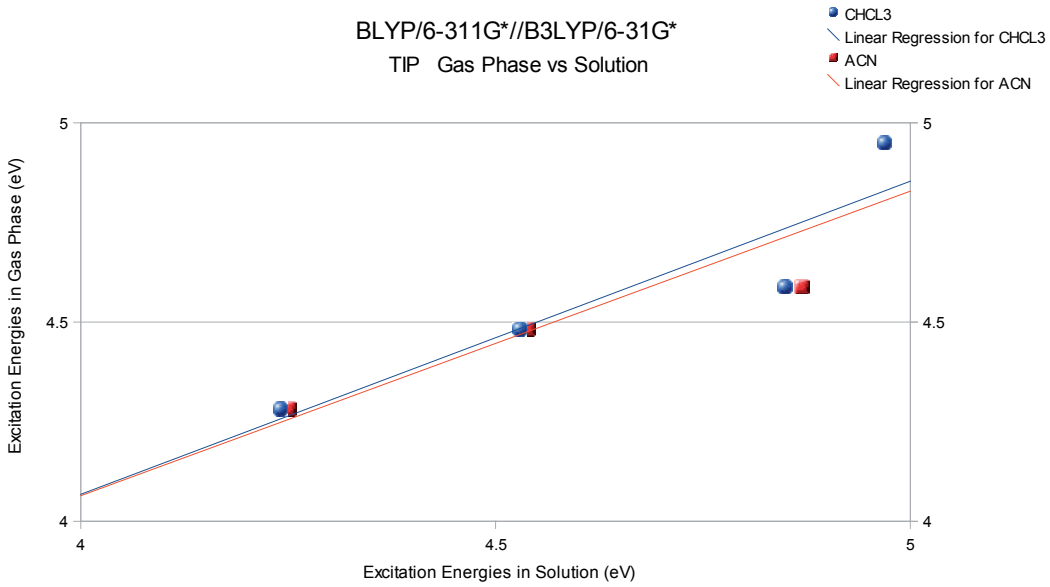

Figure 3.10: BLYP/6-311G*//B3LYP/6-31G*, correlation between gas phase and solution excitation energies for TIP

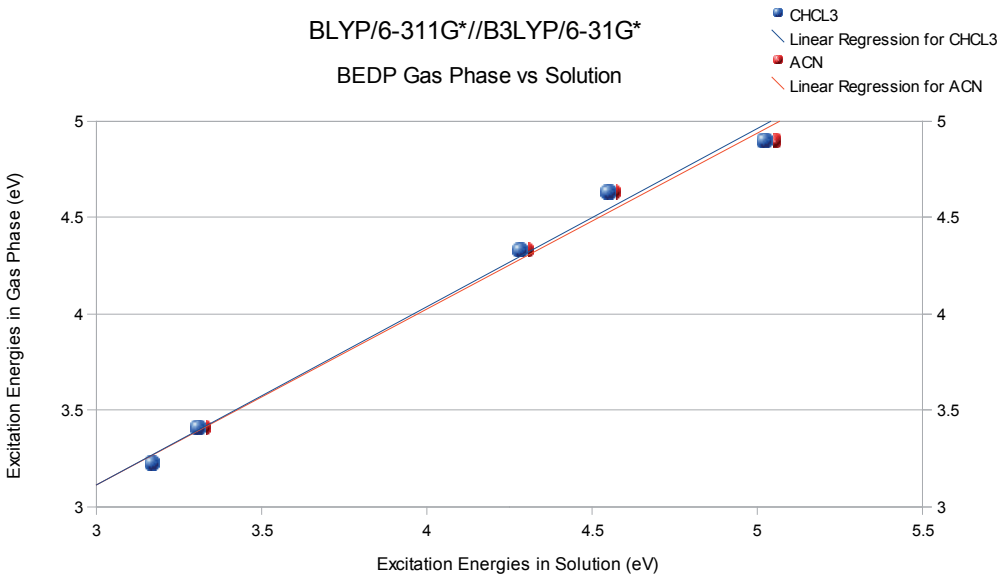

Figure 3.11: BLYP/6-311G*//B3LYP/6-31G*, correlation between gas phase and solution excitation energies for BEDP

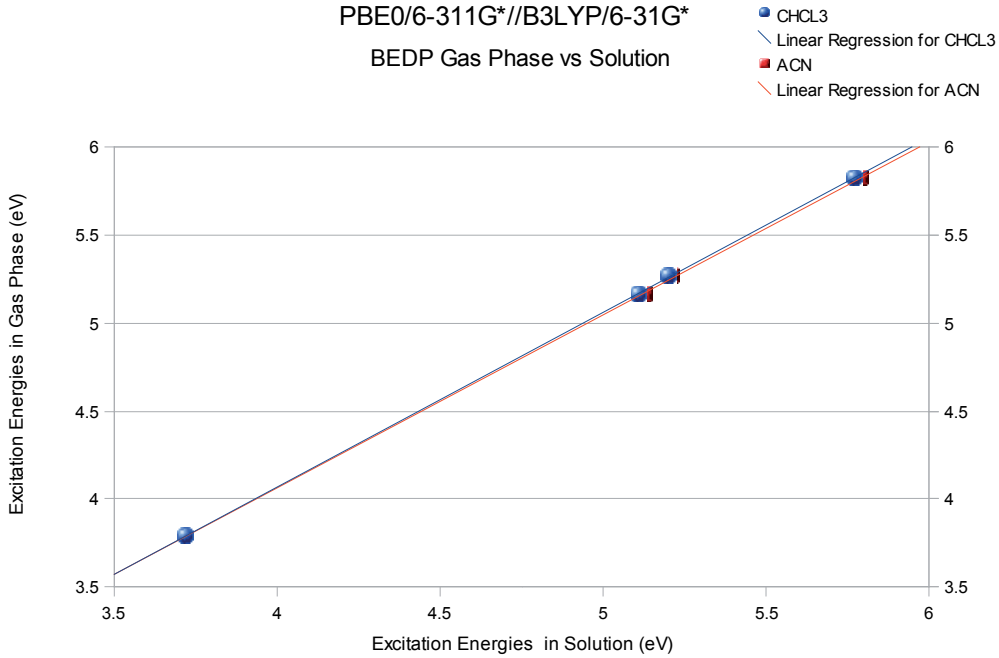

Figure 3.12: PBE0/6-311G*//B3LYP/6-31G*, correlation between gas phase and solution excitation energies for BEDP

affected by the solvent. The dynamics of the hydride transfer of the last step of the DIP synthesis reaction path has been considered through transition structures in which electron withdrawing or electron donating substituents were present on the hydride donor (TIP). In this study a good correlation has been found between the Hammond Postulate and the hydride transfer reactions considered, showing that "early" transition states (resembling more the structure of the reactants) were those where electron donor substituents were present and "late" transition structures were those where electron withdrawing groups were utilised.

4

Further studies on hydride transfer reactions

Following the studies on the hydride transfer reaction of the last step of the Dihydro-Imidazo-Phenanthridinium synthesis reaction path, studies of the hydride transfer mechanism in other heterocyclic compounds have been performed. Lee et al (1998)[107] measured the time dependent UV-vis spectra of the hydride transfer reaction of 2-heteroaryl-1,3-dimethylbenzimidazoline derivatives (HDMZ-H) with 1-benzyl-3-carbamoylpyridinium (BCPY) and 2-benzyl-5-nitrosoquinolinium (BNIQ) ions. The UV-vis spectra have been measured in a solvent consisting of four parts of 2-propanol and one part of water at 25°C.

This work is focused on :

- calculating the hydride transfer TS structures and use of Conceptual Density Functional Theory to allow determination of which electron acceptor is more suitable for these reactions .

- comparing the hydride donating strength of a 2-heteroaryl-1,3-dimethyl-benzimidazoline derivative (HDBMZ-H) and its analogue in which a -N-CH3 group within the imidazol ring has been substituted by a sulphur atom (HDBTZ-H) in which the hydride donor of fig 4.1 is species **4H** with X = $-C=CH_2$.

- calculating and thus simulating the time-dependent UV-vis spectra measured

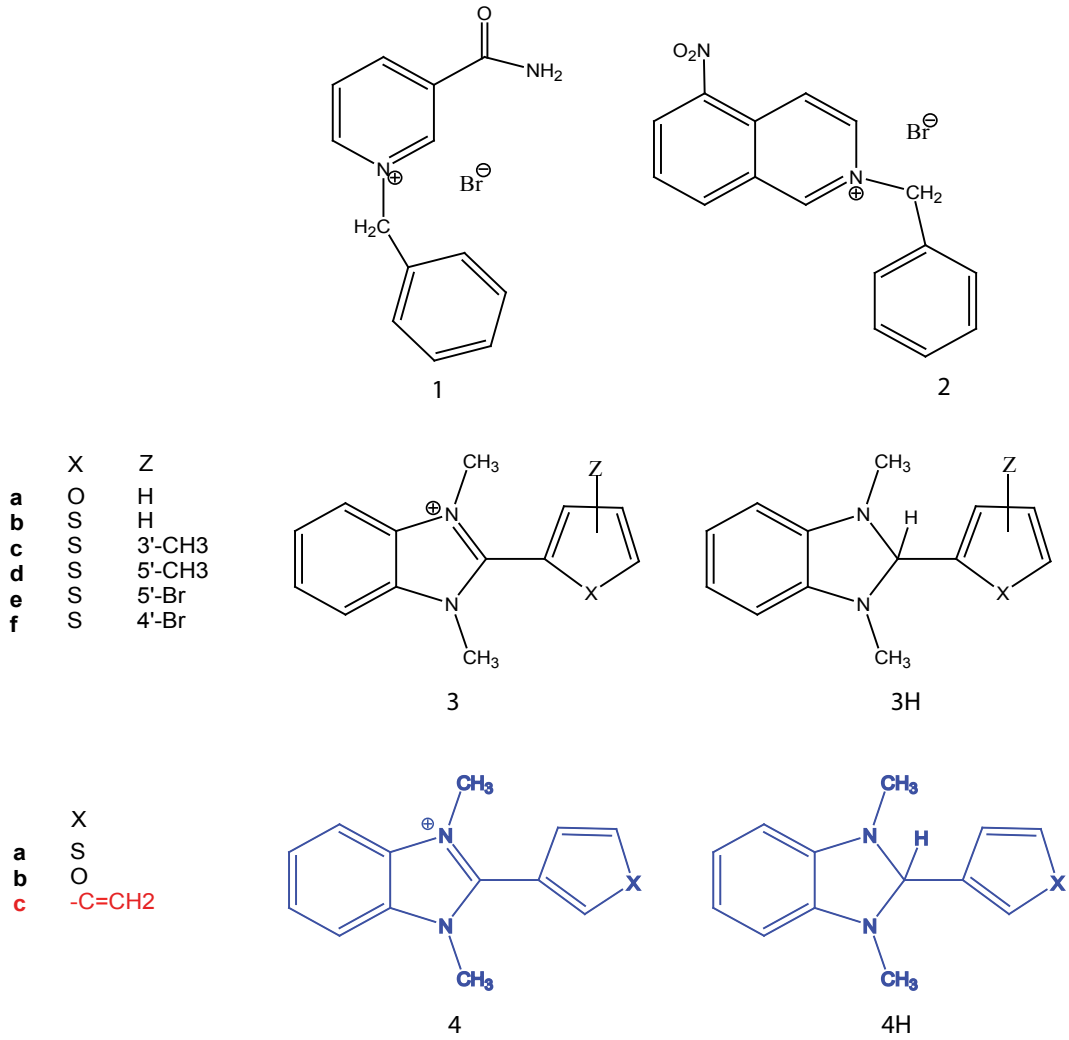

Figure 4.1: Molecules studied by Lee et al , BCPY is **1**, BNIQ is **2**, HDBMZ is **4** (c as substituent) and HDBMZ-H is 4H

experimentally by Lee et al.

Zhu et al.[108] determined, for several heterocyclic compounds, the thermodynamic driving force which is defined as enthalpy changes to release hydride anion in acetonitrile.

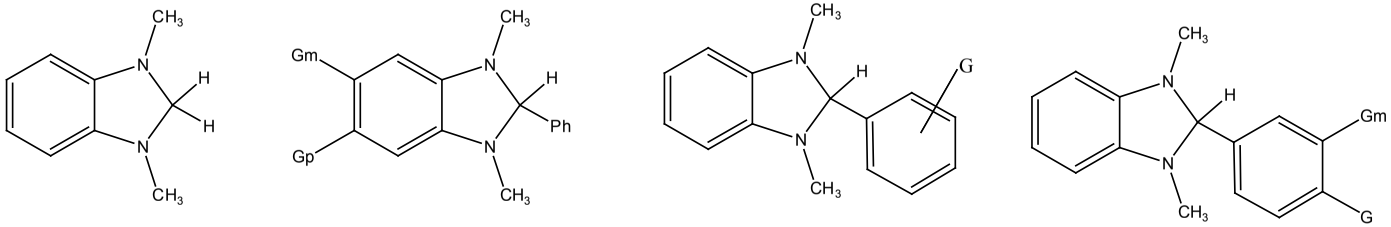

1H 2H 3H 4H

2H: Gp = OMe, Me, H, Cl, CF3 ; Gm = H, Me. **3H**: G = p-NMe2, p-OH, p-MeO, p-H, p-Cl, p-Br, p-CF3, p-CN, p-NO2, m-MeO, m-Me, M-Cl, m-Br, m-NO2, o-Me, o-Cl, o-OH. **4H**: Gm = MeO, NO2, Me, F, Br, Cl ; Gp = p-MeO, p-Me, p-H, p-Cl, p-Br.

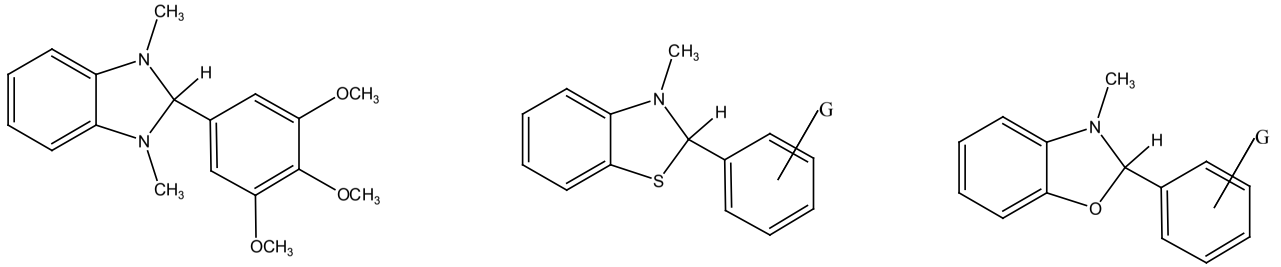

5H 6H 7H

6H: G = p-MeO, p-H, p-Cl, p-Br, p-F, p-Me, m-Me, m-Cl **7H**: G = p-MeO, p-Me, p-H, p-Cl, p-Br.

Figure 4.2: Hydride donors examined by Zhu et al.

The authors determined the enthalpy changes of the hydride donors in releasing hydride anion in acetonitrile from the hydride exchange reaction of strong organic hydride donors **1H-5H** with the strong hydride acceptor N-methylacridinium, and of the corresponding salts (6^+ and 7^+) of weak organic hydride donors 6H-7H with the strong hydride donor **3H**. The findings show that the enthalpy changes increase in the order 1H-5H (49.0 - 57.1 kcal/mol) < **6H** (69.9 - 76.9 kcal/mol) < **7H** (88.3 - 93.4) and the hydride donating abilities decrease in the order : 2,3-dihydrobenzo[d]imidazoles > 2,3-dihydrobenzo[d]thiazoles > 2,3-dihydrobenzo[d]oxazoles. This fact can be related to the aromatic properties of the hydride-removed products which are decreasing in the order : benzo[d]imidazolinium (1^+ and 5^+) > benzo[d]thiazolidinium (6^+) > benzo[d]oxazolidinium (7^+). If the enthalpy changes are compared with those of NADH models such as BNAH which is a well known strong organic hydride donor, and with HEH a medium hydride donor, it is evident as shown in fig 4.3 that the hydride donating abilities of 1H-5H are higher than that of the Hantzsch ester HEH but also than that of BNAH. In contrast the hydride donating abilities of **6H** are greater than HEH, but smaller than those of $AcrH_2$. The hydride donating abilities of **7H** are much smaller than that of $AcrH_2$. The authors also evaluates the hydrogen atom releasing and the electron-donating abilities and indicates that 1H-5H, especially those with electron-donating groups, are moderate hydrogen atom donors. The **6H** group of molecules are not good hydrogen atom donors, but could be used as the source of hydrogen atoms, like 1H-5H, when the reaction temperature is high or a stronger hydrogen atom acceptor is present. The **7H** group of molecules is not a good source of hydrogen atoms. The electron-donating abilities decrease in the order 2,3-dihydrobenzo[d]imidazoles > 2,3-dihydrobenzo[d]thiazoles > 2,3-dihydrobenzo[d]oxazoles. The electron-donating abilities of 1H-5H are larger than those of HEH, $AcrH_2$ and BNAH, indicating these compounds as strong electron donors. The 2,3-dihydrobenzo[d]thiazoles have electron-donating abilities smaller

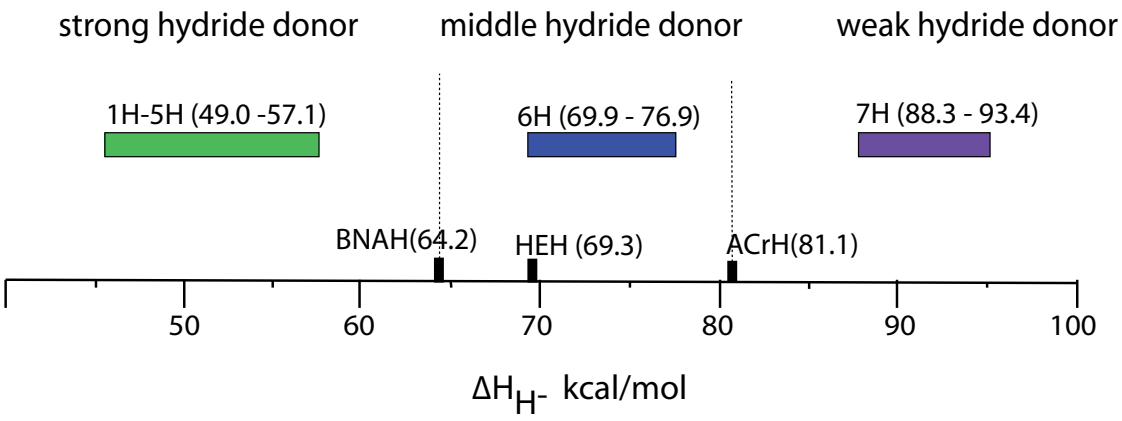

Figure 4.3: Classification of the hydride donor power from enthalpy changes of the 47 molecule analysed by Zhu et al.

than that of BNAH but larger than those of HEH or $AcrH_2$, and thus can be used as medium-strong one-electron donors. In contrast the 2,3-dihydrobenzo[d]oxazoles are poor electron donors compared with HEH or $AcrH_2$ or BNAH and therefore cannot be used as one-electron reducing agents. In conclusion, these 47 hydride donors can be divided into three classes (fig.4.3) :

- 1H-5H, which are strong hydride donors and also good electron and hydrogen atom donors,
- 6H, which are mild hydride, electron, hydrogen atom donors,
- 7H, which are poor hydride, electron, hydrogen atom donors.

The authors investigated the electron and hydrogen donating capabilities of these hydride donors because these phenomena often occur during a hydride transfer reaction. As shown in fig 4.4 the thermodynamic driving forces considered in this work are, taking **3** as example:

- 3H to release a hydride anion and hydrogen atom,
- $3H^+$ to release a proton and hydrogen atom,
- 3H to release an electron,

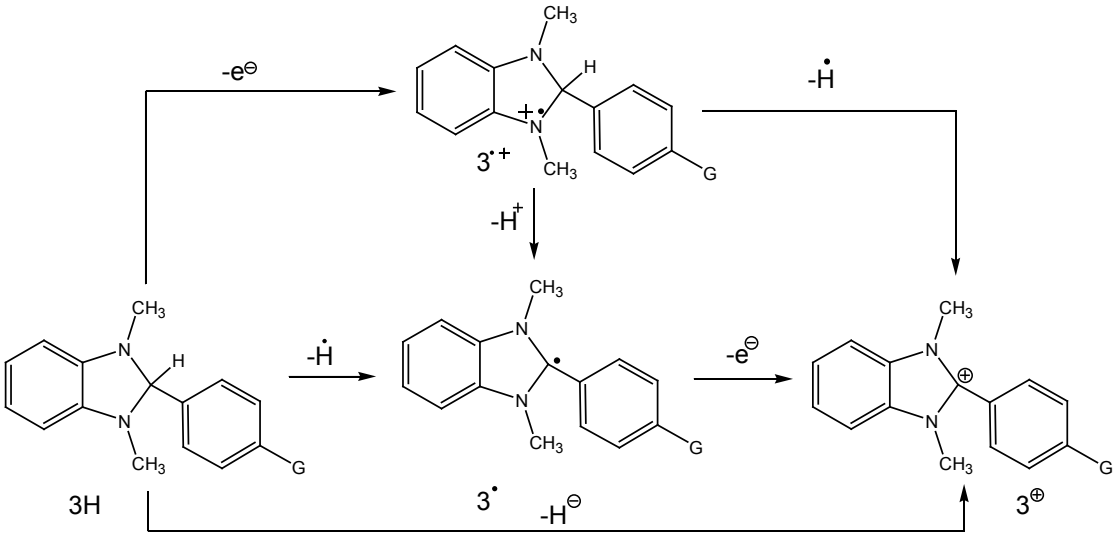

Figure 4.4: Mechanisms proposed by Zhu et al. for the hydride transfer (i.e. of 3H)

- 3^+ to accept an electron.

The system analysed is in solution and the authors point out that all these phenomena are very important in clarifying the hydride transfer mechanism.

4.1 Hydride transfer reactions comparison

HDBMZ-H + BNIQ	Reactants	TS	Products
E	-1567.8971	-1567.8599	-1567.8984
ΔE	0.00	23.34	-0.81
β_s		0.011	
R_H	1.41	0.00	1.38

Table 4.1: Energies (absolute in Hartree, relative in kcal/mol), structural proximity parameter β (eV) and distance between reactants and TS and between products and TS R_H for the hydride transfer between HDBMZ-H and BNIQ

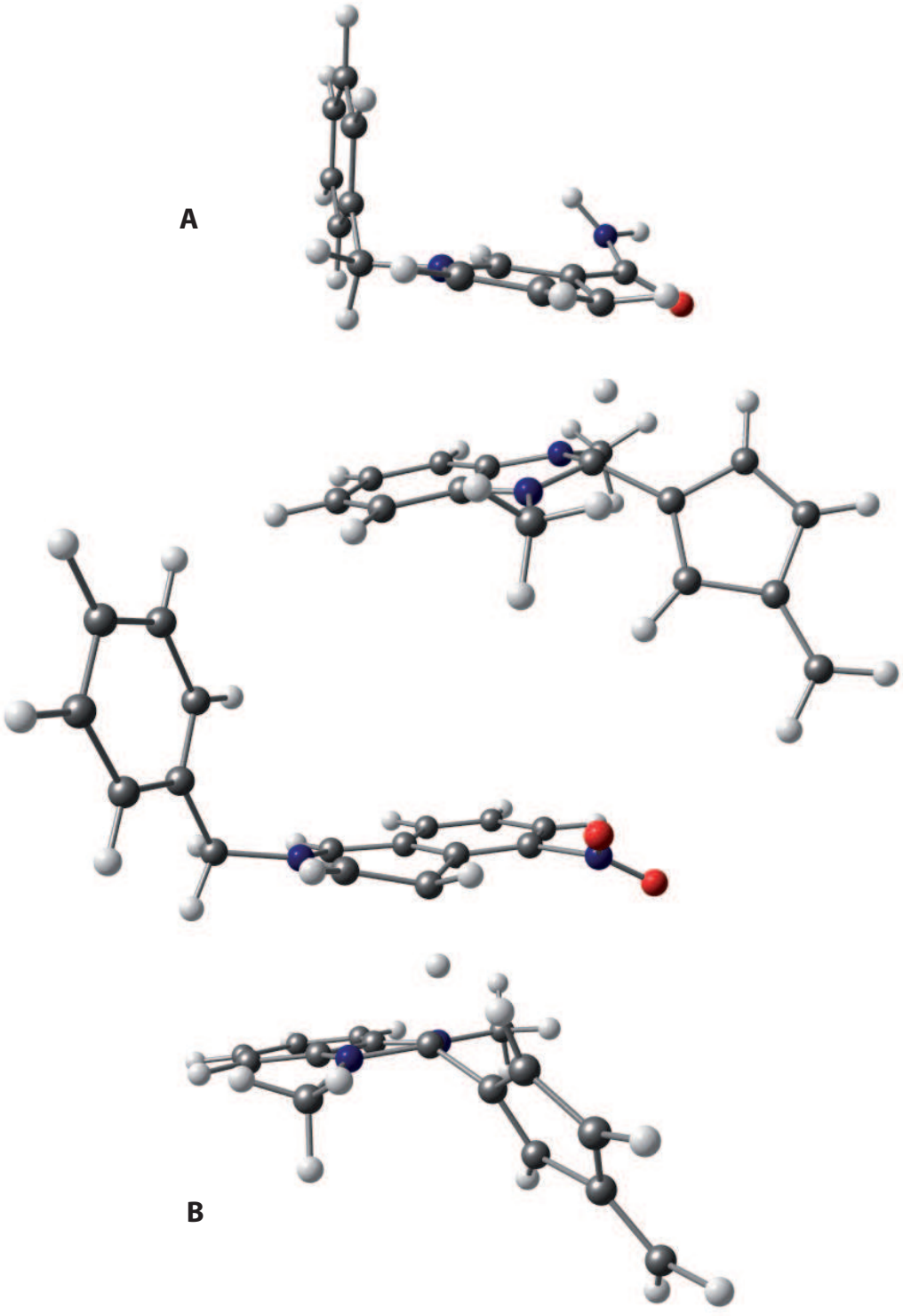

Figure 4.5: Hydride Transfer transition states between HDBMZ-H and BCPY (A) or BNIQ (B).These TS structures show that the TS between HDBMZ-H and BCPY (table 4.2) resembles more the reactants than the TS of the reaction between HDBMZ-H and BCPY. Thus, from the Hammond Postulate, the reaction of HDBMZ-H with BCPY is more favoured than with BNIQ.

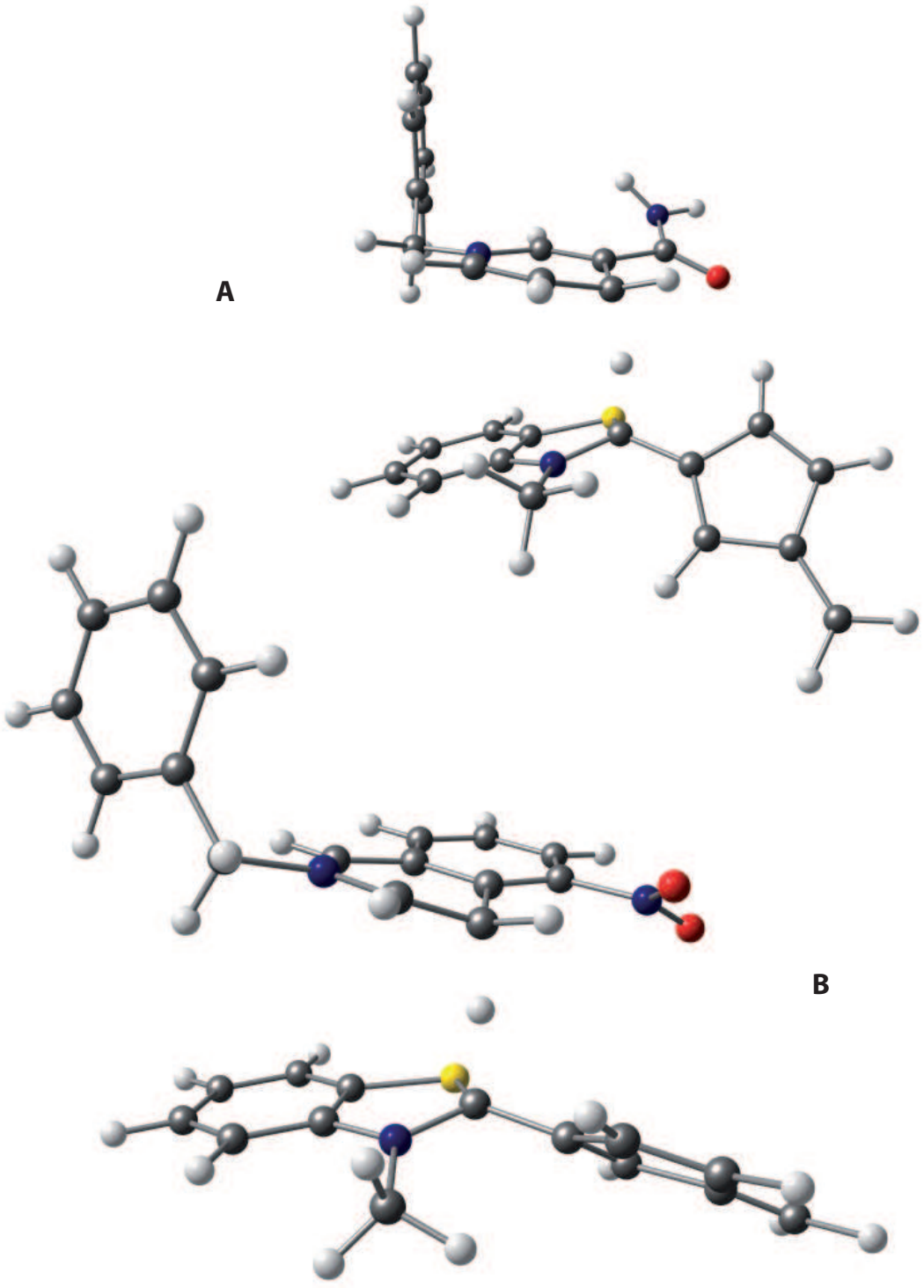

Figure 4.6: Hydride Transfer transition states between HDBTZ-H and BCPY (A) or BNIQ (B). The TS structure of the hydride transfer between HDBTZ-H and BCPY (table 4.4) does not resembles either reactants or products although the reaction is exothermic, while the TS structure for the reaction between HDBTZ-H and BNIQ (table 4.3) resembles more the products and the reaction is significantly endothermic.

HDBMZ-H + BCPY	Reactants	TS	Products
E	-1378.4556	-1378.4384	-1378.4905
ΔE	0	10.79	-21.90
β_s		-0.076	
R_H	1.29	0.00	1.50

Table 4.2: Data shown as in 4.1 for the hydride transfer between HDBMZ-H and BCPY

HDBTZ-H + BNIQ	Reactants	TS	Products
E	-1871.4256	-1871.3782	-1871.4080
ΔE	0.00	29.74	11.04
β_s		0.068	
R_H	1.49	0.00	1.30

Table 4.3: Data shown as in table 4.1 for the hydride transfer between HDBTZ-H and BNIQ

4.2 Computational details

It has been used Gaussian 03 suite of programs.[28] Geometry optimizations have been performed at B3LYP/6-31+G* level of theory. The QST3 method has been used for all transition state calculations. TDDFT calculations have been performed at B3LYP/6-311++G** level of theory including a continuum model with the IEFPCM method and ethanol as solvent.

HDBTZ + BCPY	Reactants	TS	Products
E	-1681.9819	-1681.9561	-1681.9894
ΔE	0.00	16.18	-4.7
β_s		0.003	
R_H	1.38	0.0	1.37

Table 4.4: Data shown as in table 4.1 for the hydride transfer between HDBTZ-H and BNIQ

4.3 Evaluation of the hydride transfer reactions of HDBMZ-H through conceptual DFT studies

In the previous chapter, hydride transfer reactions have been analysed with global reactivity descriptors such as the chemical potential μ, and the molecular hardness η, through the maximum hardness principle given by Pearson et al. which states that reactions tend to proceed toward species with the highest molecular hardness. In this section, the reactivity of the species participating in the hydride transfer reactions with HDBMZ-H as hydride donor will be investigated further with reactivity indexes. The reactivity indexes that will be considered and explained in this section are, in addition to μ, η, the electrophilicity index ω defined by Parr, Von Szentpály and Liu[109] and the dual descriptor introduced by Morell and coworkers.[110]

The energy stabilisation which arises when the acquisition of an electronic charge of a system from the enviroment occurs is measured by the global electrophilicity index ω. This index is given by the following expression in terms of hardness and

chemical potential :

$$\omega = \frac{\mu^2}{2\eta} \approx \frac{(\epsilon_L + \epsilon_H)^2}{4(\epsilon_L - \epsilon_H)} \tag{4.1}$$

The electrophilicity index expresses the tendency of the electrophile to acquire an additional charge driven by μ^2 (which is the square of the electronegativity $\chi = -\mu$) and the opposition of the system to exchanging electronic charge with the environment, which is described by η. In general, a good electrophile identified through this index has high value of μ and low values of η. The link between the global reactivity concept which defines the molecular hardness and the locality concept which defines the Fukui functions is given by the dual descriptor.[111–113] The electron density variation under the influence of a reagent that is approaching is an important factor. Fukui was the first to identify the importance of frontier orbitals as the principal factor determining the ease of chemical reactions. Parr and Yang[107,114] demostrated that most of this frontier theory can be conceptualised through DFT. The Fukui function of a molecule which underlies the reactivity of a site,[115,116] can be defined by :

$$f(r) = \left.\frac{\partial \rho(r)}{\partial N}\right|_{v(r)} \tag{4.2}$$

which is the electron density variation driven by a change in the number of electrons. For a molecular or atomic system, the derivative of the equation above is discontinuous and difficult to evaluate, thus three numerical definitions of Fukui functions have been provided :

$$f^+(r) = \left.\frac{\partial \rho(r)}{\partial N}\right|^{+}_{v(r)} \tag{4.3}$$

controlling of nucleophilic attack

$$f^-(r) = \left.\frac{\partial \rho(r)}{\partial N}\right|^{-}_{v(r)} \tag{4.4}$$

controlling of electrophilic attack, and

$$f^0(r) = \left.\frac{\partial \rho(r)}{\partial N}\right|^0_{\upsilon(r)} \tag{4.5}$$

controlling of radical attack

If the finite difference approximation is utilised, the Fukui functions, f, can be calculated from differences in density :

$$f^-(r) = \rho_{N=N_0}(r) - \rho_{N=N_0+1}(r) \tag{4.6}$$

which is defined when the system undergoes an electrophilic attack decreasing its number of electrons, and

$$f^+(r) = \rho_{N=N_0+1}(r) - \rho_{N=N_0}(r) \tag{4.7}$$

defined when the system undergoes a nucleophilic attack. The last function, controlling the radical attack, is defined by an average between f^+ and f^-.

In general in a molecule, considering what is said above, the charge flows from regions where f^- is large when it is attacked by an electrophilic reagent, while it accepts charge at the regions where f^+ is large when it is attacked by a nucleophilic reagent. Considering the equations above, it is possible to make the following assumption :

$$f^-(r) \approx \rho_H(r), \qquad f^+(r) \approx \rho_L(r) \tag{4.8}$$

where $\rho_H(r)$ and $\rho_L(r)$ are the densities of the highest occupied (HOMO) and lowest unoccupied (LUMO) molecular orbitals respectively.

Grand, Morell and Toro Labbé[110,117] developed the dual descriptor $\Delta(f(r))$ which can be defined through the finite difference approach as :

$$\Delta f(r) \approx \rho_{N_0+1}(r) - 2\rho_N(r) + \rho_{N-1}(r) \;\; = \;\; f^+(r) - f^-(r) \;\; \approx \rho_{LUMO}(r) - \rho_{HOMO}(r) \tag{4.9}$$

$\Delta f(r)$ will be positive in electrophilic regions and negative in nucleophilic regions as $\rho_{LUMO}(r)$ tends to be greater in electrophilic areas and $\rho_{HOMO}(r)$ in the nucleophilic ones. The dual descriptor therefore can be a simultaneous indicator of both the nucleophilic and the electrophilic regions within a molecule, hence its name "dual descriptor".

Molecule	Energy	Dipole Moment	HOMO	LUMO	μ	η	ω
BCPY-H	-688.745	8.16	-0,19	-0,04	0,07	-0,12	0,10
BCPY	-688.0144	3.27	-0,27	-0,09	0,09	-0,18	0,17
HDBMZ-H	-690.8536	4.38	-0,18	-0,08	0,05	-0,13	0,18
HDBMZ	-690.1422	1.61	-0,24	-0,10	0,07	-0,17	0,20
BNIQ-H	-878.1915	9.18	-0,20	-0,10	0,05	-0,15	0,23
BNIQ	-877.4882	10.38	-0,26	-0,12	0,07	-0,19	0,26

Table 4.5: Energies, dipole moments and reactivity parameters related to the four molecules considered, μ, η ω are in eV, Energy in Hartrees, Dipole moments in Debye.

In table 4.5, the global electrophilicity index, which describes the ability of electron acceptors to acquire an additional charge from the environment, shows that the BNIQ molecule is a stronger electron acceptor than BCPY by about 0.09eV. Some conclusions can be drawn from the transition state analysis supported by the Hammond postulate. Although the transition state of BCPY resembles the reactants more than in the case when the BNIQ molecule was the electrophile, denoting therefore a more favoured reaction, BNIQ is more electrophilic than BCPY. The reaction of the BNIQ molecule as electrophile is less favourable probably because other factors such as steric hindering play a key role in determining the success of the hydride transfer and not only the electrophilicity of the hydride acceptor. Observing the chemical potentials it is evident that a lower potential for the hydride donors and a higher potential for the hydride acceptors make the hydride transfer an allowed process. The hardness values show variations of about 0.02-

0.04eV between the molecules. Thus, it is quite difficult to give an appropriate interpretation of the values.

Yang and co-workers[114] showed that the the density change due to electron removal is given by $\rho|HOMO|^2$, while the electron-density change from adding an electron to a molecule is given by $\rho|LUMO|^2$. Thus if the orbital relaxation and the electron correlation are neglected the expression for the dual descriptor becomes $f(r) = \rho|LUMO|^2$ - $\rho|HOMO|^2$, hereafter denoted as f'. More recently, the same type of approximation has been used by Ayers et al.[117,118] in order to study the Woodward-Hoffmann Rules. The present study therefore tried to understand on which site of the electrophilic molecules BNIQ and BCPY the hydride transfer is more likely to occur. Understanding on which site of a hydride acceptor the hydride transfer is more likely to occur could save some time computationally because the transition states will be located much more quickly. Moreover, this fact can also have an important meaning from an experimental point of view with prediction of which products would be more likely to be formed. Observing fig 4.7 C, it is evident that the carbon atom of B resulting from the hydride transfer with BNIQ or BCPY shows a positive value of the dual descriptor in the direction of the hydride transfer, while looking at D it is less evident on which site the hydride transfer has occurred. In A and B of this picture, the hydrogen of HDBMZ which is involved in the hydride transfer shows negative values allowing us to estimate within the molecule which hydrogen atom could be involved in a hydride transfer reaction. Turning to fig 4.8, in A and B it is interesting to observe that the carbon atom which can actually accept a hydride anion is the site where the transfer has been found to occur within the transition state search. There is no experimental evidence about the BCPYH structure, thus these findings are not corroborated by experimental results. Fig 4.9 suggests that within the BNIQ molecule (A and B), f is better than f' in answering the question : "where can the transfer for this molecule occur?", while in BNIQH (C and D), there is a discordant prediction

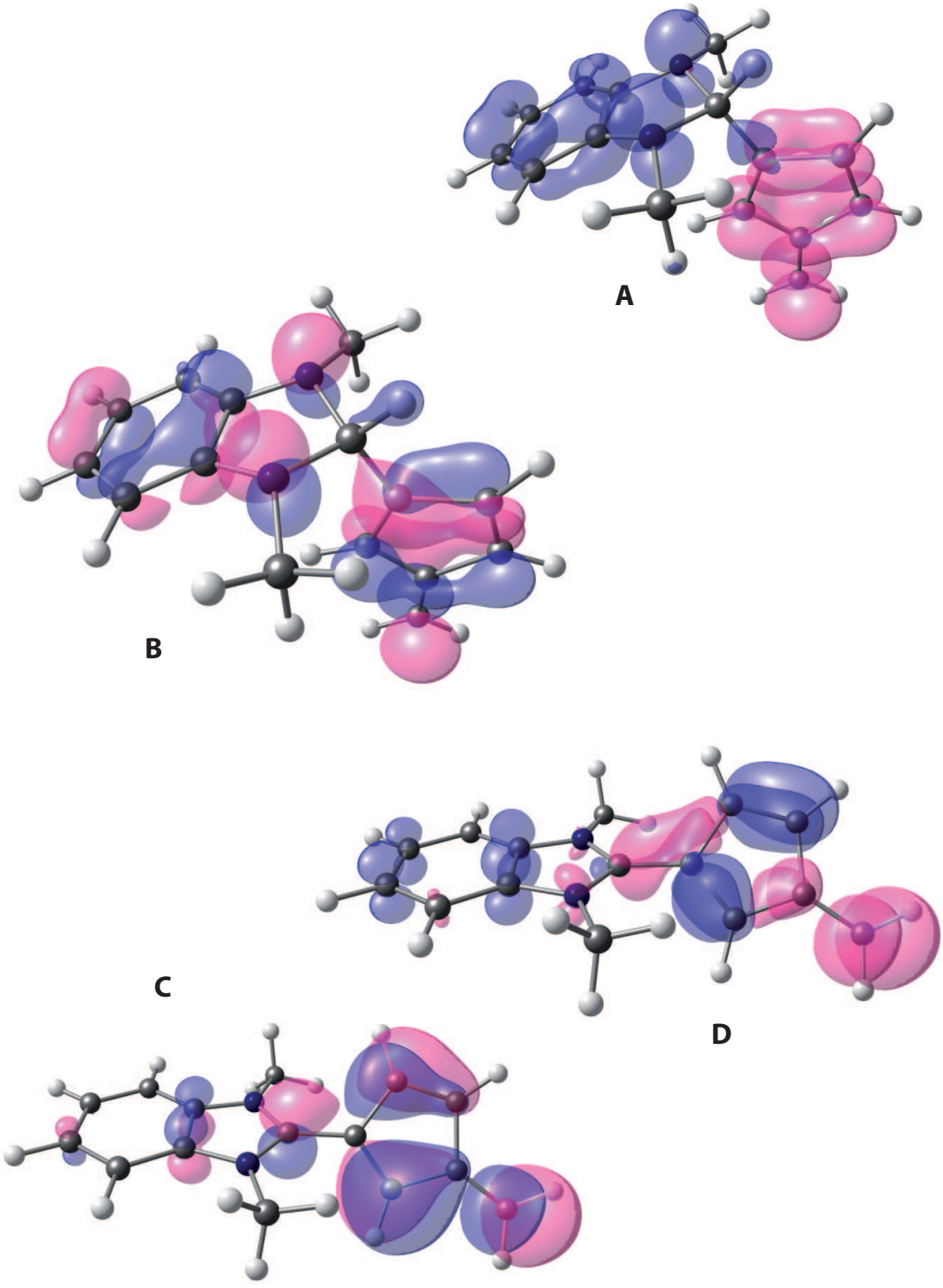

Figure 4.7: Dual descriptor of HDBMZ-H and HDBMZ molecules obtained as ρ LUMO - ρ HOMO (B and C) and as $\rho\ |LUMO|^2$ - $\rho\ |HOMO|^2$ (A and D)(The purple denotes positive values, the blue denotes negative values.)

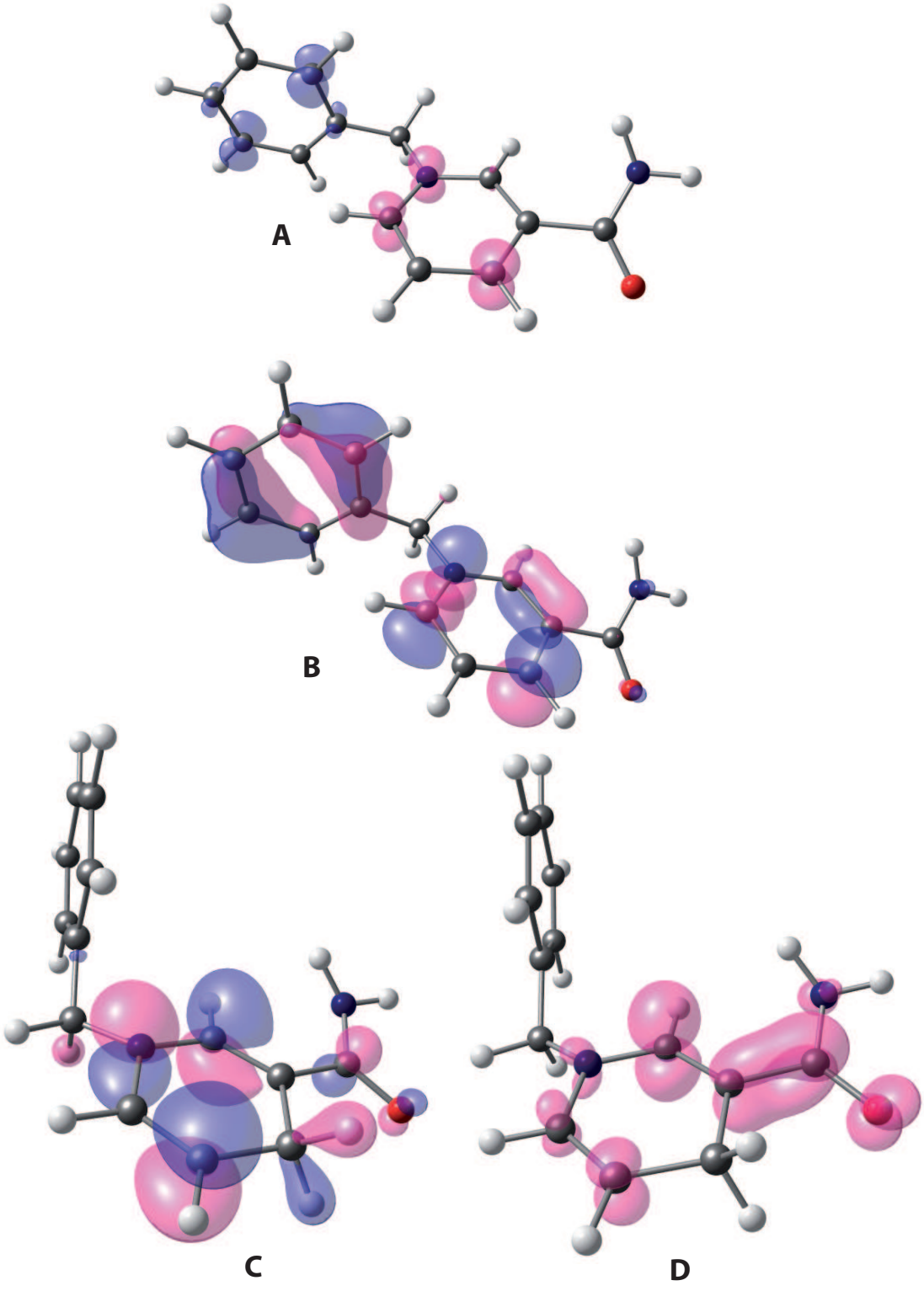

Figure 4.8: Dual descriptor of BCPY and BCPYH molecules obtained as ρ LUMO - ρ HOMO (B and C) and as $\rho\ |LUMO|^2$ - $\rho\ |HOMO|^2$ (A and D) (The purple denotes positive values, the blue denotes negative values.)

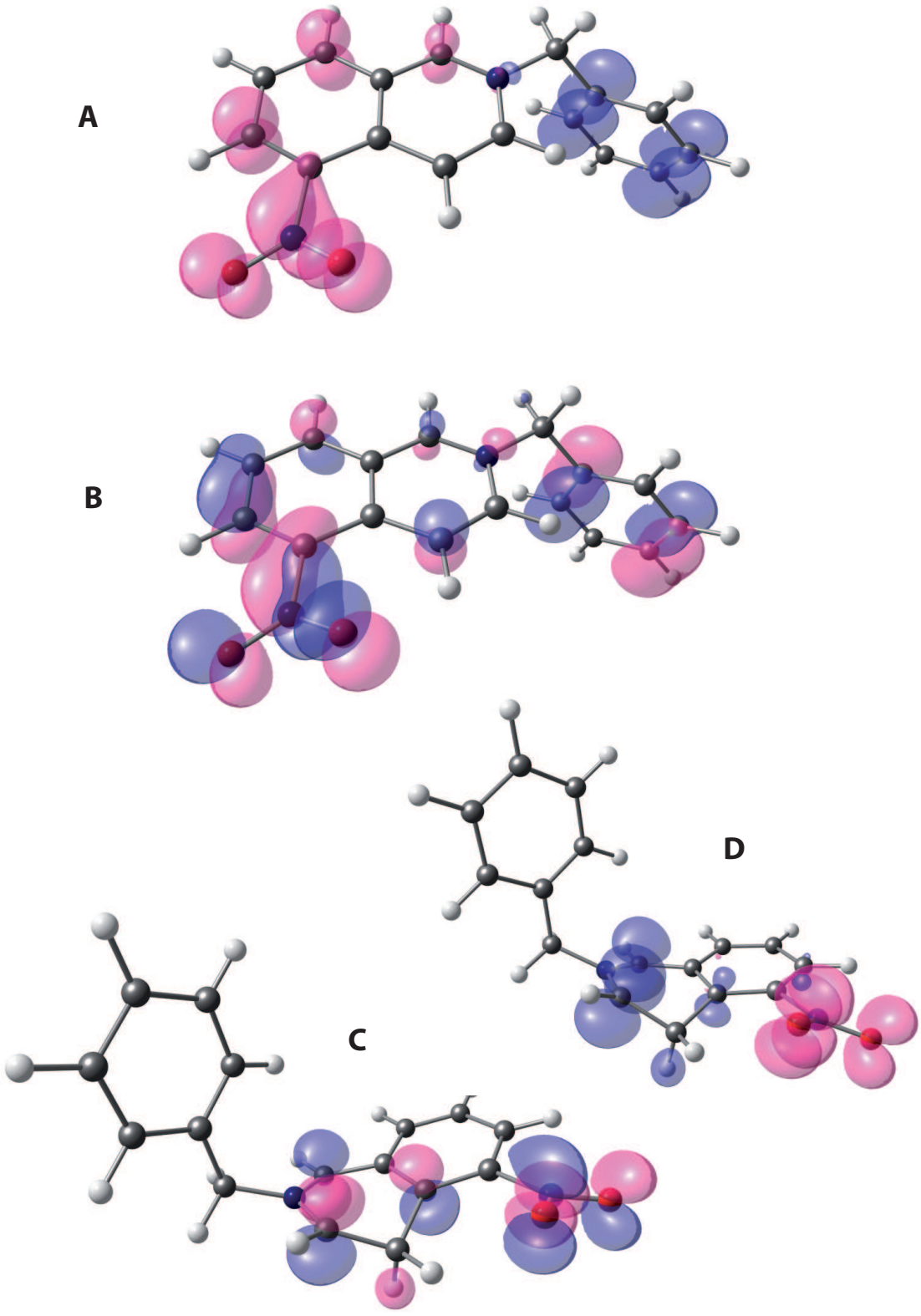

Figure 4.9: Dual descriptor of BNIQ and BNIQH molecules obtained as ρ LUMO - ρ HOMO (A and D) and as $\rho\ |LUMO|^2$ - $\rho\ |HOMO|^2$ (B and C) (The purple denotes positive values, the blue denotes negative values.)

between f and f' about which hydrogen could be donated to an acceptor. Also in this case there is no experimental evidence about the BNIQH structure.

4.4 Time-Dependent studies of the hydride transfer reaction step

TD-DFT has been employed, as previously discussed, to study several properties such as Raman spectra and UV-vis spectra of discrete molecules, but there are currently no studies directed to understanding synthesis reaction steps. It is important to remark upon the limitations within this type of analysis. The experimental Time-Dependent UV-vis spectra, help to understand the product formation from the reacting species during time. Currently, with TDDFT, it is not possible to determine the optical properties of a mixture of different molecules in GPH and even less in solution. Thus, the simplest approximation that can be employed, consists of averaging the simulated UV-vis spectra of the molecules involved within the synthesis reaction step. This is certainly an extremely approximate method for evaluating the properties of a mixture of reactant/products in solution, as can be seen in the results, but currently there are no other viable alternatives. An additional problem within this study is the representation of the solvent. The UV-vis spectra have been obtained from the GAUSSIAN 03 output through the use of the SWizard software.[119] The experimental UV-vis spectrum of the hydride transfers have been measured in a mixture of solvents (water/isopropanol 1:3). Considering all limitations, it was decided to utilise ethanol as solvent, since it has a dielectric constant similar to the mixture mentioned above. This was essential because unfortunately with GAUSSIAN03 it is not possible to solvate molecules with a solvent mixture and these problems should be addressed by the COSMO-RS[23] method developed by Klamt and co-workers. The results in fig 4.10 show the experimental UV-vis spectra of the reaction between BHDMZ-H and BCPY

and of the reaction between BHDMZ-H and BNIQ, while in fig 4.11 the simulated UV-vis of all four molecules for each hydride transfer is shown.

Fig 4.10 shows the experimental Time-Dependent UV-vis spectra of the hydride transfer between HDBMZ-H and BNIQ (A) and between HDBMZ-H and BCPY (B). The hydride transfer in A shows a λ_{max} at about 470nm with an absorbance = 2, while, the λ_{max} in B is at about 360nm with absorbance = 0.5. Turning to the calculated spectra it is possible to observe in both figures 4.11 and 4.12 that (probably) the absorbance of the products gives a major contribution to the Time-Dependent UV-vis spectra. The calculated UV-vis spectrum of BCPY-H has a λ_{max} at $\approx$ 370nm and is much less intense than that of BNIQH. The BNIQH spectrum has a λ_{max} at $\approx$ 430nm. Thus, although there is not a real correspondence between the same UV-vis spectra it is possible to hypothesize that the contribution, in this case, is given more by BCPYH and BNIQH than other molecules.

4.5 Conclusions

In this chapter the hydride transfer reaction mechanism between a 2-heteroaryl-1,3-dimethylbenzimidazoline (HDBMZ-H) or 2-heteroaryl-1,3-dimethylbenzothiazoline (HDBTZ-H), which are hydride donors, and different hydride acceptors (BCPY and BNIQ) has been computationally studied, bearing in mind the experimental findings of Lee et al and of Zhu et al. From transition state calculations, the reaction between the hydride donors and BCPY is overall the most favourable reaction with an earlier transition structure than with BNIQ, denoting its strong efficiency. The HDBMZ-H hydride donating abilities, predicted from the transition structures, is higher than HDBTZ-H, confirming the findings of Zhu et al. The calculated TD-DFT spectra of the HDBMZ-H reactions, when compared with the experimental spectra, are not in good agreement. The errors in those predictions

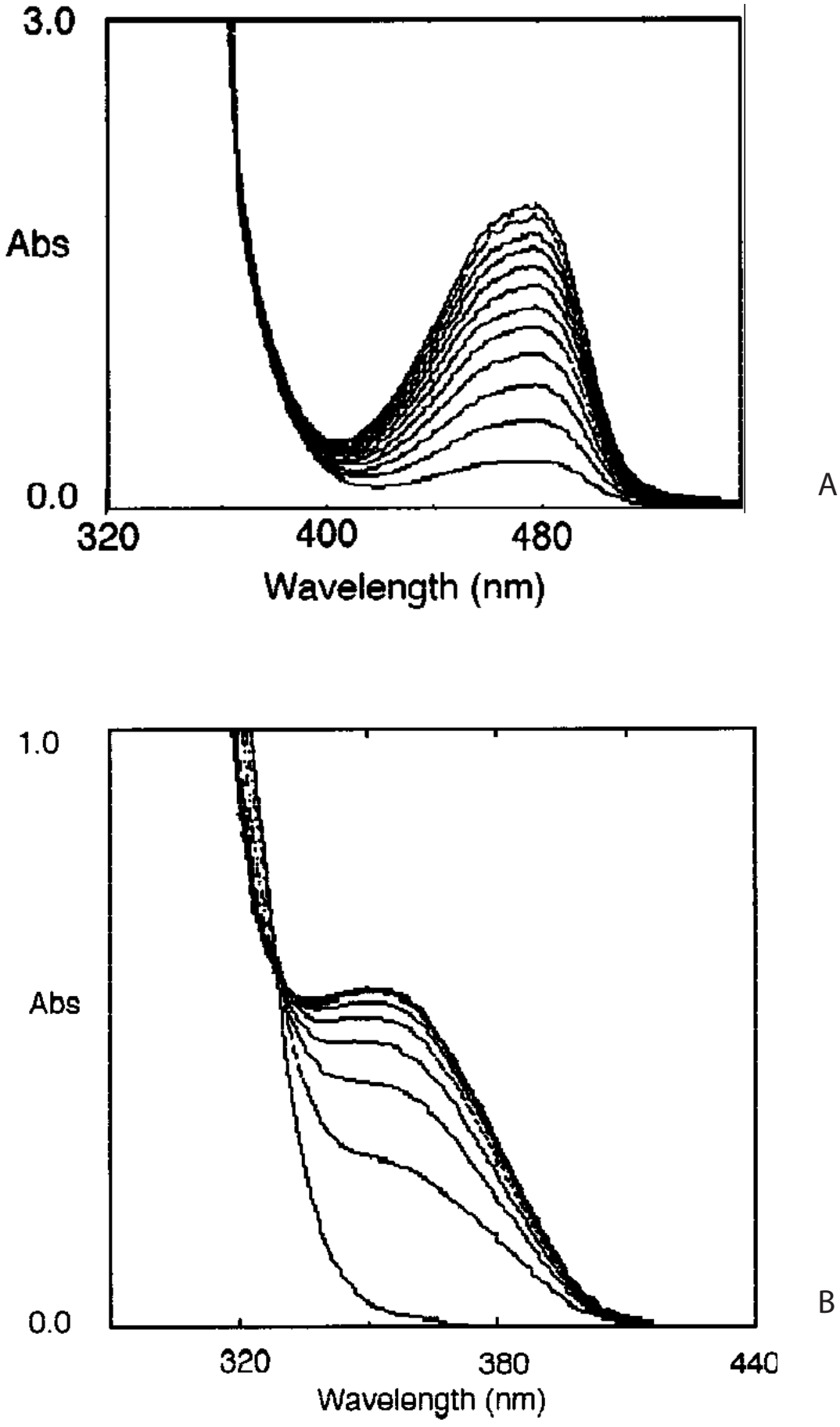

Figure 4.10: Experimental spectra of the hydride transfer between HDBMZ-H and BNIQ (A) and between HDBMZ-H and BCPY (spectra taken from Lee et al, 2007)

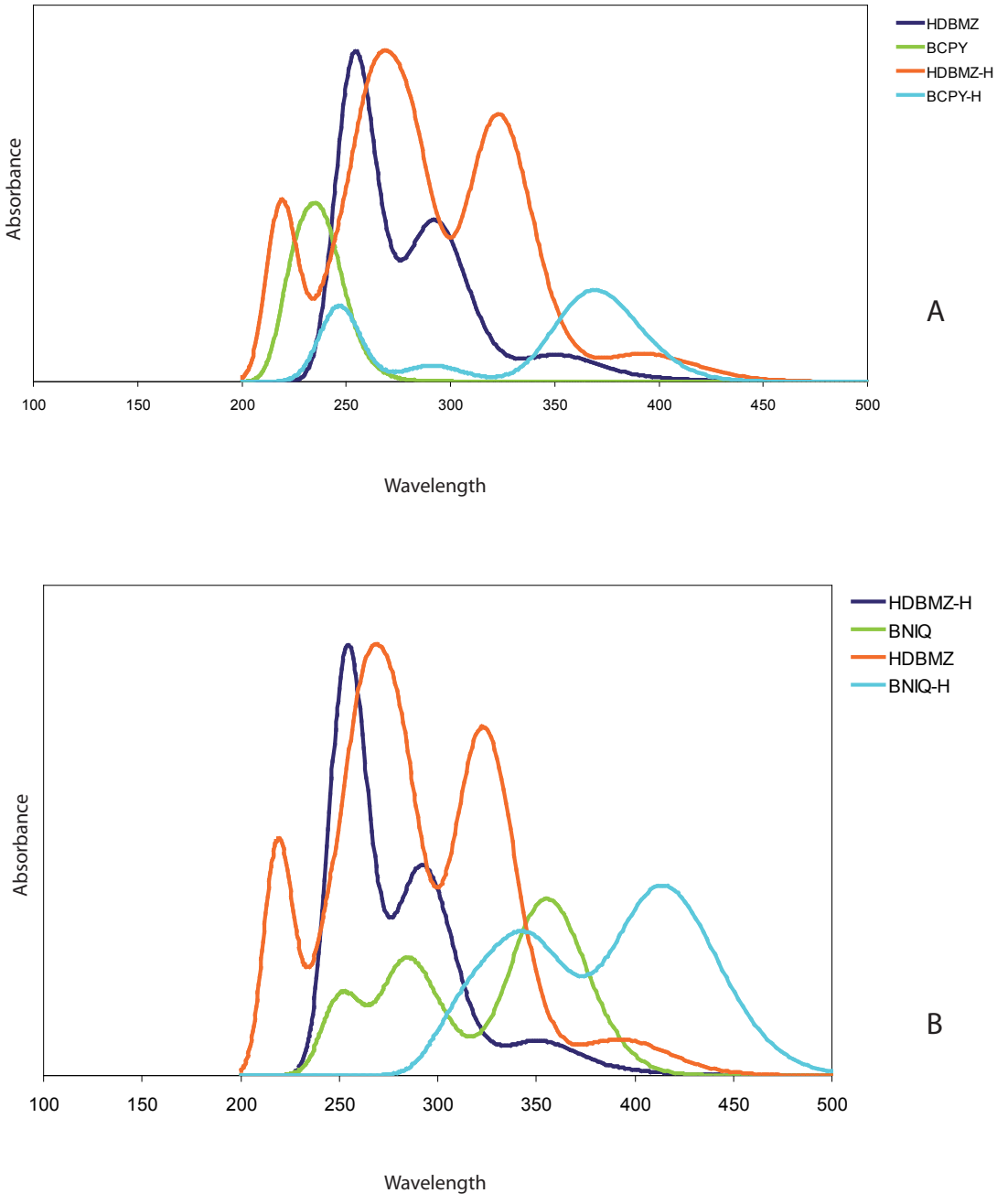

Figure 4.11: Time-dependent DFT spectra of the single molecules involved in the hydride transfer

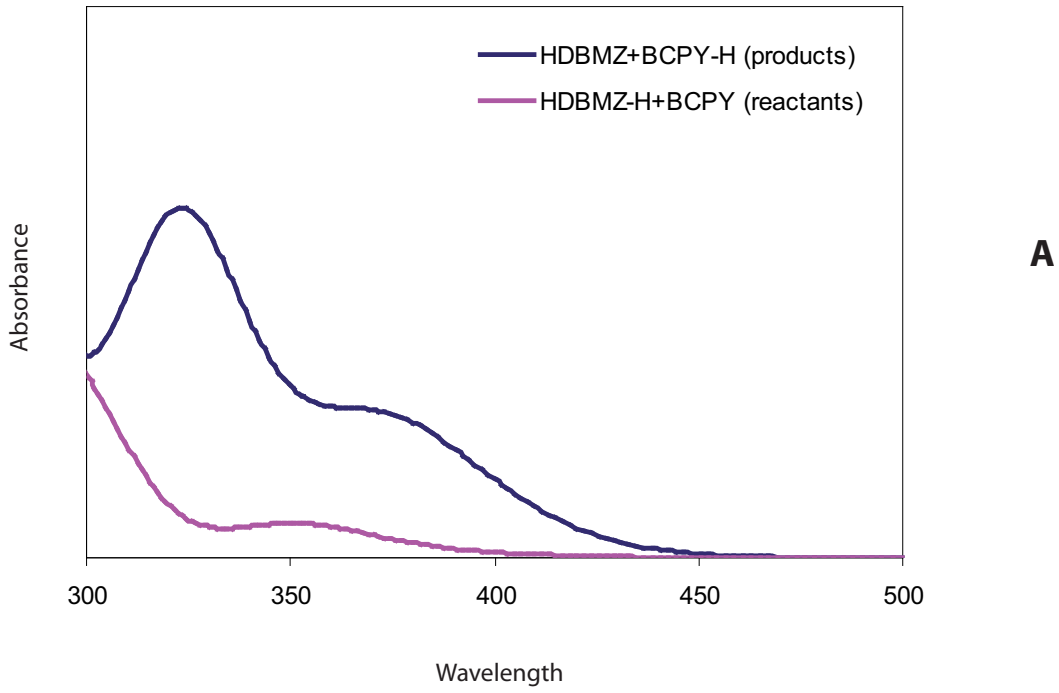

A

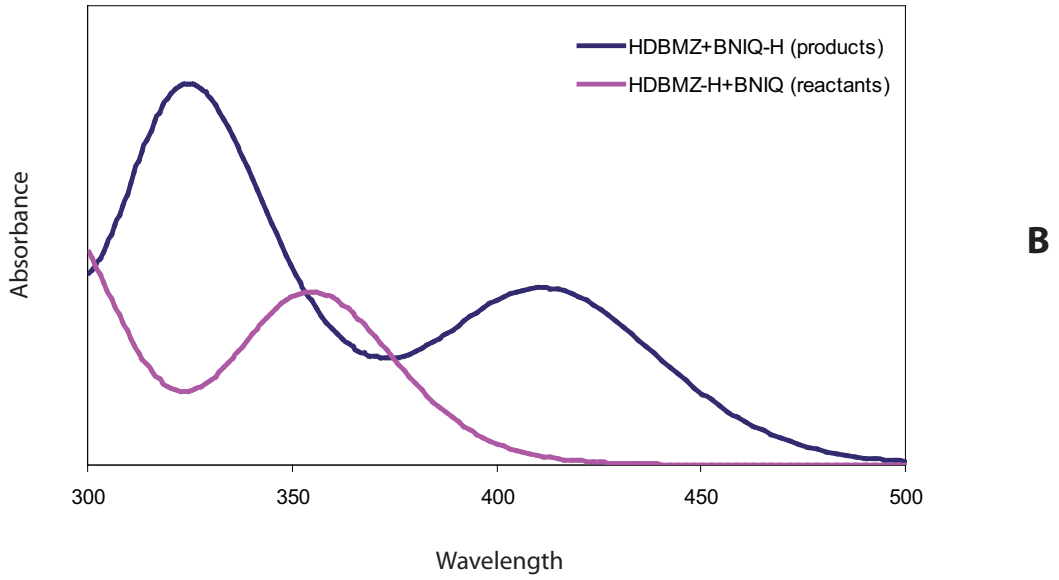

B

Figure 4.12: Time-Dependent spectra obtained averaging the spectra of the reactant molecules (purple) and the products (blue), between 300 and 500 nm

.

are probably not lying directly in the TD-DFT method but on the approximations utilised in order to obtain the time dependent UV-vis spectrum of the reaction.

5

Spin Crossover Transition in the $CsFe^{II}[Cr^{III}(CN)_6]$ Prussian Blue Analogue: A Solid State Hybrid Density Functional Study

A rare phenomenon in octahedrally coordinated transition metals is the spin crossover (SCO) which occurs in their d^4-d^7 electronic configurations. External perturbations can induce this phenomenon including variations of temperature or pressure, light irradiation or exposure to magnetic fields. Information processing and display technologies can benefit from the application of molecular electronic bistabilities among which the SCO phenomenon can be classified. The only technologically relevant molecular electronic bistabilities are those associated with an observable response of the material such as volume changes, the magnetisation, the electrical conductivity or the optical absorption. When the low spin (LS)-to-high spin (HS) ($HS \rightarrow LS$) and $HS \rightarrow LS$ switching are optically driven, showing the presence of long excited state lifetimes caused by the light-induced excited spin-state trapping, a particularly promising field can be explored. The SCO effect occurs only in materials that have a small crystal field energy splitting and a nearly equal spin pairing energy between the HS and LS configurations at the SCO-active TM. This fact is a possible explanation for the low presence of systems which manifest thermal SCO effects. Fe^{II}-N coordination complexes

show a favourable spin-pairing and crystal field energy splitting arrangement. SCO transitions in Fe^{III}, Co^{II}, Co^{III}, and Ni^{III} have also been observed[120,121] but are more rare because of the presence of several factors such as an increased crystal field splitting caused by higher oxidation states. The present study extends our use of modern computational chemistry methods and is devoted to the analysis of the thermal SCO in a novel Prussian blue analogue (PBA) $Cs^{I}Fe^{II}[Cr^{III}(CN)_6]$ which shows the first of this kind of effect observed in PBAs. In this material, when the temperature increases, there is an Fe^{II} LS ($e_g^0 t_{2g}^6$: S = 0) HS ($e_g^2 t_{2g}^4$: S = 2) transition at about 238K coupled with an isosymmetric lattice expansion of 0.38 Å(space group $F\bar{4}3m$). The reverse transition occurs at 211K and is estimated that about 11% of the Fe^{II} sites remain in the HS configuration below the critical temperature. It has been shown that X-ray illumination can induce HS-LS conversion. This fact fits with a nucleation model which demonstrates that the reaction rate decreases with a temperature increase.[122] It has been demonstrated also with combined methods that within the SCO process there is no involvement of TM redox or ligand isomerisation.

Le Guennic et al[123] studied theoretically the $Cs^{I}Fe^{II}[Cr^{III}(CN)_6]$ system, performing high level CASPT2 calculations on $[Fe(NC)_6]^{-4}$ within a point charge field and analysing the HS-LS crystal field energy splitting as a function of different charge models. In order to find a qualitative agreement with experiments the authors show that it was necessary to include the charge reorganisation across the HS→LS transition. Moreover, it is shown that the splitting is sensitive to the number of Cs ions although the proposed value of 150 kJ/mol seems to be large compared with predictions of other SCO materials. The SCO effects are interesting because the CN^- ligand possesses the ability to couple spin-bearing TM sites and gives a high structural flexibility to the lattice. The consequence is that PBAs allow variations in hydration, TM oxidation state and counterion radii.[124] Controlling the parameters previously mentioned allows the crystal field

strength to be regulated at and between the the active TM sites with the possibility to synthesise materials possessing specific SCO transition temperatures and hysteretic properties. Other interesting properties can be associated with PBAs, such as high temperature magnetic order, piezomagnetic and photomagnetic responses, pole inversions and internal electron transfer reactions.

Paulsen and Trautwein[125] give an overview of the application of DFT on SCO materials. The main limitations of DFT-based methods are in relation to the prediction of the HS-LS energy splitting and the often strong dependence of this quantity in relation to the Fock exchange content (denoted F_0 hereafter) of the functional. Studies made by Fouqueau et al[126]of the HS-LS transitions in the $[Fe^{II}(NH_3)_6]^{2+}$, $[Fe^{II}(H_2O)_6]^{2+}$ complexes demonstrated that the best agreement with CASPT2 and SORCI reference splitting energies was obtained from the VSXC meta-GGA and PBE0 ($F_0 = 25\%$). The B3LYP (F0=20%), B3LYP* ($F_0 = 15\%$), and RPBE and HCTH407 ($F_0 = 0\%$, pure GGA) functionals performed satisfactorily. Daku et al.[127] showed that the best value of F_0 was 10% within the study of the $LS \rightarrow HS$ in the $[Fe(bpy)_3]^{2+}$. The HS-LS splitting has been demonstrated to change with the strength of the Hubbard like U interaction seen in a series of DFT+U calculations for a range of Fe^{II} SCO materials. DFT calculations have been proved efficient alongside splitting energies and optimised structural parameters, and also for vibrational spectra predictions of SCO materials. Brehm et al[128]compared the normal modes of the isolated $Fe(phen)_2(NCS)_2$ complex derived from BP86 functional calculations of IR and Raman spectra, finding that an agreement was obtained only including closest-approaching groups on neighbouring complexes like in the solid state phase. Reither[129] studied the same complex and concluded that the best choice of functionals was the BP86 pure DFT approach for the vibrational analysis and the B3LYP* functional for the spin state splitting. Baranović[130] did a similar study for several SCO complexes and introduced a parameter that should simultaneously scale the computed HS-LS splitting

and mimic solute-solvent interactions, and another that describes the interaction between the complexes. This study analyses the SCO effect in $CsFe[Cr(CN)_6]$ within a periodic DFT approach. Hybrids Hamiltonians with different F_0 values are evaluated in order to understand the capacity of those functionals to characterize SCO effects. Calculated vibrational frequencies have been added to the static energetics in order to compute the transition temperatures and the relative thermodynamic parameters. Moreover, other parameters such as the bulk moduli, geometries, electronic structure and HS magnetism have been analysed.

5.1 Computational methods

The calculations carried out here have been performed with the CRYSTAL06[131] code. The basis sets utilised include contracted Gaussian-type functions of forms :

1. 1s(8)2sp(6)3sp(4)4sp(1)5sp(1)3d(4)4d(1)
   for Fe and Cr;

2. 1s(6)2sp(3)3sp(1)4sp(1)3d(1) (6-311G* in the Pople notation)
   for C and N;

3. Hay-Wadt small-core pseudopotential
   of valence 8 and 5sp(3)6sp(1) basis for Cs.

The Fe, Cr, C and N sets have all been used in previous studies of Prussian Blue and its analogues; the Cs set was obtained from the CRYSTAL06 repository found at `http://www.crystal.unito.it`, and has been optimised previously for the Cs^I state. The hybrid Hamiltonians utilised are of the form :

$$f^{xc} = \frac{100 - F_0}{100}\left(f^x_{LSDA} + 0.9\Delta f^x_{B88}\right) + \frac{F_0}{100} f^x_{UHF} + 0.81 f^c_{LYP} + 0.19 f^c_{VWN} \quad (5.1)$$

in which x and c are the exchange and correlation contributions respectively. LSDA, B88 and UHF, are the local spin density Becke-88 and spin-unrestricted Hartree-Fock exchange potentials, respectively; and VWN and LYP, the Vosko-Wilk-Nusair[132] and Lee, Yang and Parr correlation functionals, respectively. F_0 values of 0, 10, 12, 14, 16, 18, 20, 30, 90 and 100% were applied, along with pure UHF exchange. The focus on the range of $F_0 = 10 - 20\%$ is motivated by the previous theoretical work on SCO complexes, as discussed above. A value $F_0 = 20\%$ (equivalent to the B3LYP functional) has previously been shown to provide accurate band gaps and dispersions in a wide range of solids,[133] while a value $F_0 = 35\%$ has been shown to provide accurate magnetic coupling constants in a range of TM compounds.[133,134] All calculations adopt a ferromagnetic alignment of TM spin moments, except where explicitly stated otherwise. Convergence of total energies required the use of Coulomb- and exchange integral series truncation thresholds of $10^{-7}, 10^{-7}, 10^{-7}, 10^{-7}$ and 10^{-14},[131] as further described in the code documentation, and an isotropic Monkhorst-Pack reciprocal space mesh with shrinking factor 8. Optimization convergence tolerances of 10^{-7}, 0.0003 and 0.0012 a.u.. for total energy, RMS force and RMS displacement, respectively, were applied, save for in runs relating to the calculation of frequencies, magnetic coupling constants and JT distortion energies, where tighter tolerances of 10^{-9}, 0.00005 and 0.0001 a.u, respectively, were used. Atomic electron and spin populations were obtained from Mulliken analyses of the converged wavefunctions. Calculations of the zone-centre normal modes proceeded by a series of finite atomic displacements of size 0.005 a.u., using lattice symmetry to assist the filling of the mass-weighted Hessian matrix. IR intensities were obtained for selected Hamiltonians via calculation of the atomic dynamical charge tensors, as obtained from a Wannier-Boys localisation approach.[131,135]

5.2 Crystal Field Model

The model proposed by Kanamori is applied here, where the electronic interaction energies of the d-manifold electrons are expressed in terms of combinations of intra- (U) and interband (U') Coulomb- and exchange (J) integrals. The excitation energies of the LS state are obtained by the differences of the configuration energies given by the following equation for the $d^6 LS(S=0) \rightarrow$ intermediate spin (IS; S=1) excitation where B and C are the Racah parameters and Δ_{CF} is the crystal field splitting energy:

$$\Delta E[LS \rightarrow IS_1\{z^2(0)x^2 - y^2(\uparrow)xz(\uparrow\downarrow)yz(\uparrow\downarrow)xy(\uparrow)\}] = \Delta_{CF} - 3C \quad (5.2)$$

$$\Delta E[LS \rightarrow IS_2\{z^2(\uparrow)x^2 - y^2(0)xz(\uparrow)yz(\uparrow\downarrow)xy(\uparrow\downarrow)\}] = \Delta_{CF} + 2B - 3C \quad (5.3)$$

$$\Delta E[LS \rightarrow IS_3\{z^2(0)x^2 - y^2(\uparrow)xz(\uparrow)yz(\uparrow\downarrow)xy(\uparrow\downarrow)\}] = \Delta_{CF} + 6B - 3C \quad (5.4)$$

$$\Delta E[LS \rightarrow IS_4\{z^2(\uparrow)x^2 - y^2(0)xz(\uparrow\downarrow)yz(\uparrow\downarrow)xy(\uparrow)\}] = \Delta_{CF} + 8B - 3C \quad (5.5)$$

The xz and yz orbital occupancies can be interchanged without any energy variations because they possesses equivalent orbital-dependent U' and J interactions. The IS states, in which their respective excitation energy possess only one Δ_{CF} splitting have been selected amongst all possible IS = 1. This selection is supported by the understanding that Δ_{CF} must exceed the pairing energy in any material in a LS ground state. The Racah parameters are always positive, thus the most stable S = 1 configuration is the IS_1. This configuration will be called hereafter IS^L in which the "L" indicates the localisation of single occupation in two distinct orbitals. If a similar analysis is applied to the d^6 $LS \rightarrow HS(S=2)$ excitation, we have:

$$\delta E[LS \rightarrow HS_1\{z^2(\uparrow)x^2 - y^2(\uparrow)xz(\uparrow)yz(\uparrow)xy(\uparrow\downarrow)\}] = 2\Delta_{CF} + 4B - 7C \quad (5.6)$$

$$\delta E[LS \rightarrow HS_2\{z^2(\uparrow)x^2 - y^2(\uparrow\downarrow)xz(\uparrow)yz(\uparrow)xy(\uparrow)\}] = 3\Delta_{CF} + 4B - 7C \quad (5.7)$$

where three distinct $t_{2g}(\uparrow\downarrow)$ configurations lead to energetically equivalent HS_1

states, and the two $e_g(\uparrow\downarrow)$ configurations to equivalent HS_2 states. The more stable configuration HS_1 is called hereafter as HS^L, where "L" indicates the localisation of double occupation in one t_{2g} orbital. The excitation energies show the limits of the pairing energy model in which the Coulomb and the exchange contributions to the $LS \rightarrow HS^L$ energy (-4B -7C), is not an integer multiple of that for the LS-IS^L energy (-3C). A JT distortion occurs in both spin-excited lattices which results in tetragonal (tet) cell deformations lowering the point symmetry at TM sites from O_h to $D4_h$. Two other HS states are considered : the delocalised (D)
$z^2(\uparrow\downarrow)x^2 - y_2(0)xz(\uparrow \frac{1}{3} \downarrow)yz(\uparrow \frac{1}{3} \downarrow)xy(\uparrow \frac{1}{3} \downarrow)$
and the HS^L configuration in a lattice constrained to cubic (cub) geometry.

5.3 Static energetics and optimized structures

The LS ground state is stable for $F_0 \leq 18\%$, while a $HS^{L,tet}$ ground state is favoured for F_0 values higher than this. Moreover, there is no Hamiltonian in which an $IS^{L,tet}$ ground state is stable. If the spin excitation of every Hamiltonian is analyzed it is clear that its nature is of the type $LS \rightarrow HS^{L,tet}$ for $F_0 \leq 18\%$ (except at $F_0 = 0\%$, where a $LS \rightarrow HS^D$ excitation is favoured), of type $HS^{L,tet} \rightarrow LS$, for $18\% < F_0 \leq 60\%$, and of type $HS^{L,tet} \rightarrow IS^{L,tet}$ for $F_0 > 60\%$. The $HS^{L,tet}$ and $IS^{L,tet}$ states are not energetically stable at the $F_0 = 0\%$ limit, with an electronic structure that relaxes back to the LS configuration upon release of the initial spin and eigenvalue constraints. The relative energies of those states have been approximated by extrapolation of fourth order polynomial fits of the obtained data. In the same way, any attempt to have a stable HS^D state above $F_0 = 60\%$ results in a relaxation to the corresponding LS state. Furthermore, the HS^D - HS^L increases rapidly to a value of 270 kJ/mol at the HS^D stability limit. The orbital relaxation therefore seems to be of great importance in the determination of the relative spin state energies in Hamiltonians

with fractions of Fock exchange. The relative spin state energies show that as F_0 increases, there is a progressive dominance of Coulomb and Exchange interactions over the crystal field splittings.

Analysing the optimised structures, it is evident that the $LS \rightarrow HS$ transition always results in an increase in molar volume. The best agreement with the experimental values is obtained from the $F_0 = 0\%$ functional, although all functionals give volume differences reasonably close with the experimental ones. The majority of the structural effects come from the elongation of the Fe-N bonds because of the occupation of the antibonding Fe^{II} e_g-orbitals. Fractional charges in Cr-C and distances relative to LS values are, in all Hamiltonians, less than approximately 4% and 2%, respectively, of the fractional change in the mean Fe-N distance.

A set of LS and HS state energy-volume curves are shown in fig 5.2 as obtained from the $F_0 = 14\%$ functional. The bulk modulus K_0 is obtained from polynomial fits via fourth order functions shown in 5.2, giving values of approximately 60 and 51 GPa for LS and $HS^{L,tet}$ configurations respectively.

$$K_0 = V_0 \frac{\partial^2 E}{\partial V^2}\Big|_{V_0} \tag{5.8}$$

Similar values are obtained within range of Hamiltonians where the LS configuration is favoured. The occupation of the Fe^{II} e_g-orbitals therefore leads to increased Fe-N bond lengths but also to an increased lattice compressibilities. This fact is in agreement with previous studies and if the difference in equilibrium molar volume is also taken in account, it can be quite important for a better understanding of the piezomagnetic effect of the material analyzed. Further comparisons with experiments are not possible because experimental values are unavailable. The Franck-Condon excitation energies (such as spin excitation energies obtained with nuclear positions fixed as in the initial state) have been calculated and are shown in fig 5.2. The $LS \rightarrow HS$ and the $HS \rightarrow LS$ excitation energies, with values of 171.80 and 100.87 kJ/mol respectively, are higher than the optimized states at the same volumes. Those energies normally are correlated to optical transitions but

are forbidden in this material because of parity and spin selection rules.

5.3.1 Electronic Structure

Fig 5.2 shows the atomic charges, net spin populations and d-orbital occupancies obtained from Mulliken analyses of the converged wavefunctions. Absolute values must be analysed with care because of basis set dependence, but the relative variations related to the change of the Hamiltonian and the spin state are more reliable. The absolute charges (q) in the LS state are all of lower magnitude than the respective formal values, with exception of the Cs sites. The Cr charges are very low and have values closer to those expected for the Cr^{II} state. Those effects can be due to a spin-paired density transfer from the CN^{-} ligands to the Fe and Cr e_g orbitals. The presence of the HS^{D} when $F_0 = 0\%$ and the HS^{L} in the functionals containing Fock exchange can be confirmed by observing the Fe orbitals occupancies.

Variations of orbital occupations and charges within the $HS \rightarrow LS$ transitions show that the summed Fe e_g-orbital occupations increase, by amounts ranging from 1.2eV at $F_0 = 0\%$, to 1.8eV in the UHF method, while the summed Fe t_{2g}-orbital occupations decrease, by 1.6eV and 2.0eV, in the same Hamiltonians. The HS Fe charges are generally larger than those in the LS configuration. Those variations correlate well with the summed changes in the neighbouring N charges. This phenomenon can be explained by the fact that the Fe e_g-orbitals in the HS state limit a density transfer from N to Fe sites due to intraband Coulomb interactions which disfavour double occupation. C and Cr charge variations are small during the transition in all functionals examined.

The net spin moments (μ), are generally in agreement with the formal, spin-only values for both spin states. Unpaired density in the LS Fe t_{2g}-orbitals with the Cr spins is of interest for the insights provided on the Cr-Cr magnetic coupling. If it is assumed that the fundamental excitation of the LS lattice is related to an $Fe \rightarrow Cr$

charge transfer, a partial delocalisation of Fe $t_{2g}(\beta)$ density onto Cr sites is given by the mixing of some fraction of excited state into the ground state, which is driven by the concomitant reduction in kinetic energy. If variations in the $HS \rightarrow LS$ transition are closely examined, it can be observed that the summed Fe e_g and t_{2g}-moments increase by amounts ranging from 1.65 and 1.91μB, respectively, at $F_0 = 0\%$, to 1.94 and 1.99μB, respectively, in the UHF method. The N moments are larger in the HS state, while the changes of the C and Cr values within the states are very small.

This study is related to the magnetism of the HS configuration alone. The double occupation of a single t_{2g}-orbital and associated JT distortion introduce some degree of anisotropy. The magnetic model introduced here allows the orientational dependence of the coupling to be understood (which can be difficult from first principles), separating the in-plane-(IP, Jxy) and out-of-plane (OOP, Jz) exchange coupling constants. The spin Hamiltonian utilised is of the form :

$$\hat{H}_{spin} = \hat{H}_0 + \frac{J_{xy}}{2} \sum_{ij}^{nn,IP} \overrightarrow{S_i}\overrightarrow{S_j} + \frac{J_z}{2} \sum_{ij}^{nn,OOP} \overrightarrow{S_i}\overrightarrow{S_j} \tag{5.9}$$

$\hat{H}_0$ is the putative non-magnetic energy, the first sum runs over nn pairs of Fe^{II} and Cr^{III} spin moments (S) in the same xy-plane, and the second, over nn OOP pairs. Positive J values favour antiferromagnetism in this sign convention, while restricting to nn pairs implies modelling of coupling mediated by single CN^- ligands alone. In this study four magnetic orders are considered, these are the ferromagnetic (FM), type 1 antiferromagnetic (AF1; AF alignment IP and FM alignment OOP), AF2 (AF IP, AF OOP), and AF3 (FM IP, AF OOP) states. The energies per TM ion of those states can be found through the following equations

:

$$E[FM] = E_0 + 2J_{xy}\bar{S}^2 + J_z\bar{S}^2 \tag{5.10}$$

$$E[AF_1] = E_0 - 2J_{xy}\bar{S}^2 + J_z\bar{S}^2 \tag{5.11}$$

$$E[AF_2] = E_0 - 2J_{xy}\bar{S}^2 - J_z\bar{S}^2 \tag{5.12}$$

$$E[AF_3] = E_0 + 2J_{xy}\bar{S}^2 - J_z\bar{S}^2 \tag{5.13}$$

$$\tag{5.14}$$

and the effective squared spin is :

$$\bar{S}^2 = \sqrt{S_{Cr}(S_{Cr}+1)S_{Fe}(S_{Fe}+1)} \tag{5.15}$$

where $S_{Cr} = \frac{3}{2}$ and $S_{Fe} = 2$. Mapping these expressions within the related computed total energies allows the coupling constants to be obtained. The optimised FM $HS^{L,tet}$ structures appropriate to each functional have been used for all four magnetic states. The coupling constants, are derived twice, in order to check for consistency: once from the FM, AF1 and AF2 energies (set I), and the other from the FM, AF2 and AF3 energies (set II).

Table 5.3 presents the relative magnetic energies and coupling constants obtained from the $F_0 = 30$ and 40% Hamiltonians. The couplings are consistent: the set I and II values vary from their respective mean value by only 2.6 and 6.7% for J_{xy} and J_z respectively at $F_0 = 30\%$, and by 2.3 and 5.9% for the same coupling constants at $F_0 = 40\%$. The couplings increase in their value in going from $F_0 = 40\%$ to 30% and the IP coupling is FM while the OOP coupling is AF in which the former has a larger value than the latter. Interpolation between the respective average values yields estimates at $F_0 = 35\%$ of -3.64, +2.78 and $-1.5cm^{-1}$ for J_{xy}, J_z and $\bar{J} = \frac{1}{3}(2J_{xy} + J_z)$ respectively. The latter Hamiltonian thus has been able to give reliable coupling constants. In order to interpret the couplings the computed directionally averaged coupling $\hat{J}$ of -1.5 cm^{-1} with the experimental value of -1.9

cm^{-1} inferred from bulk susceptibility measurements above $T_{\frac{1}{2}}$ can be compared, revealing a good agreement.

F_0	V (LS)	V ($HS^{L,tet}$)	V (HS^D)	c/a (HS^D)	ΔH_{static} (HS-LS)	ΔH $HS^D - HS^{L,tet}$	ΔH_{JT} ($HS^{L,cub} - HS^{L,tet}$)
0	276.27	—	308.24	—	+94.58D	—	—
10	280.00	316.43	308.37	1.0024	$+46.17^{L,tet}$	+31.73	+0.043
12	280.76	317.01	308.37	1.0019	$+34.99^{L,tet}$	+41.78	+0.029
14	281.51	317.54	308.35	1.0014	$+24.59^{L,tet}$	+50.20	+0.019
16	282.20	318.01	308.31	1.0010	$+13.97^{L,tet}$	+61.75	+0.013
18	282.94	318.42	308.24	1.0006	$+4.11^{L,tet}$	+72.02	+0.009
20	283.60	318.78	308.15	1.0004	$-2.28^{L,tet}$	+81.90	+0.008
30	286.74	320.11	307.44	0.9991	$-46.42^{L,tet}$	+132.74	+0.022
40	289.27	320.72	306.29	0.9983	$-80.61^{L,tet}$	+181.65	+0.038
50	291.03	321.02	304.80	0.9978	$-108.78^{L,tet}$	+227.70	+0.057
60	292.51	321.04	303.11	0.9975	$-132.74^{L,tet}$	+270.59	+0.075
70	293.28	320.85	—	0.9973	$-153.71^{L,tet}$	—	+0.089
80	294.03	320.52	—	0.9971	$-170.42^{L,tet}$	—	+0.106
90	294.52	320.12	—	0.9971	$-187.12^{L,tet}$	—	+0.110
100	294.80	319.52	—	0.9970	$-202.77^{L,tet}$	—	+0.116
UHF	318.59	343.78	—	0.9955	$-309.82^{L,tet}$	—	+0.196
Expt.	275.58	306.95		—	—	—	

Table 5.1: Variation with F_0 (%) of the optimised LS, $HS^{L,tet}$ and HS^D cell volumes, V (Å/molecule), c/a ratio of $HS^{L,tet}$ state lattice constants, and static HS-LS, $HS^D - HS^{L,tet}$ and $HS^{L,cub} - HS^{L,tet}$ enthalpy differences, ΔH (kJ/mol; superscripts indicate lowest energy HS state)

F_0	State	q (μ) Cs	q (μ) C	q (μ) N	Metal	q (μ) Total	n (n_S) z^2	n (n_S) xz	n (n_S) yz	n (n_S) x^2-y^2	n (n_S) xy
0	LS	0.99 (0.00)	-0.28 (-0.07)	-0.41 (0.10)	Cr	1.74 (2.59)	0.66 (0.08)	0.95 (0.80)	0.95 (0.80)	0.66 (0.08)	0.95 (0.80)
					Fe	1.41 (0.27)	0.59 (0.00)	1.76 (0.09)	1.76 (0.09)	0.59 (0.00)	1.76 (0.09)
	HS^D	0.99 (0.00)	-0.27 (-0.05)	-0.48 (0.15)	Cr	1.72 (2.55)	0.67 (0.08)	0.95 (0.79)	0.95 (0.79)	0.67 (0.08)	0.95 (0.79)
					Fe	1.79 (3.85)	1.20 (0.83)	1.24 (0.73)	1.24 (0.73)	1.20 (0.83)	1.24 (0.72)
14	LS	0.99 (0.00)	-0.27 (-0.08)	-0.43 (0.09)	Cr	1.80 (2.87)	0.62 (0.09)	0.95 (0.89)	0.95 (0.89)	0.62 (0.09)	0.95 (0.89)
					Fe	1.41 (0.09)	0.47 (0.00)	1.84 (0.03)	1.84 (0.03)	0.47 (0.00)	1.84 (0.03)
	$HS^{L,tet}$	0.99 (0.00)	-0.28 (-0.08)^{x,y} -0.25 (-0.05)^{z}	-0.48 (0.13)^{x,y} -0.49 (0.12)^{z}	Cr	1.79 (2.89)	0.62 (0.09)	0.94 (0.90)	0.94 (0.90)	0.63 (0.10)	0.96 (0.88)
					Fe	1.75 (3.79)	1.14 (0.88)	1.00 (0.97)	1.00 (0.97)	1.12 (0.90)	1.89 (0.07)
UHF	LS	0.99 (0.00)	-0.22 (-0.16)	-0.59 (0.14)	Cr	2.16 (3.15)	0.38 (0.09)	0.99 (0.98)	0.99 (0.98)	0.38 (0.09)	0.99 (0.98)
					Fe	1.69 (-0.01)	0.16 (0.00)	1.98 (0.00)	1.98 (0.00)	0.16 (0.00)	1.98 (0.00)
	$HS^{L,tet}$	0.99 (0.00)	-0.24 (-0.18)^{x,y} -0.21 (-0.14)^{z}	-0.60 (0.17)^{x,y} -0.62 (0.13)^{z}	Cr	2.15 (3.15)	0.38 (0.09)	0.99 (0.98)	0.99 (0.98)	0.39 (0.09)	0.99 (0.98)
					Fe	1.86 (3.94)	1.06 (0.96)	1.00 (0.99)	1.00 (0.99)	1.05 (0.97)	1.98 (0.01)

Table 5.2: Atomic charges, q(e), and spin moments, $\mu(\mu_B)$, and TM d-orbital electron, n, and spin, nS, occupation numbers obtained from $F_0 = 0$, 14%, and UHF calculations in the LS- and lowest energy HS states

F0	Set	$\Delta E(AF_2FM)$	$\Delta E(AF_1FM)$	$\Delta E(AF_3FM)$	J_{xy}	J_z	$\bar{J}$
30	I	+0.5657	+0.8960	—	-3.95	+2.91	-1.66
	II	+0.5657	—	-0.3776	-4.16	+3.33	-1.66
40	I	+0.4546	+0.7157	—	-3.15	+2.30	-1.34
	II	+0.4546	—	-0.2944	-3.30	+2.59	-1.34
		Expt	–	—	—	—	-1.9

Table 5.3: Magnetic energy differences, δE (kJ/mol per TM ion), and Fe-Cr coupling constants, J (cm^{-1}), obtained from $F_0 = 30$ and 40% calculations in the $HS^{L,tet}$ state. Each set of coupling constants obtained from the energy differences shown. $\bar{J}$ denotes the average coupling $\frac{1}{3}(2J_{xy} + J_z)$

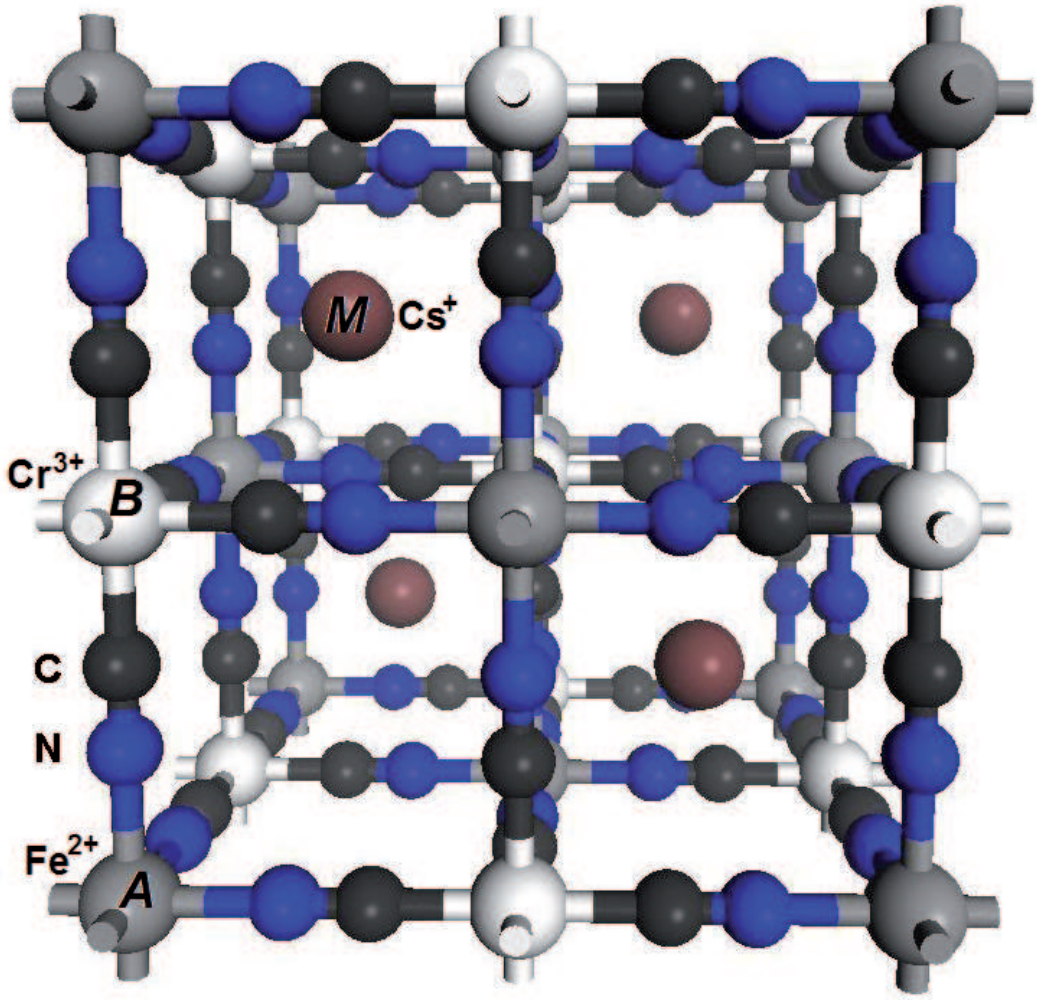

Figure 5.1: The $F\bar{4}3m$ symmetry conventional cell of $CsFe^{II}[Cr^{III}(CN)_6]$

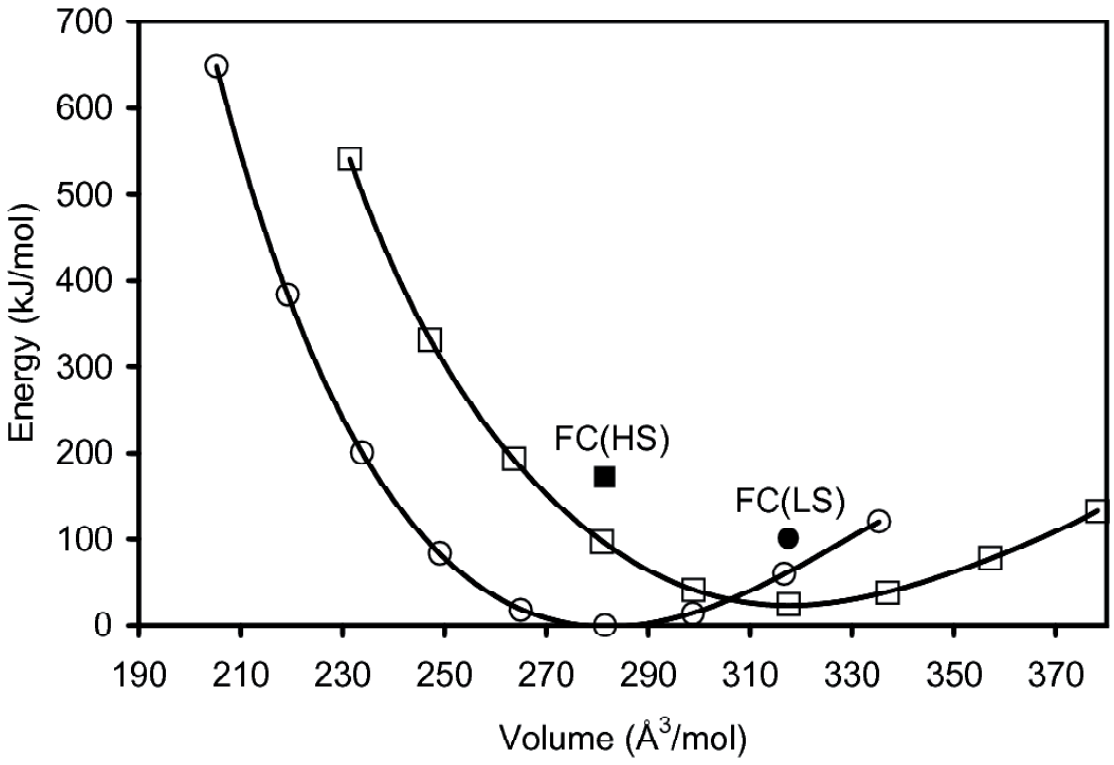

Figure 5.2: Energy-Volume variations. The energies are those of the the optimised LS lattice of the LS (circle) and tetragonal HS^L(square) lattices for F_0 =14%. Also shown are the relative energies of the corresponding Franck-Condon excited states (FC, filled symbols), i.e. the HS state in the optimised LS geometry and vice-versa. Lines show fourth-order polynomial fits

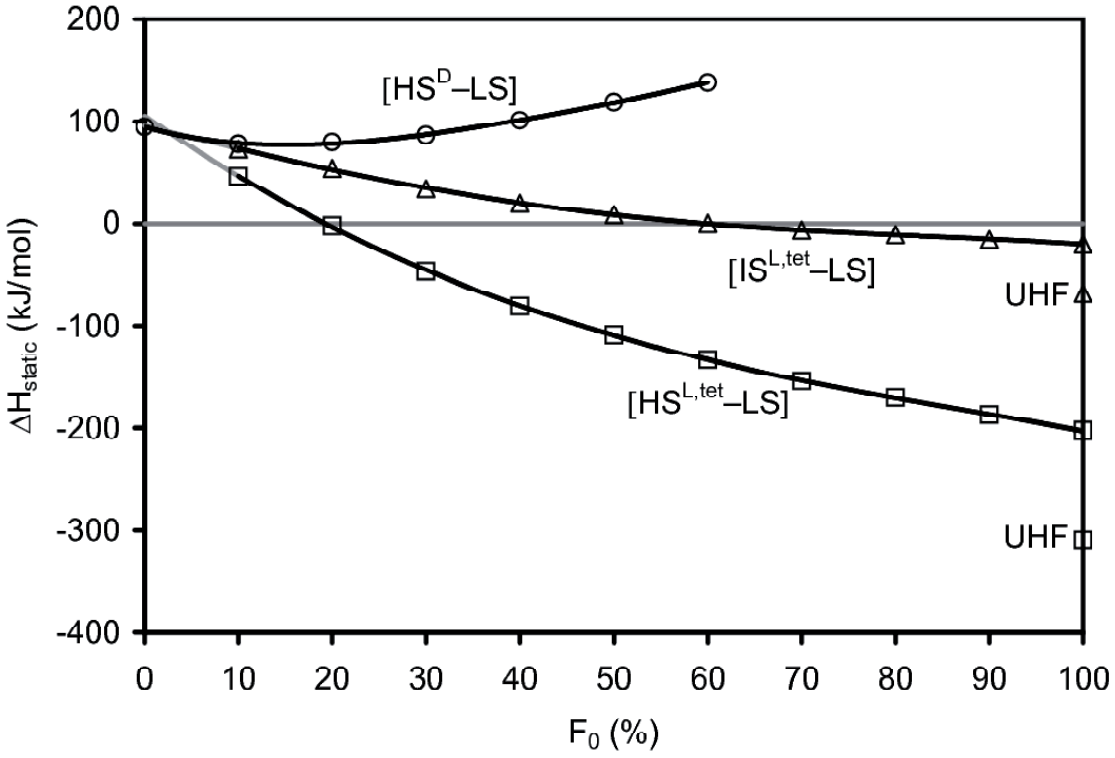

Figure 5.3: variation with $F_0(\%)$ of the energies of the optimised cubic HS^D, tetragonal HS^L, and tetragonal IS^L states relative to the optimised LS lattice

5.4 Conclusions

In this chapter the spin crossover of a Prussian Blue analogue has been analysed, in which the CRYSTAL06 code has been utilised in order to deepen the understanding of the $LS \rightarrow HS$ transition in this compound which experimentally can be observed when the temperature increases at about 238K. Through the model proposed by Kanamori, the energetics of the possible spin states have been considered varying the Fock exchange content in hybrid functionals showing that when $F_0 \leq 18\%$ (except when F_0 =0%) the nature of the spin excitation was of $HS^{L,tet} \rightarrow LS$, when $60\% \leq F_0 \leq 18\%$ this was of $HS^{L,tet} \rightarrow LS$ and for $F_0 > 60\%$ this was of $HS^{L,tet} \rightarrow IS^{L,tet}$. The optimized structures show that the $LS \rightarrow HS$ transition leads to an increase in molar volume. Within the magnetic model employed in this work, orientational in plane and out of plane coupling constants have been calculated. Notably the couplings increase in their value in

going from $F_0 = 40\%$ to 30% with the IP coupling shown to be FM while the OOP coupling is AF.

6

Looking Forward

Computational Chemistry has been proven to be very useful in this work in tackling interesting problems in computational organic chemistry, mainly related to reaction mechanisms and the interaction of molecules with light in solution. Many other different and challenging questions in this field are still awaiting an answer which will hopefully be found with increasing availability of computational resources. Full solution of the Schrödinger equation is still a dream and will require an extremely high integration between sciences such as chemistry physics and computer sciences, in that collaborating in common projects will allow the full development of quantum computers and therefore an invaluable tool for the scientist. Recently L.DiCarlo et al (2009)[136] developed the first two qu-bit superconducting processor with implementation of a quantum algorithm, fig 6.1 (figure found at `http://futurity.org`). Other frontiers for computing which are currently under study are related to the development of optical transistors which are constituted by just one or few organic molecules where the information is transported not by electrons but by photons which probably will dramatically increase the amount of information transported. The development of theoretical methods that study electron transport and the interaction of light with organic molecules will be extremely important in helping chemists in designing new materials utilised in solar cells and other electronic devices. The development of those materials, coupled with a lower production cost, will enormously benefit the spreading of such technologies.

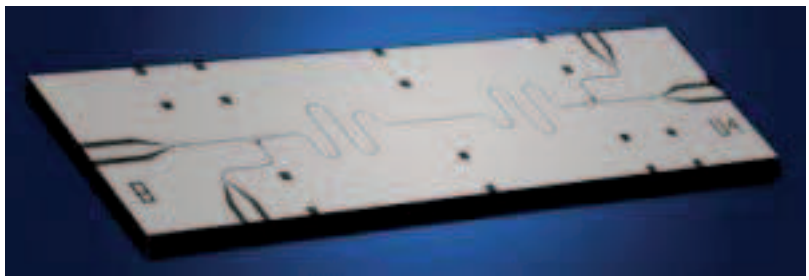

Figure 6.1: First solid state quantum processor which is also able to run simple algorithms

A better understanding of mechanisms in organic chemistry will be of great importance in saving production costs especially in reactions where many steps are involved. Many limitations are still present within the methods currently utilised for example in the study of the modulating effect of solvent on the reaction mechanism or in the treatment of radicals. The development of new organic hydrides can be quite interesting from different point of views such as the production of powerful or more selective reducing agents. Thus, an increasing knowledge on reactions of hydride transfer can be quite important, especially if Conceptual Density Functional Theory is employed as a tool for understanding better the acceptor site in which the hydride will be transferred. Moreover being able to choose the best solvent in which an hydride transfer can occur can be extremely useful although there are limitations related to the compound solubility and others...

Cyclisation reactions happen in numerous biochemical mechanisms that are very important for the survival of microorganism and humans. Sometime those reaction steps could be rate determining in the synthesis reaction path of a compound depending probably also on the solvent chosen which can perhaps modulate the reactivity by acting on nucleophilicity, steric effect and many other physical properties. Thus, learning more about how to increase the efficiency of those reactions and also computationally predicting the favourability of one cyclisation compared to another can be a valuable tool for the organic chemist.

References

[1] P. Echenique and J. L. Alonso, *Mol. Phys.*, 2007, **105**(23-24), 3057–3098.

[2] T. Bredow and K. Jug, *Theor. Chem. Acc.*, 2005, **113**, 1–14.

[3] C. J. Cramer, *Essentials of Computational Chemistry*, John Wiley and Sons Ltd, 2001.

[4] C. H. Moller and M. Plesset, *Phys. Rev.*, 1934, **46**, 1–5.

[5] F. Bernardi, A. Bottoni, and M. Gravelli, *QSAR*, 2002, pp. 1–21.

[6] F. Neese, *J. Biol. Inorg. Chem.*, 2006, **11**(6), 702–711.

[7] W. Koch and M. C. Holthausen, *A Chemist's Guide to Density Functional Theory*, Wiley-VCH, Weinheim, Germany, 2001.

[8] X. Hua, X. Chen, and W. A. G. III, *Phys. Rev. B*, 1997, **55**(24), 1–7.

[9] A. D. Becke, *Phys. Rev. A*, 1988, **38**(3098).

[10] A. J. Cohen, P. Mori-Sanchez, and W. Yanga, *J. Chem. Phys.*, 2008, **129,**, 1–4.

[11] A. J. Cohen, P. Mori-Sanchez, and W. Yang, *Phys. Rev. B*, 2008, **77**(115123), 1–6.

[12] P. Mori-Sanchez, A. J. Cohen, and W. Yang, *Phys. Rev. Lett.*, 2008, **100**(1464).

[13] A. J. Cohen, *Science*, 2009, **321**(792), 1–4.

[14] E. E. Santiso and K. E. Gubbins, *Mol. Simul.*, 2004, **30**(11-12), 699–748.

[15] K. Burke, J. Werschnik, and E. K. U. Gross, *J. Chem. Phys.*, **123**(6), 622–626.

[16] P. Elliott, K. Burke, and F. Furche, *Rev. Comput. Chem.*, pp. 91–165.

[17] N. T. Maitra, K. Burke, and C. Woodward, *Phys. Rev. Lett.*, 2002, **89**(2), 1–4.

[18] E. Runge and E. K. U. Gross, *Phys. Rev. Lett.*, 1984, **52**, 997–1000.

[19] J. Tomasi, B. Mennucci, and R. Cammi, *Chem. Rev.*, 2005, **105**, 2999–3093.

[20] Q. Cui, *J. Chem. Phys.*, 2002, **117**(10), 4720–4728.

[21] J. Gao and T. R. Furlani, *Comput. Sci. & Eng.*, 1995, pp. 1–10.

[22] M. F. Iozzi, M. Cossi, R. Improta, N. Rega, and V. Barone, *J. Chem. Phys.*, 2006, **124**(18), 184103.

[23] A. Klamt, F. Eckert, and M. Hornig, *J. of Comput-Aided Mol. Des.*, 2001, **15**, 355–365.

[24] D. M. Chipman, *J. Chem. Phys.*, 2004, **120**(12), 1–10.

[25] M. Orozco, C. Alhambra, and X. Barril, *J. Mol. Model.*, (2), 1–15.

[26] C. J. Cramer and D. G. Truhlar, *Acc. Chem. Res.*, 2008, **41**(6), 760–768.

[27] C. Cramer and D. Truhlar, *Chem. Rev.*, 1999, **99**(8), 2161–220.

[28] Gaussian 03, revision d.02. M. J. Frisch, G. W. Trucks, H. B. Schlegel, G. E. Scuseria, M. A. Robb, J. R. Cheeseman, J. A. M. Jr, T. Vreven, K. N. Kudin, J. C. Burant, J. M. Millam, S. S. Iyengar, J. Tomasi, V. Barone, B. Mennucci, M. Cossi, G. Scalmani, N. Rega, G. A. Petersson, H. Nakatsuji, M. Hada, M. Ehara, K. Toyota, R. Fukuda, J. Hasegawa, M. Ishida, T. Nakajima, Y. Honda, O. Kitao, H. Nakai, M. Klene, X. Li, J. E. Knox, H. P. Hratchian, J. B. Cross, V. Bakken, C. Adamo, J. Jaramillo, R. Gomperts, R. E. Stratmann, O. Yazyev, A. J. Austin, R. Cammi, C. Pomelli, J. W. Ochterski, P. Y. Ayala, K. Morokuma, G. A. Voth, P. Salvador, J. J. Dannenberg, V. G. Zakrzewski, S. Dapprich, A. D. Daniels, M. C. Strain, O. Farkas, D. K. Malick, A. D. Rabuck, K. Raghavachari, J. B. Foresman, J. V. Ortiz, Q. Cui, A. G. Baboul, S. Clifford, J. Cioslowski, B. B. Stefanov, G. Liu, A. Liashenko, P. Piskorz, I. Komaromi, R. L. Martin, D. J. Fox, T. Keith, M. A. Al-Laham, C. Y. Peng, A. Nanayakkara, M. Challacombe, P. M. W. Gill, B. Johnson, W. Chen, M. W. Wong, C. Gonzalez, and J. A. Pople; Gaussian Inc., Wallingford CT, 2004.

[29] S. M. Bachrach, *Computational organic chemistry*, 2007.

[30] J. d Thompson, C. J. Cramer, and D. G. Truhlar, *J. Comput. Chem.*, 2003, **24**, 1291–1304.

[31] C. P. Kelly, C. J. Cramer, and D. G. Truhlar, *J. Chem. Theory Comput.*, 2005, **1**, 1133–1152.

[32] A. Klamt, *J. Phys. Chem.*, 1996, **100**, 3349–3353.

[33] M. J. Kamlett and R. W. Taft, *J. Org. Chem.*, 1982, **47**, 1734.

[34] B. Mennucci, *Theor. Chem. Acc.*, 2006, **116**(1-3), 31–42.

[35] A. Berezhkovskii, *Chem. Phys.*, 1992, **164**, 331–339.

[36] M. Cossi and V. Barone, *J. Phys. Chem. A*, 2000, **104**, 10614–10622.

[37] M. Caricato, B. Mennucci, J. Tomasi, F. Ingrosso, R. Cammi, S. Corni, and G. Scalmani, *J. Chem. Phys.*, 2006, **124**(124520), 1–13.

[38] M. Caricato, F. Ingrosso, B. Mennucci, and J. Tomasi, *J. Chem. Phys.*, 2005, **122**(15), 154501.

[39] J. E. Baldwin, *Chem. Comm.*, 1976, pp. 734–736.

[40] J. March and M. B. Smith, *Advanced Organic Chemistry*, Wiley-Interscience, New York, 5 edition ed., 2001.

[41] J. Mikosch, S. Trippel, C. Eichhorn, R. Otto, U. Lourderaj, J. X. Zhang, W. L. Hase, M. Weidemuller, and R. W. r, *Science*, 2008, **319**(183), 1–5.

[42] H. B. Burgi, J. D. Dunitz, J. M. Lehn, and G. Wipff, *Tetrahedron*, **30**, 1563–1572.

[43] C. D. Johnson, *Acc. Chem. Res.*, 1993, **26**, 476–482.

[44] J. E. Baldwin, R. C. Thomas, L. I. Kruse, and L. Silberman, *J. Org. Chem.*, 1977, **42**(24), 1–7.

[45] N. C. J. Chokotho, T. C. Jarvis, C. D. Johnson, C. C. Lewis, and M. E. A. Astudillo, *Tetrahedron*, 1985, **41**(24), 5919–5928.

[46] J. Piccirilli, *Chem. & Biol.*, 1999, **6**(3), 1–6.

[47] K. D. Janda, C. G. Shevlin, and R. A. Lerner, *Science*, 1993, **259**, 1–4.

[48] K. Gruber, B. Zhou, K. N. Houk, R. A. Lerner, C. G. Shevlin, and I. A. Wilson, *Biochemistry*, 1999, **38**, 7062–7074.

[49] C. Chatgilialoglu, C. Ferreri, M. Guerra, V. Timokhin, G. Froudakis, and T. Gimisis, *J. Am. Chem. Soc.*, 2002, (124), 10765–10772.

[50] H. Ishibashi, *Chem. Record*, 2006, **6**(1), 23–31.

[51] H. Ishibashi, N. Nakamura, T. Sato, M. Takeuchi, and M. Ikeda, *Tetrahedron Lett.*, 1991, **32**(14), 1725–1728.

[52] J. Friedrich, K. Walczak, M. Dolg, F. Piestert, T. Lauterbach, and D. W. andl Andreas Gansauer, *J. Am. Chem. Soc.*, pp. 1–9.

[53] V. V. Speybroeck, K. Hemelsoet, M. Waroquier, and G. B. Marin, *Int. J. Quantum Chem.*, 2003, **96**(6), 568–576.

[54] X. Guan, D. Lee, and P. D. Yang, *J. Org. Chem*, 2005, **71**, 1984–1988.

[55] P. d'Antuono, A. Fritsch, L. Ducasse, F. Castet, and P. James, *J. Phys. Chem. A*, 1904, **110**, 3714–3722.

[56] Y. Yamamoto, M. Ohno, and S. Eguchi, *J. Org. Chem*, 1997, **61**, 9264–9271.

[57] I. V. Alaburgin and M. Manoharan, *J. Am. Chem. Soc.*, 2005, **127**, 9534–9545.

[58] T. Yamazaki, S. Hiraoka, J. Sakamoto, and T. Kitazume, *J. Phys. Chem. A*, 1999, **103**, 6820–6824.

[59] K. Ando, *J. Org. Chem*, 2004, **69**, 4203–4209.

[60] S. Olivella and A. Sole', *J. Am. Chem. Soc.*, 2000, **122**, 11416–11422.

[61] I. V. Alaburgin and M. M. Manoharan, *J. Am. Chem. Soc*, 2005, **127**, 12583–12594.

[62] L. Liu, Q. Chen, Y. D. Wu, and C. Li, 2004, **70**, 1539–1544.

[63] A. D. C. Parenty, L. V. Smith, A. L. Pickering, D.-L. Long, and L. Cronin, *J. Org. Chem.*, **69**, 5934–5946.

[64] C. J. Richmond, A. D. C. Parenty, Y.-F. Song, G. Cooke, and L. Cronin, *J. Am. Chem. Soc.*, 2008, **130**, 13059 – 13065.

[65] M. Cossi, C. Adamo, and V. Barone, *Chem. Phys. Lett.*, 1998, **297**, 1–7.

[66] X. Chen and J. I. Brauman, *J. Am. Chem. Soc.*, 2009, (130), 15038–15046.

[67] C. K. Regan, S. L. Craig, and J. I. Brauman, *Science*, 2009, **295**, 2245–2247.

[68] I. Adamovic and M. S. Gordon, *J. Phys. Chem. A*, 2004, **109**, 1629–1636.

[69] A. D. Boese, J. M. L. Martin, and N. C. Handy, *J.Chem. Phys.*, 2003, **119**(6), 1–10.

[70] H. Buck, *Int. J. Quantum. Chem.*, 2004, **101**(4), 389–395.

[71] L. M. McDonough PhD thesis, University of Washington, 1960.

[72] E. M. Arnett, R. A. Flowers, A. E. Meekhof, and L. Miller, *J. Am. Chem. Soc.*, 1993, **115**, 12603.

[73] E. M. Arnett, R. A. Flowers, R. T. Ludwig, A. E. Meekhof, and S. A. Walek, *J. Phys. Org. Chem.*, 1997, **10**, 499.

[74] R. M. Nicoll, I. H. Hillier, and D. G. Truhlar, *J.Am.Chem.Soc.*, 2001, **123**, 1459–1463.

[75] C. Alhambra, J. C. Corchado, M. L. S. nchez, J. Gao, and D. G. Truhlar, *J. Am. Chem. Soc.*, 2000, **122**, 8197–8203.

[76] S. Gronert and J. R. Keeffe, *J. Org. Chem*, 2006, **71**, 5959–5968.

[77] S. Hammes-Schiffer, *ChemPhysChem*, 2002, **3**, 33–42.

[78] S. Hammes-Schiffer, *Curr. Opinion in Structural Biology*, 2004, **14**, 192–201.

[79] C. G. Swain, R. A. Wiles, and R. F. W. Bader, *J. Am. Chem. Soc*, 1961, **83**(1945).

[80] P. Y. Ayala and H. B. Schlegel, *J. Chem. Phys.*, 1997, **107**(2), 1–10.

[81] A. D. Becke, *J. Chem. Phys.*, 1993, **98**, 5648–56.

[82] A. Toro-Labbe', *J. Phys. Chem. A*, 1999, **103**, 4398 – 4403.

[83] R. G. Pearson, *PNAS*, 1986, **83**(22), 8440–8441.

[84] D. Dipankar, *J. Phys. Chem.*, 1992, **96**(6), 2409–2410.

[85] M. J. G. Peach, T. Helgaker, P. Saek, T. W. Keal, O. B. Lutnæs, D. J. Tozer, and N. C. Handy, *Phys. Chem. Chem. Phys*, 2006, **8**, 558–562.

[86] R. J. Magyar and S. Tretiak, *J. Chem. Theory Comput.*, 2007, **3**, 976–987.

[87] N. T. Maitra, *J. Chem. Phys.*, 2005, **122**(23), 234104.

[88] A. Dreuw, J. L. Weisman, and M. Head-Gordon, *J.Chem. Phys.*, 2003, **119**(6), 1–4.

[89] M. J. G. Peach and D. J. Tozer, *J. Mol. Struct.*, 2009, **3**.

[90] M. J. G. Peach, P. Benfield, T. Helgaker, and D. J. Tozer, *J. Chem. Phys.*, 2008, **128**, 44118.

[91] J. P. Perdew, K. Burke, and M. Ernzerhof, *Phys. Rev. Lett.*, 1996, **77**, 3865 – 3868.

[92] D. Jacquemin, E. A. Perpète, G. E. Scuseria, I. Ciofini, and C. Adamo, *J. Chem. Theory Comput.*, 2008, pp. 123–135.

[93] E. A. Perpète, F. Maurel, and D. Jacquemin, *J. Phys. Chem. A*, 2007.

[94] D. Jacquemin, M. Bouhy, and E. A. Perpète, *J. Chem. Phys.*, 2006, **124**(20), 204–221.

[95] W. Valerie, A. Jean-Marie, E. A. Perpète, and J. Denis, *J. Phys. Chem. A*, 2006, **110**, 8145–8150.

[96] D. Jacquemin, V. Wathelet, J. Preat, and E. A. Perpète, *Spec. Acta Part A*, 2007, pp. 334–341.

[97] J. Preat, D. Jacquemin, and E. A. Perpete, *Dyes and Pigments*, 2007, **72**, 185–191.

[98] J. Preat, P.-F. Loos, X. Assfeld, D. Jacquemin, and E. A. Perpète, *Int. J. Quantum Chem.*, 2007, **107**(3), 574–585.

[99] P.-F. Loos, J. Preat, A. le D Laurent, C. Michaux, D. Jacquemin, E. A. P. te, and X. Assfeld, *J. Chem. Theory Comput.*, 2008, **4**, 637–645.

[100] D. Jacquemin, E. A. Perpete, I. Ciofini, and C. Adamo, *Theor. Chem. Acc.*, 2008, **120**(4-6), 405–410.

[101] D. Jacquemin, J. Preat, V. Wathelet, M. le Fontaine, and E. A. Perpète, *J. Am. Chem. Soc.*, 2006, **128**, 2072–2083.

[102] J. N. Woodford, *Chem. Phys. Lett.*, 2005, **410**, 182–187.

[103] D. Varsano, R. D. Felice, M. A. L. Marques, and A. Rubio, *J. Phys. Chem. B*, 2006, **110**, 7129–7138.

[104] F. Santoro, V. Barone, and R. Improta, *J. Comput. Chem.*, 2008, **29**(6), 957–964.

[105] R. Improta, *Phys. Chem. Chem. Phys.*, 2008, **10**(19), 2656–2664.

[106] J. A. Pople, M. Head-Gordon, D. J. Fox, K. Raghavachari, and L. A. Curtiss, *J. Chem. Phys.*, 1989, **90**(10), 1–8.

[107] I.-S. H. Lee, H. J. Kil, and Y. R. Ji, *J. Phys. Org. Chem.*, 2007, **20**(7), 484–490.

[108] X.-Q. Zhu, M.-T. Zhang, A. Yu, C.-H. Wang, and J.-P. Cheng, *J. Am. Chem. Soc.*, 2008, **130**, 2501–2516.

[109] R. G. Parr, L. V. Szentpaly, and Liu, *J. Am. Chem. Soc.*, 1999, **121**, 1922 – 1924.

[110] C. Morell, P. W. Ayers, A. Grand, S. Gutierrez-Olivac, and A. Toro-Labbe', *Phys. Chem. Chem. Phys.*, 2008, **10**, 7239–7246.

[111] J. V. Correa, P. Jaque, J. Oláh, A. Toro-Labbé, and P. Geerlings, *Chem. Phys. Lett.*, 2009, **470**(4-6), 180–186.

[112] T. Fievez, N. Sablon, F. D. Proft, P. W. Ayers, and P. Geerlings, *J. Chem. Theory Comput.*, 2008, pp. 1065–1072.

[113] P. Geerlings, F. D. Proft, and W. Langenaeker, *Chem. Rev.*, 2003, **103**, 1793–1873.

[114] C. Lee, W. Yang, and R. G. Parr, *Phys. Rev. B*, 1988, **37**(785).

[115] J. Korchowiec and R. Nalewajski, *Int. J. Quantum Chem.*, 1992, **44**, 1027–1040.

[116] R. K. Roy, S. Krishnamurty, S. Pal, and K. Hirao, *J. Chem. Phys.*, 2001, **115**(7), 2901–2907.

[117] C. Morell, A. Hocquet, A. Grand, and B. Jamart-Gregoire, *Theochem*, 2008, **849**, 56–51.

[118] P. W. Ayers, C. Morell, F. D. Proft, , and P. Geerlings, *Chem. Eur. J.*, 2007, **13**, 8240–8247.

[119] Swizard program, http://www.sg-chem.net/, ccri, ottawa, canada. S. I. Gorelsky; University Of Ottawa, Ottawa, Canada., 2008.

[120] P. Gutlich, A. Hauser, and H. spiering, *Angew. Chem. Int. Ed.*, 1994, **33**(2024).

[121] P. Gutlich, *Struct Bonding (Berlin)*, 1981, **44**(83).

[122] D. Papanikolaou, W. Kosaka, S. Margadonna, H. Kagi, S. Ohkoshi, and K. Prassides, *J. Phys. Chem. C*, 2007, **11**, 8086.

[123] B. L. Guennic, S. Borshch, and V. Robert, *Inorg. Chem.*, 2007, **46**, 11106 – 11111.

[124] K. R. D. Verdaguer and R. A. Heintz, *Prog. Inorg. Chem.*, 1997, **45**.

[125] H. Paulsen and A. X. Trautwein, *J. Phys. Chem. Solids*, 2004, **65**(4), 793 – 798.

[126] A. Fouqueau, M. E. Casida, L. M. L. Daku, A. Hauser, and F. Neese, *J. Chem. Phys.*, 2005, **122**, 44110.

[127] L. M. L. Daku, A. Vargas, A. Hauser, A. Fouqueau, and M. E. Casida, *Chem. Phys. Chem.*, 2005, **11**(6), 1393 – 1410.

[128] G. Brehm, M. Reiher, and S. Schneider, *J. Phys. Chem. A*, 2002, **106**, 12024 – 12034.

[129] M. Reiher, *Inorg. Chem.*, 2002, **41**, 6928 – 6935.

[130] G. Baranovic, *Chem. Phys. Lett.*, 2003, **369**(5), 668 – 667.

[131] R. Dovesi, V. Saunders, C. Roetti, R. Orlando, C. M. Zicovich-Wilson, F. Pascale, B. Civalleri, K. Doll, N. Harrison, I. Bush, P. DArco, and M. Llunell, *CRYSTAL06 User's Manual*, 2008.

[132] S. H. Vosko, L. Wilk, and N. Nusair, *Can. J. Phys.*, 1980, **58**(1200).

[133] D. Middlemiss and C. Wilson, *Phys. Rev. B*, 2008, **77**, 155129.

[134] D. Middlemiss, L. Lawton, and C. Wilson, *J. Phys. Condens. Matter*, 2008, **20**, 335231.

[135] C. M. Zicovich-Wilson, R. Dovesi, and V. R. Saunders, *J. Chem. Phys.*, 2001, **115**, 9708.

[136] L. DiCarlo, J. M. Chow, J. M. Gambetta, L. S. Bishop, B. R. Johnson, D. I. Schuster, J. Majer, A. Blais, L. Frunzio, S. M. Girvin, and R. J. Schoelkopf, *Nature*, 2009, **460**(7252), 240 – 244.